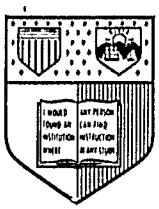

Energy Program

Sibley School of
Mechanical and Aerospace Engineering

Cornell University Ithaca, New York 14853

Exhaust Gas Measurements in a Propane Fueled Swirl-Stabilized Combustor

by

M.S. Aanad

E-82-4 August 1982

This report is the thesis of Mr. Mathagondapally Srinivasan Aanand, presented to the Faculty of the Graduate School of Cornell University in partial fulfillment for the Degree of Master of Science, June 1980. The work was supported by a grant from the Lewis Research Center of the National Aeronautics and Space Administration (Grant NO. NSG-3019). C.J. Marek was the technical monitor.

EXHAUST GAS MEASUREMENTS IN A PROPANE FUELED SWIRL-STABILIZED COMBUSTOR

A Thesis

Presented to the Faculty of the Graduate School

of Cornell University

in Partial Fulfillment for the Degree of

Master of Science

by

Mathagondapally Srinivasan Anand

August 1982

ABSTRACT

Exhaust gas temperature, velocity and composition are measured and combustor efficiencies are calculated in a lean premixed swirl-stabilized laboratory combustor. These data should be valuable in understanding the combustion and fluid mechanical processes in such a combustor with an aim to reduce pollutant emissions and maintain high combustion efficiencies in order to develop new combustor designs for practical applications. This work is part of an overall combustion research program at Cornell University directed towards the characterization of swirling turbulent reacting flows.

The combustor consists of two confined co-axial swirling jets. The inner jet is premixed fuel-air mixture while the outer jet is air only. The amount of swirl can be varied in both the jets. The outer jet can be swirled in the same direction (co-swirl) or in the direction opposite (counter-swirl) to that of the inner jet. Combustion is stabilized in front of a swirl-induced recirculation zone.

In the first phase of measurements, radial traverses measuring temperature, velocity and gas composition are made at the exit plane for varying outer swirl conditions using propane as fuel. These data are compared with previous results for methane firing. In the second phase, measurements are made under cold flow (nonreacting) conditions to investigate fuel distribution at the inlet and

exit planes. In addition, data similar to those obtained in the first phase are obtained for methane firing for comparison with data for propane firing as well as previous results.

Temperature measurements are made with an uncoated Pt/Pt-10%Rh fine wire thermocouple. A transverse cylindrical probe is used to measure velocity as well as to draw gas samples. In situ calibration of the probe is found necessary for velocity measurements to correct for turbulence effects. Samples are analyzed for oxides of nitrogen in a chemiluminescence analyzer equipped with an NO_2-NO converter. Analyses for the major species are done by gas chromatography. A novel scheme to significantly reduce the analysis time for the gas chromatographic analysis of the products of propane combustion is developed.

Results show significant differences in the radial profiles of the data between the co- and the counter-swirl cases. Co-swirl cases show evidence of poor turbulent mixing across the combustor in comparison to the counter-swirl cases. NO_x levels are low in the combustor but substantial amounts of CO are present. Combustion efficiencies are low and surprisingly constant with varying outer swirl in contradiction to previous results under a slightly different inner swirl condition. This difference in the efficiency trends is expected to be a result of the high sensitivity of the combustor to changes in the inner swirl. Combustor

operation is found to be the same for propane and methane fuels.

A mechanism is proposed to explain the combustor operation and a few important characteristics determining combustor efficiency are identified. Future experiments to substantiate the proposed mechanism are suggested.

BIOGRAPHICAL SKETCH

M.S.Anand was born on April 21,1957 in Bangalore, India where he had most of his early education. Keenly interested in model making from an early age, Anand, as he is called, held copyrights for some of his model kits while in high school. He was placed within the top ten in all the three state-level examinations for the Secondary Schools Leaving Certificate and the I and II year Pre-University Course, in recognition of which he was awarded the National Merit Scholarship. Anand received his B.Tech. degree, First Class with Distinction, from the Indian Institute of Technology, Madras in 1978. He joined Cornell University in the fall of 1978 to pursue graduate studies. He is currently doing his Ph.D. at Cornell University. His hobbies include music, badminton and cricket.

To my parents

Srinivasan and Vasantha

ACKNOWLEDGEMENTS

The author would like to thank Prof. F.C.Gouldin, chairman of the author's special committee, for his guidance and discussions during the course of this work. Thanks are also extended to Prof. P.C.T.De Boer and Prof. J.T.Jenkins for serving as minor members on the special committee. Special appreciation is expressed for the technical assistance by Ed Jordan and his readiness to help. The author wishes to thank fellow graduate students for their discussions during the course of this research and Govindaraj Kuntimad for his valuable help during the typing of this thesis.

This work was supported in part by the NASA Lewis Resaerch Center, Cleveland, Ohio, Grant NSG-3019. Dr. C.J.Marek was the technical monitor.

TABLE OF CONTENTS

LIST OF TABLES

LIST OF FIGURES

CHAPTER 1

INTRODUCTION

1.1 Swirl-Stabilized Combustion

Swirling flows have been studied for many years because of their potential for stabilization of high intensity combustion processes [1,2]. Swirl has been used to stabilize subsonic combustion systems[3] and is proposed for use in supersonic combustion processes as well[4]. The attractive features of reacting vortex flows are better flame stability resulting from the formation of one or more recirculating flow zones, reduced combustion length and increased mixing through turbulence generation. These large scale effects have been demostrated by numerous experimental studies involving both diffusion and premixed flame combustors, e.g.,[3,5,6,7,8]. Unfortunately, the simultaneous presence of swirl, shear, turbulence and heat release makes the reacting vortex flow a very complex object of study and as a consequence these flows are poorly understood.

Recirculation in flows with swirl is known to depend on the swirl number S, the ratio of the axial flux of angular momentum to the axial flux of linear momentum, and the Reyolds number of the flow[1]. As the swirl number is increased a pronounced deceleration or even a reversal of the flow along the flow axis may occur. Below a critical swirl number no back flow occurs. Above this critical level of

swirl the phenomenon of vortex breakdown[9,10] occurs which is characterized by the formation of a free stagnation point on the vortex axis, followed by reversed flow in a region of limited axial extent. Various forms of vortex breakdown are possible[9,11]. Notable among them are the axisymmetric and the spiral forms, both of which appear capable of stabilizing combustion[12]. Continued reasearch is required to understand and characterize combustion processes in swirling flows and to develop combustor designs with such flows.

One of the present applications of the swirl-combustor is in gas turbine engines. It is hardly necessary to stress the increasing role of gas turbines in the present day world. Gas turbines are the major power systems for military and commercial aircraft. Also, gas turbines are used for marine propulsion, in the 'Spruance' class of destroyers, for example. A recent application is in electric power generation as peaking-power units, mid-range and even as baseload power[13] units. In the combined cycle concept a gas turbine topping cycle generates power and its exhaust is used to provide heat to the bottoming cycle[14]. As a result of the high operating temperatures possible with new high temperature alloys and ceramic materials, automotive gas turbines are under serious consideration[15].

1.2 Pollutant Emissions and Control

With the growth in applications and the widespread use of gas turbines, the problem of pollutant emissions from gas

turbines also has grown. The need to limit pollutant emissions from combustion systems is widely recognized[16,17,18,19,20]. The U.S. Environmental Protection Agency (EPA) has proposed stringent emission standards for new aircraft[21] and stationary gas turbines[22]. The three major pollutants from gas turbine combustors are carbon monoxide (CO), unburned hydrocarbons (UHC) and oxides of nitrogen (NO_x) which comprise nitric oxide (NO) and nitrogen dioxide (NO_2). Soot and sulphur oxides emissions can occur under certain conditions but do not currently pose problems for gas turbines.

1.2.1 Unburned Hydrocarbons

Unburned hydrocarbons (UHC) are a direct indication of inefficient combustion. In addition, they are intimately connected with oxides of nitrogen in the formation of photochemical smog in the atmosphere. Higher UHC emissions are caused by increasingly lean conditions which lead to lower flame temperatures and to thermal quenching of the hydrocarbon breakdown reactions. Thermal quenching can be described as the cooling of the gases below the temperature at which a given reaction can effectively take place. Sawyer[23] experimentally determined that the quenching temperature for heavy unburned hydrocarbon oxidation is in the range of approximately 1500 to 1700°K. Also, large droplets with long burning times can contribute directly to increased UHC as they may persist into the secondary dilution zone or hit the cool

combustor liner and remain unreacted. Thus premixed, prevaporized combustion in a near stoichiometric mixture is likely to reduce or eliminate UHC emissions.

1.2.2 Carbon Monoxide

In addition to being highly toxic, carbon monoxide in the gas turbine exhaust is also an indication of inefficient combustion. It is well accepted that the oxidation of CO to CO_2 in combustion systems follows the reaction[24]

$$CO + OH = CO_2 + H \ . \qquad (1.1)$$

Reaction (1.1), which proceeds rapidly at high temperatures, is hindered at low temperatures due to reduced levels of OH. At stoichiometric conditions the CO concentrations are kept to a minimum in the primary zone of the combustor where high flame temperatures are reached and combustion is complete. CO increases in rich mixtures due to lack of oxygen and in lean mixtures due to thermal quenching by excess air. This similarity between HC and CO trends in lean flames is due mainly to the tendency of oxidation reactions to increase with temperature. However, since the CO oxidation is slower than hydrocarbon reactions, CO is more prone to thermal quenching and persists unreacted for many (5-6) milliseconds in fuel lean flames (ϕ=0.8)[17]. The quenching temperature for CO has been experimentally determined[17] to be about 1270°K at atmospheric pressure and approximately 1500°K at 3 atmospheres below which temperature CO can remain unreacted

indefinitely if quenching is fast enough. These observations[17] are consistent with the approximation that flame generated trace species such as O, H, H_2 and OH remain equilibrated among themselves and decay together as the temperature falls, but CO is not necessarily equilibrated with the others. Since the CO reaction with OH can be slow compared to the decay of the trace species, CO can remain largely unreacted as the others decay. At high temperatures, however, CO can occur due to dissociation of CO_2. Reduction in CO emissions can be achieved by uniform, stoichiometric or lean premixed combustion with reduced thermal quenching rates.

1.2.3 Oxides of Nitrogen

NO and NO_2 are highly toxic. In addition, they play an important role in smog formation and depletion of ozone in the stratosphere[16]. Since, at ground level, an interconversion between NO and NO_2 is possible in the presence of atmospheric oxygen, there has been little interest in specific emissions of NO and NO_2, and emissions have been measured in terms of NO_x. In the stratosphere the catalytic ozone destruction cycle promotes a steady-state balance between the oxides of nitrogen on a relatively short time scale[19] regardless of the initial amounts of each. Smog formation, however, may well be affected by high NO_2 levels, since ozone does not begin to form until NO has been converted to NO_2 in the atmosphere. It has also been suggested

that locally high NO_2 emissions in the lower stratosphere could, under some conditions, result in a more rapid removal of NO_x via conversion to nitric acid[25]. Thus the relative amounts of NO and NO_2 are important and in recent studies the two species are reported separately.

In combustion systems, NO formation is a prerequisite for NO_2 formation. It is generally accepted that NO formation in fuel-lean mixtures follows the Zel'dovich mechanism (thermal NO) where fuel-bound nitrogen is insignificant[26]. Formation of NO is associated with high temperatures of 1900°K and above[23]. Under lean conditions in a combustor NO increases with increasing equivalence ratio, following a trend opposite that of CO and UHC, due to the increase in temperature with increasing equivalence ratio. But even at high temperatures NO formation is fairly slow and occurs on a time scale of several milliseconds. Hence NO is formed in the primary zone where the two main prerequisites for NO formation are met, namely, high temperatures and sufficient residence time. This understanding suggests two methods of NO control. First, the peak temperatures in the combustor should be lowered by methods such as lean premixed combustor operation and exhaust gas recirculation. In the case of liquid fuels whose individual droplets burn at locally stoichiometric conditions, prevaporization and premixing of fuel seems necessary. Second, the residence time in the primary combustion zone should be reduced by the rapid addition of secondary air through turbulent mixing. Schefer and Sawyer[26] have pre-

sented results for turbulent, lean, premixed combustion, of their own work as well as others which show substantial reductions in the levels of NO_x emissions over the NO_x emissions from current conventional turbulent diffusion flame gas turbine combustors. Gouldin[27] points out that while turbulent mixing is desirable both to reduce residence times in high temperature zones and to enhance the stabilization of the lean combustion suggested above, the intensity and small scale of the turbulence required could result in a prohibitive combustor pressure drop.

The preceeding discussion applies to NO formed from N_2 in atmospheric air. Nitrogen is also found in some fuels, especially in those derived from coal. Fuel nitrogen conversion to NO_x occurs at lower temperatures than reactions with molecular nitrogen and may result in larger amounts of NO than in pure hydrocarbon flames[28]. It is suggested that flame generated nitrogeneous species such as HCN, CN and NH_x play important roles in NO_x formation in flames of fuels containing nitrogen compounds[28]. Also, in fuel-rich hydrocarbon flames, some NO formation proceeds by a mechanism similar to that for fuel-bound nitrogen involving the formation of intermediate species such as HCN and CN[29].

The formation of NO_2 is less completely understood than the formation of NO though several explanations have been tendered. A consistent mechanism for NO_2 formation must be able to explain the high fractions of NO_2 that have been mea-

sured in or near laminar flame fronts[30,31,32] as well as in turbulent combustors[26,33,34,35]. The most plausible mechanism for NO to NO_2 conversion invokes Reaction (1.2) in quenching zones where the temperature is falling and the free radical concentrations exceed their equilibrium values[25,31,32,35].

$$NO + HO_2 = NO_2 + OH \qquad (1.2)$$

Fenimore[32] has shown that with the assumption of local equilibrium for the Reactions (1.2), (1.3) and (1.4) the ratio of NO_2/NO can be found by assuming equilibrium for Reaction (1.5) when oxygen atoms are determined by the equilibration of Reaction (1.4).

$$H + O_2 + M = HO_2 + M \qquad (1.3)$$

$$H + O_2 = OH + O \qquad (1.4)$$

$$NO + O = NO_2 \qquad (1.5)$$

Calculations by Anderson, et al.[25] have shown that under after burning conditions in a supersonic transport engine, superequilibrium concentrations of HO_2 can result in unexpectedly large values for NO_2/NO through Reaction (1.2). This supports Fenimore's results although in Fenimore's case the excess HO_2 results from hydrocarbon oxidation rather than from Reaction (1.3). Thus, Fenimore's mechanism with excess HO_2 due to hydrocarbon oxidation appears to be the most plausible explanation of NO_2 formation in gas turbines. Further

support for this mechanism comes from the study by Chen, et al.[36] who showed that when a partially reacted sample containing unburnt fuel is quenched (either by mixing or in a probe), large concentrations of HO_2 are produced during low temperature hydrocarbon oxidation. Reaction (1.2) is therefore favored in quenching zones, and the high NO_2/NO_x fractions can be attributed to quenching zones in the combustor.

1.2.4 Pollution Control

Some conditions under which pollutant emissions can be reduced have been mentioned in the preceding subsections. Pollution control in gas turbines and other continuous flow combustors has been accomplished by trying to achieve these conditions primarily by alterations or additions to existing designs. Since conditions minimizing NO_x formation tend to maximize CO and UHC emissions, and vice versa, a trade off is inevitable. Flame temperatures have been reduced by leaner fuel-air mixtures, by steam or water injection into the combustion zone and by exhaust gas recirculation. Fuel injection has been improved and combustor liners have been modified to change air flows. Lefebvre[37], in a review of gas turbine pollution control, concludes, as do Rudy and Reck[16] and many others, that only advanced and radically new combustor designs involving concepts such as prevaporized premixed combustion, variable geometry and swirl-augmented combustion can achieve the required emissions reduction levels. These are the very concepts which form the basis for the swirl-

stabilized combustion research at Cornell.

1.3 Swirl-Stabilized Combustor Research at Cornell

Research at Cornell in this area, going on since the early seventies, is a continuing program directed towards the study of the interrelationships between chemical kinetics and turbulent mixing in a research combustor with premixed prevaporized fuel and variable swirl. The aim of the overall program is to completely characterize the swirling flows in the combustor under both reacting and nonreacting conditions and perhaps to develop numerical models to predict these flows. This characterization of the combustor which entails flow and turbulence measurements in nonreacting flows and detailed measurements of velocity, temperature and composition as well as flow visualization in combusting flows, is key to developing new and viable combustor designs for practical applications.

1.3.1 The Swirl Combustor

The combustor under investigation (Figure 1-1) is a lean, premixed combustor in which the flame is stabilized by a swirl-generated recirculation zone. The combustor consists of two co-axial swirling jets confined in a long cylindrical test section of 10.2 cm I.D. The inner jet, 4.8 cm in diameter, consists of premixed fuel and air. Swirl in the inner jet is generated by tangential air injection well upstream of the combustor inlet. The outer jet flow is air only and has

an outer diameter (D_o) of 10.2 cm. Swirl in the outer jet, which is generated by varying-angle vanes upstream of the combustor inlet, can be either co-swirl (outer and inner swirls in the same direction) or counter-swirl (outer and inner swirls in the opposite directions). The fuel, commercial grade methane or propane, is injected radially from the inner jet centerline five combustor diameters ($5D_o$) upstream of the inlet. Ignition is accomplished by a long reach spark plug. A more detailed account of the combustor can be found in Chapter 2.

The swirl number as defined in Section 1.1 is non-dimensionalized by the outer radius of the jet. The swirl number for the inner or the outer flow is then given by

$$S = \frac{2\pi\rho \int_{r_i}^{r_o} u\, v\, r\, dr}{2\pi\rho\, r_o \int_{r_i}^{r_o} u^2\, r\, dr} \qquad (1.6)$$

where r_i and r_o are the inner and outer radii of the jet under consideration, u and v are the time-mean axial and tangential velocities respectively. The swirl number is positive as defined. A negative sign is used for the outer swirl number under counter-swirl conditions.

The principal operating variables of the combustor are the inner and outer swirl numbers, the inner and outer jet flow rates and the fuel flow rate. The axial velocity ratio is

the ratio of the volumetric mean axial velocity of the inner jet to that of the outer jet. The combustor is operated at atmospheric pressure without preheat.

1.3.2 Results from Previous Studies

A series of studies as part of the overall program have been made examining different aspects of combustor operation. Martin[38], who also built the combustor, and Martin, et al.[39] measured stability and blow-off limits for methane in the combustor. Their[38,39] results show that the lean blow-off limits are very close to the lean inflammability limits and are independent of outer swirl. The rich blow-off limits, however, are lower than the rich inflammability limits and show significant variations with outer swirl, the limits being higher for higher outer swirl numbers and higher axial velocity ratios, thus indicating the importance of swirl-generated recirculation zone size and turbulent mixing for the rich limits. Also, flame instability was encountered in rich mixtures and combustion instability is the likely cause for blow-off at the rich limits. Their[38,39] visual observations are the following: co-swirl cases have long cylindrical flames while counter-swirl cases have much shorter bubble-like flames. The flames for lower axial velocity ratios are smaller in size than flames under high axial velocity ratios. They conclude that high rich blow-off limits and best flame stability are achieved under high counter-swirl conditions.

Oven and Oven, et al.[33,40,41] have made NO-NO_x, temperature and species concentration measurements at various axial and radial locations in the combustor for methane firing. Yetter and Yetter and Gouldin[42,43] have made temperature, velocity and composition measurements at the exhaust with methane as fuel. These investigators[33,40,41,42,43] report large concentrations of unburned fuel and CO in the exhaust which they attribute to quenching in the inter-jet shear layer, but NO_x emissions are low. Oven, et al.[33] report large fractions of NO_2/NO_x in the exhaust, especially in counter-swirl cases, which they attribute to quenching in the shear layer and turbulent mixing. Yetter's[42] and Yetter and Gouldin's[43] results show poor combustion efficiencies in general, though efficiency is significantly improved in going from high counter-swirl to high co-swirl and as the axial velocity ratio approaches one. These results are discussed in greater detail and compared with results from the present work in Chapter 3.

Lee[44] made Laser Doppler velocity measurements under cold flow (without combustion) conditions. Results show a recirculation zone for the counter-swirl case, but no such zone is seen in the co-swirl case in cold flow. However, centerline profile measurements[44] under combusting conditions show that a recirculation zone develops for the co-swirl case as well, while little alteration of the recirculation zone due to combustion is seen in the counter-swirl case. Visual observations of the ignition sequence, with

video photography at 20 frames per second, made by Halthore[45] show, in combination with Lee's measurements[44], that in the counter-swirl case the flame is stabilized in front of the recirculation zone whereas in the co-swirl case the flame is first stabilized in the wake of the ignitor electrodes, a recirculation zone is then formed and the flame is stabilized in front of this recirculation zone. Halthore[45] also made blow-off measurements with propane in order to compare with Martin's results for methane[38]. He found that the lean blow-off limits for propane are nearly the same as those for methane and are also independent of the outer swirl. The rich blow-off limits for propane are however slightly higher than those for methane. Beyler[46] and Beyler and Gouldin[47] made emission spectroscopy measurements of the flame for methane firing in order to characterize the flame structure and the mechanism of flame stabilization. The results of his investigation establish that the stabilization of combustion occurs in front of the recirculation zone in a region of low velocity which, in the mean, is largely free of recirculation zone influence through heat and mass transfer. Beyler also found that the structure of the reaction zone in the forward regions of the combustor is the same for both co- and counter-swirl conditions but differences are seen further downstream.

1.4 Present Work

The present work is one of the steps in the overall research program outlined earlier in this section. In the first phase of the present study the combustor is operated with prevaporized propane. Temperature, velocity and composition measurements including NO-NO_x are made for varying swirl conditions along the radius of the combustor at the exhaust plane, six combustor diameters ($6D_o$) downstream of the combustor inlet. Temperature measurements are made with an uncoated Pt/Pt-10%Rh thermocouple. A two-holed pressure probe is used for velocity measurements. Composition measurements other than those of oxides of nitrogen are made with a gas chromatograph. NO and NO_x are measured with a chemiluminescent analyzer used in conjunction with a NO_2 to NO converter. A cylindrical water-cooled probe is used to draw gas samples for composition measurements. From these data chemical and thermal efficiencies are calculated for various operating conditions.

Propane is chosen as the fuel for two reasons. First, propane is more representative of the commercially used fuels than methane, the previously studied fuel. Second, the results for propane can be compared with the previous results for methane (see Section 1.3.2) to investigate the effect of possible differences in the chemical processes on the combustion of the two fuels in the combustor thereby getting a better insight into the operating characteristics of the

combustor. In the second phase of the study cold flow measurements (without combustion) are made for propane in order to determine the distrubution of the fuel in the exhaust plane as well as at the inlet to the combustor. Cold flow measurements are made for methane fuel also. In addition, the measurements made in the first phase of the present study are repeated using methane fuel. These results are compared with previous results for methane (Section 1.3.2) as well as the results for propane obtained in the first phase of the present study.

Chapter 2 of this thesis contains the details of the experimental set-up and the measurement techniques. Results are presented and discussed in Chapter 3. Chapter 3 also contains details of the calculation of combustor efficiencies. The conclusions from the present study are noted, and suggestions for future studies are made in Chapter 4.

CHAPTER 2

EXPERIMENTAL

2.1 Test Facility

A schematic layout of the test facility is shown in Figure 2-1. Ambient air is supplied to the combustor by a single blower, a belt driven Buffalo Forge centrifugal fan, model 7E, run by a 25 HP General Electric motor. Air supplied by the blower is divided into two streams the inner and outer flows for the combustor. Downstream of the blower each stream passes through a metering station, a settling chamber and a variable swirl generator. Butterfly valves in each line permits adjustment of the inner and outer flow rates which are measured with annubar elements (Ellison Instrument Division, model 710, Dietrich Standard Co.). Temperature measurements by copper-constantan thermocouples and pressure measurements from wall pressure taps are recorded at each metering station allowing for density corrections of the measured flow rates. Area integrated mass flow rates, obtained under nonreacting conditions without swirl, from the combustor exit velocity and temperature profiles were used to determine the calibration constant for each annubar. The accuracy of the calibration is estimated to be $\pm 2\%$ of the instantaneous flow rate. These calibrations were originally made by Martin[38] and were repeated by subsequent researchers who have worked on the test rig. The calibrations were not repeated in the course of the present work. Flow

straightening sections are placed upstream of the metering station to eliminate radial and tangential velocity components and to obtain fully developed flow profiles.

Both inner and outer flows pass through separate settling chambers and variable swirl generators (Figure 2-2). Air leaves the variable swirl generators and enters the combustor through two confined co-axial jets . The inner jet, 4.76 cm in diameter, is premixed with fuel and the outer annular jet, 10.16 cm in diameter, is air only. The combustor test section is 58.3 cm long, 10.16 cm in I.D., and made of quartz tubing. The inner diameter of the test section is the 'combustor diameter' (D_o). Variable swirl in the inner flow is obtained by injecting air both tangentially and axially into a mixing section approximately five combustor diameters upstream of the combustor inlet. Swirl in the outer jet is regulated by variable angle vanes with both co- and counter-swirl conditions possible. A long reach spark-plug is inserted near the centerline close to the inlet for the purpose of ignition. The exhaust gases exit through a 10.16 cm I.D. stainless steel tube section and out through a chimney. Measurements of gas composition, velocity and temperature in the exhaust were made at a station six combustor diameters downstream of the combustor inlet, by means of probes inserted radially and supported by the stainless steel exhaust tube.

The fuel, either commercial grade propane or methane, is

injected radially from the inner jet centerline $5D_o$ upstream of the combustor inlet through eight orifices symmetrically positioned around the circumference of a 0.45 cm O.D. stainless tube. Fuel metering is accomplished by a Brooks (Type 1110-08H2G1A) rotameter calibrated for propane at 4.8×10^5 N/m^2 (69.7 psia) and 21°C. For other metering conditions density corrections are made using the temperature obtained with a Cmega Engineering (Model 199) iron-constantan thermocouple and pressure obtained with a bourdon-tube (Maxisafe A.I.S.I 316) pressure gauge. Two propane cylinders partially filled with liquid propane supply the fuel. The two cylinders are placed in a water bath, whose temperature can be controlled by a flow of suitable amounts of hot and cold water from the building water lines. The water bath supplies the heat for vaporization of the fuel. (See Reference 42 for methane metering.)

The combustor, which is operated at atmospheric pressure without preheat, has a maximum overall inlet velocity of 45 m/s. A more detailed account of the combustor design, construction and instrumentation has been given by Martin[38]. Equations for determining the combustor operating conditions are listed in Appendix A.

2.2 Composition Measurements

Exhaust gases are sampled from radial locations in the exhaust plane ($6D_o$ downstream of the inlet) and analyzed for nitric oxide (NO), total oxides of nitrogen (NO_x), carbon

dioxide (CO_2), carbon monoxide (CO), unburnt propane (C_3H_8), lower hydrocarbons (e.g., ethane (C_2H_6), ethylene (C_2H_4) and methane (CH_4)), oxygen (O_2) and nitrogen (N_2).

2.2.1 Sampling Probe

A water-cooled cylindrical probe spanning the diameter of the combustor is used to sample the exhaust gases in this experiment. A transverse cylindrical probe is felt to have certain advantages over the conventional L-shaped probe. For a cylindrical probe, in flows with very low radial velocities, sample hole alignment to the flow is accomplished by simply rotating the probe to balance pressures at two taps located at equal angular displacements on either side of the sampling hole on the surface of the cylinder. Also the distrubance to the flow is more symmetric with a cylinder spanning the diameter than an L-shaped probe inserted into the flow. Finally, the cooling passage design is simplified, resulting in a smaller overall probe diameter since cooling water flows in one direction only.

Oven[40] considered various materials and designs for the probe and found that the probe shown in Figure 2-3 was best suited for sampling in the exhaust plane. Considerations in the choice were coolness of the probe to prevent catalytic reactions in the hot center piece (i.e. the thermal conductivity of the center piece material) and minimum probe interference to the flow.

The same probe shown in Figure 2-3 is used in the present work. Two pressure taps, a sampling hole and a cooling water hole are drilled into a solid cylindrical brass piece of 7.9 mm diameter. Looking at the cylindrical cross-section, one sees that the pressure taps are located 59° on either side of the sampling hole. Pieces of stainless steel tubing, silver-brazed to this center piece, form the pressure and sample lines. Stainless steel tubing of 7.9 mm outer diameter forms the outer jacket of the probe, providing a cooling water flow passage as well as structural support. The sample line of the probe is connected to the sample train which draws the sample for analysis. The pressure lines are connected to either ends of a micromanometer enabling pressure measurements for velocity calculations as well for alignment of the probe to the flow direction.

The need for rapidly quenching chemical reactions in the gas sample when once inside the probe, to preserve sample composition, is widely recognized[30,42,48,49]. Hence the probe is cooled by a water flow through it. Cooling water is supplied to the probe at room temperature.

Gouldin[50] has shown that low velocity sampling or isokinetic sampling are not satisfactory techniques for sampling in regions of large density and velocity fluctuations such as, for example, turbulent reaction zones, since the effect of the above turbulent fluctuations is to cause the probe to draw a sample which is not truly representative of the mean

composition in the flow. He suggests either choking the flow at the sampling hole or sampling with a large pressure drop across the sampling orifice. In the present work a bellows pump provides a large pressure drop for sampling but the flow is not choked in general. Moreover, the sampling is done in the exhaust plane where density fluctuations are much lower than in the reaction zone.

Alignment tests were performed by Oven[40] to determine the effect of probe (sample hole) misalignment with the flow direction on the composition measurements. His results showed that probe misalignment upto 60 degrees had little effect on the composition measurements in the present combustor. In the present experiment, however, the probe is aligned with the direction of the flow (see Section 2.3 for the method used to determine the flow direction).

The probe is supported horizantally across the diameter of the combustor by two brass sleeves, fitted diametrically opposite each other, to the walls of the combustor. A scale attached on the outside, to the combustor wall, and a dial protractor attached to the cylindrical probe serve to position the sample hole and pressure taps at desired radial locations and to determine the angle of rotation (about its own axis) of the probe.

2.2.2 Sample Train

Figure 2-4 shows the sample transfer system. As with the

probe it is necessary to prevent any reactions in the sample transfer lines in order to preserve sample composition. The same material and temperature considerations pertinent to the probe apply to the sample lines. All lines are 6.4 mm O.D. stainless or polyethylene tubes with stainless steel and brass fittings.

The main sample line is connected to the probe sample line and thus draws the sample into the transfer system. The main line is then divided into branches --(a) the NO_x analyzer line and (b) the syringe sampling line. In line (a) a stainless steel diaphragm pump (Metal Bellows MB-41) draws off 0.15 l/min. of sample and pressurizes it to atmospheric pressure to pass through the NO_x converter. From the converter the sample is bled across a needle valve to the chemiluminescence reaction chamber which is maintained at 5 torr by a vacuum pump. The main line and the sample lines upto the reaction chamber are resistance heated to 50°C by nichrome wire, to prevent removal of NO_2 by water condensation in the lines. It is expected that potential reactions in the sample lines are avoided since stainless steel tubes are nonreactive with respect to oxides of nitrogen at temperatures less than 100°C [51]. The lines are electrically insulated with asbestos material, wrapped with nichrome wire, and wrapped with an additional layer of asbestos insulation.

Sample gas is drawn into the syringe sampling line (b) by another metal bellows pump (MB-41). Since water gives long

tailing peaks on most chromatographic columns, the sample line (b) passes through two ice baths to condense out the water. Initially a mixture of dry ice and acetone was used in the second bath, but it was found that an ordinary ice bath was able to condense out all the water in this experiment. The syringe sampling port is a septum fitted kajon fitting in the sampling line.

2.2.3 NO, NO_x Measurements

NO and NO_x are measured with a chemiluminescent analyzer constructed at Cornell University in conjunction with a Thermo Electron (N-CV-1526-36) NO_x converter (Figure 2-4). The NO_x converter, a stainless steel tube heated to 1023°K, converts NO_2 to NO. The chemiluminescent analyzer is sensitive to NO only. In combination with the converter the total NO_x can be measured; when the converter is bypassed, NO alone is detected. The difference between the above two measurements gives the amount of NO_2 in the sample. A brief but comprehensive description of the principle and operation of the chemiluminiscent analyzer can be found in Reference 52.

In the present study the reaction chamber is maintained at 5 torr by means of a vacuum pump, with approximately 0.15 l/min sample flow and 0.03 l/min ozone/oxygen flow. The ozone flow is obtained by passing oxygen through a 15 KV alternating electric field in an ozonator constructed at Cornell. Though a measurement of the amount of ozone produced was not made in this study, it is expected that a mixture of

about 2.5 percent ozone in oxygen leaves the ozonator according to tests conducted by Homan[53]. The oxygen pressure in the ozonator is about 1.13×10^5 N/m^2 (16.4 psia). The output current from an uncooled EMI photomultiplier tube operated at 900 volts is converted into a voltage drop across a 5.6 Megohm resistance and read out on a Dana digital voltmeter. The NO_x converter is operated at atmospheric pressure. It was observed that the output signal from the photomultiplier tube is very sensitive to the pressures in the ozonator and reaction chamber and the sample and oxygen flow rates. Hence care is taken to keep these readings steady and constant throughout a test run.

As mentioned earlier, all lines in the chemiluminescence system and the sample transfer lines are maintained at 50°C (323°K) by heating to prevent removal of NO_2 by water condensation in the lines. Significant reduction in measured NO_2 has been observed when water vapor is allowed to condense in the lines[53,54]. Tuttle, et al.[55] have reported that particulate matter, especially soot, trapped in sample filters affect NO_2 measurements since NO_2 is absorbed or reduced by the carbon and hence larger analysis times are required before accurate NO_2 readings are obtained. In the present case, however, no particulates are evident in the exhaust because of premixing and the nature of fuel used. Even so, about two minutes are provided for each measurement to allow the detector to reach its full response and to account for any effects of particulates which could have been trapped in

the system during use of the analyzer in other experiments.

It is now well known that the presence of CO, CO_2, hydrocarbons and H_2 cause interference in NO_x measurements by reduction reactions in which NO_2 and NO are reduced to N_2 and perhaps NH_3[55,56,57]. Interference depends on converter history and conditioning, oxygen level in the sample or overall equivalence ratio and converter temperature. Studies[55,56,57] indicate that interference is serious only when the levels of the above mentioned interfering compounds are high, the fuel-air mixture is rich or when the converter is not conditioned. The results of Sigsby, et al.[56] and Breithenbach and Shelef[58] which are also listed in Reference 55 suggest that as long as the sum of CO and HC concentrations in the sample is less than the oxygen level and the converter is conditioned at close to operating temperature by flowing air through it for about two hours, accurate NO_x measurements can be obtained with the converter operating at 1023°K. Sigsby, et al.[56] suggest that preconditioning will oxidize the metallic surface of the converter and prevent the exposure of any reducing agents on the surface to the sample stream. In the present experiment H_2 is not present in the exhaust gas, combined levels of CO and HC are far less than oxygen levels in the sample and the sample gas is oxidizing (oxygen rich) in character. Hence all the above conditions for reliable and accurate NO_x measurements are satisfied. The converter is conditioned at 1023°K with air flow for at least one hour prior to every test run and operated at 1023°K. In

addition the entire system including the converter is purged with air between every data point. In this way oxidation of the metal surface of the converter is ensured.

Some attenuation in the detector output is caused by collisional deactivation of NO_2^* by O_2, N_2, CO_2 and H_2O. Deactivation by N_2 is accounted for in the detector calibration. To correct for the remaining species, a quenching efficiency is calculated for each species based on its respective cross-section for collisional deactivation of NO_2^* and its concentration in the sample. Based on the method described in Reference 59, calculations by Oven[40] show that the combined effects of O_2, CO_2, and H_2O attenuate the detector output by less than 3%. It is expected that the results of the calculations will be no different for the present experiment due to the similarity in the sample gas composition with Oven's experiment. Moreover, the sample is predominantly N_2 whose effects of collisional deactivation are accounted for in the calibration. Since the effects of collisional deactivation of NO_2^* due to other species is expected to be minimal based on Oven's calculations, no corrections are made to the $NO-NO_x$ data presented in this thesis.

The analyzer is calibrated before and after every run. The linearity of the instrument is well accepted. Hence a straight line calibration curve is drawn between the voltage corresponding to the photomultiplier dark current and that corresponding to 423 ppm of NO in N_2 calibration gas. The

analyzer can indicate the concentration to within 0.5 ppm based on the noise in the voltage signal.

2.2.4 Analysis by Gas Chromatography

The objective of the analysis is to obtain the relative amounts, in a dry mixture of combustion products of propane, of oxygen, nitrogen, carbon monoxide, carbon dioxide, unburnt propane and other possible hydrocarbons like ethane,ethylene and methane, in a simple way preferably with a single injection of sample and a short analysis time. Samples are transferred from the sample line to the chromatograph by syringe.

Sample Transfer Via Syringes

The sampling port in the sample transfer line is equipped with a septum allowing insertion of a syringe needle for sample extraction. Hamilton 1005 5 ml gas tight syringes are used to remove and store samples before injecting them into the gas chromatograph for analysis. Syringes are flushed while inside the sampling line by repeatedly drawing and ejecting the gas sample, before finally drawing the sample for analysis. The septum in the sampling port maintains air-tightness while flushing the syringe and collecting the sample. About 2.5 ml of gas sample is slowly drawn into the syringe over a period of about 10 seconds. The pressure in the sample line at the sampling port is just above atmospheric. Hence when the syringe is taken out of the sampling port, outside air cannot enter the syringe due to the

slightly higher pressure inside the syringe. The syringe is then immediately inserted into a specially made stand such that the needle tip pierces a septum, at the bottom of the stand which blocks the needle hole and prevents air diffusion into the syringe.

A maximum of 9 samples are taken during any one test run. All syringe samples are analyzed within 2.5 hours of sampling to minimize errors due to leakage. Samples stored for longer periods of time showed, upon analysis, significant air leakage into the syringe. Oppegaard[60] has identified the various problems facing a syringe injection with septum and suggested ways to overcome them. The procedures followed in the present analysis concur with most of his suggestions, except that the new injector design suggested by him is not used.

Selection of Column and Technique

The problems facing a simplified analysis involving a single injection are the following. Firstly, there is no single column material which allows complete separation of all the aforementioned gases in the sample, without requiring a long time for analysis (50 minutes or more). Secondly, a few column materials irreversibly adsorb some gases. For example, molecular sieve, which is the most efficient column to obtain nitrogen/oxygen split, irreversibly adsorbs carbon dioxide. Porous polymers and silica gel which allow separation of carbon dioxide are incapable of separating oxygen from nitrogen and of separating carbon monoxide from the com-

posite air peak at room temperature or above.

To overcome the problem of separating carbon dioxide and carbon monoxide as well as oxygen and nitrogen, Alltech Associates provides a concentric column (CTR column)[61] which is a column within a column and thus permits the use of two different packings in parallel. Carbon dioxide is separated by the inner poropak column while oxygen,nitrogen and carbon monoxide are seperated (in that order) by the outer molecular sieve column. The separation of any mathane in the sample is also accomplished by the molecular sieve column with the methane peak occuring between the nitrogen and carbon monoxide peaks. The entire analysis is isothermal, takes about 6 minutes and is accomplished with a single sample injection. The CTR column, however, is unsuitable for the samples of interest in the present analysis. Firstly, ethylene and ethane eluted from the inner poropak column overlap the oxygen and nitrogen eluted from the molecular sieve column. Secondly, though propane can be eluted from the poropak within 10 minutes by temperature programming, it takes nearly 80 minutes to elute from molecular sieve. Thus a subsequent injection of sample is delayed for 80 minutes.

The possibility of two separate injections on two different columns, one a molecular sieve and the other a poropak, was also investigated. In this scheme the molecular sieve would separate O_2, N_2, CO and CH_4, while the second injection into poropak enables the separation of CH_4, CO_2, C_2H_4, C_2H_6

and C_3H_8. This scheme also poses problems. The propane injected into the molecular sieve column is retained for a long time during which a second injection is not possible. In addition, to obtain concentrations on a relative percent basis with schemes involving two separate injections, either exactly equal amounts of sample should be injected with each of the injections or there should be at least one common peak in the two chromatograms whose relative areas can then be used to relate the areas of the other peaks in the chromatograms. In the above scheme, the only common peak is that of methane which may or may not be present in the actual samples obtained from the combustor. Even if present, it may be in very small amounts, whereas it is desirable that the common peak be a major component in the sample. Also, injecting precisely the same amount in both the injections using syringes is difficult.

Kaiser[62,63] synthesized a new material called the carbon molecular sieve, for use in gas chromatography. The use of carbon molecular sieve for analyses of various gas samples have been demonstrated by Zlatkis, et al.[64], Bollman and Mortimore[65] and others. Unfortunately, none of the analyses produced the oxygen/nitrogen split and at the same time gave elution of propane in a short time. Bollman and Mortimore[65] used carbon molecular sieve marketed by Supelco Inc. (Bellefonte,PA) under the name of carbosieve B[66]. Supelco introduced a new type of carbosieve called carbosieve S[67,68] in 1976. Carbosieve S is spherical in shape

and has increased surface area. It is best suited for the separation of permanent and sulphur gases. Carbosieve S gives separations similar to carbosieve B and hence Carbosieve S alone cannot solve all the problems posed in the present analysis. Using a carbosieve S column and temperature programming upto 230°C (503°K) it is possible to obtain complete separation of all the gases in the sample of interest. But in order to get a good oxygen/nitrogen split the column must be long and the initial temperature must be close to room temperature. These conditions increase the time of elution of propane to approximately 40 minutes resulting in a total cycle time (including cooling of the oven) of 45 to 50 minutes.

It is crucial to keep the analysis time per sample, short. The combustor is allowed to run for a while to reach a steady state of operation. The samples from about 9 radial locations are then collected and stored in syringes, over a period of 45 minutes to 1 hour. It is desirable not to run the combustor for longer periods of time in order to conserve fuel. If each sample analysis were to take 50 minutes the total time for analysis of all the samples collected in a single run would be 7 to 9 hours. Substantial leakage of ambient air into the syringes during this period of time would cause unacceptale contamination of the last few samples. Though it is possible to store samples in evacuated bottles or sampling bulbs, which makes the sampling system more complicated, it is nevertheless desirable to have a

short analysis time.

To overcome all these difficulties a scheme using two columns in series, with a 4-port switching valve is used. After a careful study of the properties of various columns, it was found that columns of poropak Q and carbosieve S would be most suitable for the purpose.

Figure 2-5 shows a schematic of the column arrangement and the flow path. The 4-port valve switches between the two flow arrangements, 'A' and 'B'. In position 'A' the two columns are in series and the elutants from the poropak Q go through the carbosieve S column. In position 'B' the carbosieve column is bypassed and the elutants from poropak go directly to the detector.

The gas chromatograph conditions are as follows.

Column 1	: Poropak Q, 1/8"x6 ft., SS
Column 2	: Carbosieve S, 1/8"x8 ft., 100/120 mesh, SS
Oven temperature	: 50°C for 4 minutes and programmed at 25°C/min. to 175°C
Carrier gas	: Helium
Flow rate	: 47 ml/min.
Detector	: Thermal Conductivity, 270°C, 160 MA, 0.5 mV range
Sample size	: 0.5 ml.

Figure 2-6 shows a chromatogram obtained under the above conditions for a sample withdrawn from the combustor. The

time axis between the peaks in the chromatogram is compressed to accomodate all the peaks.

The sample is injected with the 4-port valve in position 'A'. A composite peak of air, carbon monoxide, methane (if present) and carbon dioxide elutes within 0.8 min. from the poropak and passes on into the carbosieve column. The valve is switched to position 'B' at the end of 2 minutes. Ethylene and ethane, which elute in that order at 2.5 minutes from poropak, pass directly to the detector. (Ethylene and ethane are not present in the sample and hence are not seen in Figure 2-6).

The valve is switched back to position 'A' immediately after the elution of ethane (i.e. after approximately 3 minutes). Oxygen elutes from the carbosieve column at about 3.5 minutes (the exact time depends on how long the valve is kept in position 'B'), followed by nitrogen and carbon monoxide. The valve is again switched at the end of 6 minutes to position 'B'. Propane eluting from the poropak passes directly to the detector and can be detected at about 6.8 minutes. The valve is then switched back to position 'A'. Methane elutes from the carbosieve at 9.5 minutes followed by carbon dioxide at 11.2 minutes. The column oven temperature is then reset to the initial temperature, 50°C. In this way the entire sample analysis including propane, ethane and ethylene can be done within 12 minutes. In addition, the columns are ready for the next sample as soon as they reset

to the initial temperature. Hence the total cycle time is only 15 to 16 minutes.

Data Reduction and Error Estimation

The gas chromatograph used for the composition analysis is a Varian Model 3700. The detector output is recorded on a Varian Model 9176-02 strip chart recorder which has a built-in triangular trace electronic integrator. The number of transverse line crossings of the integrator trace is proportional to the area of the peak. The operating conditions and the columns used are described in the previous subsection on technique. Area data of the peaks are reduced by a relative percent method to obtain concentrations as mole fractions. In order to do this, nitrogen, being the major species in the sample, is chosen as reference and a response factor is obtained for each of the other species by calibration using calibration gases. Calibration gases used are mixtures of the gas species of interest, whose concentrations are known to within ±2% accuracy. The calibration gases were obtained from Alltech Associates and their compositions are listed in Table 2.1. Response factors (b_i) are defined as

$$b_i = \frac{\text{Response(peak area) per unit concentration of } N_2}{\text{Response per unit concentration of species i}} \qquad (2.1)$$

which gives,

$$b_i = \frac{A_{N2}\, a_{N2} / X_{cN2}}{A_i\, a_i / X_{ci}} \qquad (2.2)$$

where:

A = the area of the peak

a = detector attenuation(set on the gas chromatograph)

X_c = mole fraction of the species in the calibration gas sample.

It can be seen from the above expression that response factors can be determined for each species in a calibration chromatogram indepedent of the the other species. The response factor for nitrogen is 1 by definition. With these response factors the mole fractions(X_i) of the various species in a sample gas can be determined by,

$$X_i = \frac{A_i \; a_i \; b_i}{\sum_j A_j \; a_j \; b_j} \qquad (2.3)$$

In this method the area of each species is converted into an quivalent area of a nitrogen peak of the same concentration as that of the species. The numerator in Equation 2.3 represents an equivalent nitrogen peak area for species i. The denominator is the sum of all such areas for each species including nitrogen. Hence the resulting concentration will be in mole fraction units.

The advantage of the relative percent method is that it is independent of the sample volume injected. A disadvantage is that an error in measuring the area of one component peak will propogate through out the numbers for the other components as well. Also, since the total of the concentrations

must always add up to 100 percent, unmeasured species can introduce error if their concentrations are significant. Results presented in this study should be free of errors of this type since all the species present in any significant amount are measured.

A number of calibration injections are done for each of the calibration gas mixtures and response factors are calculated for every calibration injection. These data were statistically analyzed to obtain standard deviations for the response factors. The mean of the response factors for each of the species is used in calculations using Equation 2.3. Error analysis of Equation 2.3 shows that contributions to the error in X_i come mainly from the error in the response factor for the species i and the uncertainity, arising from the detector noise and the least count of the integrator markings on the chart paper, in determining the area of the peak for the species i. Neglecting the higher order contributions from cross terms from other species in the sample, the fractional error in X_i is given by

$$(\sigma_{Xi}/X_i) = \sqrt{(\sigma_{bi}/b_i)^2 + (\sigma_{Ai}/A_i)^2} \qquad (2.4)$$

where (σ_{bi}/b_i) and (σ_{Ai}/A_i) are fractional errors in b_i and A_i respectively. It is seen from Equation 2.4 that the actual error in X_i depends on the actual area of the species. Representative concentrations of each of the species were chosen to calculate typical values for errors in X_i. Table 2.2 lists the values of the response factors and estimated

errors in calculated species concentrations. Obviously, the errors will be slightly smaller for species concentrations larger than those listed in the table and slightly larger for lower species concentrations. It should be noted that the estimated errors do not take into account the possible air leakage into the syringes and the sampling lines which could be a serious problem if proper care is not taken to prevent leaks. Response factors for ethane and ethylene are not listed in Table 2.2 since those species are not encountered in the exhaust gases.

Based on the noise levels, the lowest attenuation and the detector response to the various species, the minimum detectable amounts were calculated to be 40 ppm for CO_2 and aproximately 70 ppm for the other species.

Injection technique and consistency in injection are found to be critical for good results. Very fast or very slow injection results in improper peak shapes and erronous data.

2.3 Velocity Measurements

The pressure taps in the sampling probe are used for velocity measurements also. The taps, 0.8 mm in diameter, are located 118 degrees apart in the same axial plane. They are located symmetrically about the sampling hole which is at an axial distance of 8 mm from the plane of the pressure taps. The pressure lines from the probe are connected to the two sides of a micromanometer.

The reference for determining the flow direction (θ) is taken to be the plane containing the flow direction on the centerline so that $\theta=0$ on the centerline. The axisymmetry of the θ values measured from this reference (see Section 3.2) supports the choice of this reference. The direction (θ) of the mean total velocity (neglecting radial components) with respect to the reference plane is located by rotating the probe about its axis, with the two pressure taps facing upstream towards the flow. When the pressures in the two taps are equal, as indicated by a null balance on the micromanometer, the local flow direction is aligned with the bisector of the angle between the pressure taps. The angle made by the bisector with the reference plane gives ,which is read from the circular dial protractor attached to the probe (see Figure 2-7). One of the pressure lines is then disconnected from the micromanometer and the pressure at the other pressure tap, P_{59}, which corresponds to the pressure on the surface of the probe at a 59^{o} angle from the flow direction, is read. The probe is then rotated by 59^{o} (see Figure 2-7) to align the pressure tap to the local mean flow and the total pressure P_T is measured. The difference between the two readings gives (P_T-P_{59}). Readings are taken along the radius of the combustor at 5 mm inter'als.

Velocity measurements in turbulent swirling flows using a transverse cylindrial probe is affected by stream turbulence and swirl in the following manner. Turbulence in the flow affects the pressure distribution around the surface of the

probe in two ways. Firstly, increased turbulence in the flow accelerates the transition from a laminar to a turbulent boundary layer[69] and secondly, the separation point for the turbulent boundary layer is further downstream on the probe surface than for the laminar boundary layer[69]. Hence the calibration of the probe done in a laminar flow may not be valid in a turbulent flow.

Bilger[48] points out the possibility of secondary flow along the probe towards the vortex core due to the positive mean pressure gradient in the radial direction in swirling flows. The effect of the secondary flow is such that the velocity measured by the probe at a given radial location actually corresponds, in the undisturbed flow, to a farther radial location approximately 0.09 of the probe diameter from the measurement point[70]. Density gradients in reacting flows may affect the velocity measurements in a way similar to swirl by means of pressure gradients in the flow.

The diameter of the probe used in this study is small compared to the diameter of the combustor. Hence swirl and density gradients are not likely to cause appreciable distortions to the flow when the probe is introduced.

The probe was first calibrated in laminar flow using a calibration jet of 2 inch diameter, to obtain a relationship between (P_T-P_{59}) and (P_T-P_S) where P_S is the static pressure. Whether a correction is required and the magnitude of such a correction for the turbulent swirling flow in the combustor

were determined subsequently. The calibration jet was non-swirling and unconfined and hence the static pressure was atmospheric. Readings of pressures P_T and P_{59} were taken for various velocities of the jet and the relationship between (P_T-P_{59}) and (P_T-P_S) was found to be

$$(P_T-P_S)_1 = 0.76075\ (P_T-P_{59}) + 0.0042 \qquad (2.5)$$

in the velocity range of interest, where $(P_T-P_S)_1$ and (P_T-P_{59}) are in inches of water. The subscript 1 denotes that the calibration was done in a low turbulent intensity (laminar) jet.

Using the values of P_T-P_{59} obtained from the probe readings and Equation 2.5, the values of $(P_T-P_S)_1$, which are the dynamic pressures, are calculated. The mean total velocity at each radial location is calculated from the dynamic pressure as follows

$$V_1 = \sqrt{(2\rho_m g h R_a T/P_S)} \qquad (2.6)$$

where

ρ = density of the manometer fluid (water)=1 gm/cc

g = acceleration due to gravity = 9.81 m/s

h = dynamic head = $(P_T-P_S)_1 \times 0.0254$ meters

R_a = Gas Constant for air = 2154.69 (mm-Hg)cm^3 /gm^oK

T = local gas temperature in ^oK

P_S =local pressure, assumed atmospheric.(see Section 3.3.2).

Substitution of the above values gives

$$V_1 = \sqrt{(1073.9(P_T-P_S)_1 T/P_{atm})} \qquad (2.7)$$

where $(P_T-P_S)_1$ is in inches of water and P_{atm} is in mm of Hg.

Since the turbulent intensities in the combustor are high (about 10% of the mean flow velocity) there is a need to check the validity of the probe calibration (Equation 2.5) in the combustor. Laser Doppler Velocity (L.D.V.), described in Reference 71, was used to measure velocities in the combustor (without the probe in place) and compared with the velocities measured by the probe using the calibration in Equation 2.5. It was found that the velocities measured by L.D.V. were about 20% lower than those obtained by the laminar calibration of the probe. Hence the velocity obtained by Equations 2.5 and 2.7 has to be multiplied by a correction factor, f_c, in order to get the correct velocity, V. It was found that f_c was a function of V_1 alone. The f_c values obtained with varied outer swirl and at various radial locations under both hot and cold flow conditions are plotted gainst V_1 in Figure 2-8. It is found that f_c changes very slightly with V_1 and is in the range the range of 0.73 to 0.88 for all operating conditions in this study. Since the f_c values were not found to depend on the swirl condition or the temperature gradients in the flow, it can be concluded the presence of swirl and density gradients in the flow does not affect the measurement of velocity using the cylindrical probe. The correction factor f_c corrects for any probe blockage effects also since L.D.V. measurements are made without the probe in place and then compared with the probe measurements to obtain f_c.

The corrected mean total velocity (V), and the horizontal (u) and vertical (v) components of the mean velocity are calculated from

$$V = V_1 x f_c \quad , \quad u = V \cos\theta \quad \text{and} \quad v = V \sin\theta \ . \qquad (2.8)$$

Obviously, calculations of velocities require local temperature information (Equation 2.7). Measurement of temperature is described in the next section.

Figure 2-9 shows the pressure distribution on the surface of the cylindrical probe as measured by the two pressure taps for a typical flow condition in the combustor. θ is the angle subtended by the bisector between the two pressure taps with the flow direction. The Figure shows a symmetric pressure distribution around the probe. The peaks at +59 and -59 degrees correspond to the total pressure measured by the two pressure taps. Each of the two pressure taps measures the same pressure when the bisector is aligned with the flow direction (i.e. at θ=0 in the figure) indicating that the probe can measure the flow direction accurately. Measurements of flow direction with L.D.V and with the cylindrical probe agree to within half a degree.

Detailed additional measurements in cold flow comparing cylindrical probe velocity measurements with L.D.V. and measurements with a 5-hole pitot probe previously tested in cold swirling flows[72,73] show that while perturbations to the flow due to either of the probes are negligible in counter-swirl, in co-swirl, under cold flow conditions, both probes

alter the flow drastically. The velocity profiles measured by the two probes and L.D.V (with the probe in place) resemble those in front of a recirculation zone with strong deceleration on the centerline. The reason for the drastic flow alteration is the following. For the co-swirl case in cold flow there is no recirculation zone formed near the inlet and flow is on the verge of vortex breakdown. Therefore, introduction of any probe in the flow can cause a drastic flow alteration resulting in the formation of a recirculation zone.

2.4 Temperature Measurements

An uncoated fine wire Pt/Pt-10%Rh thermocouple probe is used to measure temperatures at radial locations in the exhaust plane (Figure 2-10). The thermocouple bead was formed by butt welding 0.127 mm diameter Platinum and Platinum- 10% Rhodium wires. The thermocouple lead arms are made of 0.254 mm diameter wires for rigidity and support. Mean thermocouple e.m.f is obtaind by putting the thermocouple output through a TSI averaging circuit. A time constant of 10 seconds is used and each measurement is averaged for approximately 1 minute. Averaging is required due to large temperature fluctuations (of the order of $100^{o}K$), especially in the hot central core of the combustor exhaust.

The possibility of catalytic reactions on the thermocouple junction was investigated by comparing an SiO_2 coated thermocouple and an uncoated thermocouple. A difference of about

5^{o} was found around $1300^{o}K$. At higher temperatures and higher velocities in the core it was found that the coating could not last long enough to obtain any meaningful data. However, since the observed difference is small, an uncoated thermocouple is used throughout the experiment.

The measured temperatures can be corrected for thermocouple radiation losses to the surroundings, by equating the heat transferred from the gas to the probe to that lost by the probe due to radiation. The correction is[24]

$$T_g - T_c = \epsilon \sigma d (T_c^4 - T_w^4)/2k \qquad (2.9)$$

where ϵ is the emissivity of the wire material, σ the Stephen-Boltzmann Constant (5.64×10^{-5} erg cm^{-2} ^{o}K sec^{-1}), d the diameter of the bead and k the thermal conductivity of the gas. The temperature subscripts w,c and g refer to the wall, thermocouple and gas, respectively. $\epsilon\sigma (T_c^4 - T_w^4)$ is the heat loss rate by radiation per unit area of the probe. For a small diameter spherical bead such that the Reynolds number is much less than 1, the heat transferred by the gas per unit area of the bead is given by $(2k/d)(T_g - T_c)$.

The emissivity ,ϵ, is a function of temperature. Though values of ϵ for platinum are not available in literature for the entire range of temperature, values listed in References 74 and 75, which are collections of data, suggest a value of about 0.1 at $1000^{o}K$ and about 0.2 at $2000^{o}K$ with almost a linear variation with temperature. The value of k also

depends on the temperature. Since air and nitrogen have approximately the same thermal conductivity as well as the fact that the exhaust gas is mostly nitrogen, the values of thermal conductivity for nitrogen listed in Reference 76 for various temperatures were used. With a maximum value of ϵ=0.2 for the entire calculation and with values of k from Reference 76 the temperature corrections were found to be 89.5°K for T_c=1923°K and 0.6°K for T_c=460°K with T_w=340°K. The corrections are quite small upto about 800°K. Hence the corrections do alter the temperatures but only in the hot central core of the combustor. These corrections did not significantly alter the velocities nor the calculated thermal efficiency. The velocities on the centerline increases by approximately 2%, and the thermal efficiency increases by less than 2%. The reason for this is that the temperature correction affects only a small central region and does not contribute greatly to altering the efficiency. The temperature profiles presented in this work have not been corrected for radiation losses unless otherwise noted.

A method for obtaining corrections for conductions losses has been presented by Frock, et al.[77]. The expression is

$$(T_g-T_c) = (T_g-T_w)/(\text{Cosh } 2a\sqrt{h/d\lambda}) \qquad (2.10)$$

where h is the film coefficient of heat transfer for a wire of diameter d, λ is the thermal conductivity of the wire and a is the depth of immersion from the junction to the probe supporting tube. The thermocouple used in the present study

has a small wire diameter and a long immersion depth of 1.3 cm making the conduction losses negligible.

2.5 Experimental Procedure and Test Conditions

Exhaust composition, velocity and temperature data are taken for varying outer swirl, keeping the equivalence ratio, inner swirl, axial velocity ratio and overall axial velocity at the inlet more or less constant for all the runs. It was intended to study variations due to outer swirl since it was believed, based on previous results[41,42], that the outer swirl was the single most important parameter affecting the operation of the combustor. The actual test conditions are shown in Table 2.3.

The apparatus is allowed to warm up and reach steady state by running the blower for about half an hour before igniting the combustor. After ignition the combustor is allowed to run for about 10 minutes to reach steady state operation. Measurements are then taken along a radius at intervals of 5 mm starting from 1 mm away from the wall. The pressure taps are first moved to the desired radial location, the flow direction determined and the pressure readings taken. The sample hole is then moved to the radial location and aligned to the flow. After allowing about a minute for the sample line to flush completely NO and then NO_x measurements are taken. A sample is collected in a syringe at the sample port for gas chromatographic analysis. The pressure taps in the probe are then moved to the next radial location and the

entire procedure is repeated. In the intervals between taking data, the NO_x converter is flushed with ambient air through a side valve to preserve the oxide coating on the converter walls. After traversing the entire radius the combustor is turned off to remove the sample probe and introduce the thermocouple probe. The combustor is re-ignited and temperature measurements are made at the same radial locations used for velocity measurements. Either probe can be positioned at the desired radial location to better than ±0.5 mm accuracy. Gas chromatographic analysis of the sample is not made at all the radial locations to keep the total analysis time short, but is restricted to 10 mm intervals and in regions of large concentration gradients to 5 mm intervals.

It was seen after a few runs and analyses of data that combustor operation is highly reproducible (to within 3% of each other as seen by temperature and velocity profiles for repeated runs). Hence it was possible to make individual measurements of composition, temperature and velocity from separate combustor runs instead of in the same run. This reduced the duration for which the samples are stored in the syringes.

The axi-symmetry of temperature, velocity and composition in the combustor have been established in previous experiments by Oven[40], Yetter[42] and other authors[44,46]. Hence data in the present study are taken only across half the diameter of the combustor and symmetry is assumed in cal-

culations. Additional data, taken in the present study, to support the assumption of axi-symmetry are presented in Section 3.2.

In the second phase of experiments, data are taken for combustor operation with methane as the fuel. This is done for comparison with the propane runs as well as with results obtained by Yetter[42]. The test conditions for methane are also listed in Table 2.3. In addition, composition measurements are made for cold flow (without combustion) for propane at the exhaust plane to study the fuel distribution. Fuel distribution at the inlet is also studied for propane and methane without combustion. To measure the inlet fuel distribution a simple hypodermic stainless steel tube in the shape of an L, with the hole facing the flow, is used to withdraw samples.

Swirl numbers are obtained by integration of inlet velocity profiles measured under nonreacting conditions using a five-hole pitot probe. These measurements were originally performed by Martin[38] and repeated for calibration checks by Yetter[42] and Halthore[45]. These measurements were not made in the present study.

CHAPTER 3

RESULTS AND DISCUSSION

3.1 Introduction

The results are presented and discussed in two stages; results for propane firing (Phase 1) followed by those for cold flow and methane firing (Phase 2). The presentation of results is preceeded by two other sections. Section 3.2 deals with the axisymmetry of conditions in the combustor and with the reproducibility of results. In Section 3.3 the methods for calculating average exhaust composition values and efficiencies are given.

The results for propane firing (Phase 1) are presented in Section 3.4. In Section 3.5 the propane results are compared with previous results for methane firing[40,42]. The comparison shows some disagreements between the two sets of data. In an attempt to resolve these disagreements Phase 2 experiments were performed as follows. Cold flow measurements were made and the results of these measurements are presented in Section 3.6. However, the results of the cold flow measurements could not explain the differences. Hence experiments were done with methane as the fuel. The methane firing results are presented and discussed in Section 3.7. A mechanism for the operation of the combustor which can explain the previous and the present results is proposed in Section 3.8.

Composition results are presented on a dry basis in Figures (3-11 - 3-18,3-25,3-26) and on a wet basis in the Tables (3.2-3.5,3.7,3.8).

The folowing terminology will be used in the discussion. 'Quenching' refers to the reduction in reaction rates due to cooling (thermal quenching) as well as to the freezing or stopping of the reactions by the decay and removal of active free radicals. Quenching occurs due to the 'dilution' with the cold outer air, of zones where reactions are occuring. 'Combustion zone' refers specifically to the region close to the combustor inlet (upto about $1.5D_o$ axial distance from the combuster inlet) where most of the combustion is taking place. The region downstream of the combustion zone will be referred to as the 'post-combustion zone'. The oxidation of CO to CO_2 and NO to NO_2, which takes several milliseconds and is slower by orders of magnitude compared to the fuel break-up reactions, occurs in the post-combustion zone.(See Section 1.2 in support).

3.2 Axisymmetry and Reproducibility of Results

Axisymmetry and reproducibility of results in the combustor are discussed in Section 2.5. Additional results to demonstrate axisymmetry and reproducibility of combustor operation are presented in this section.

Figure 3-1 shows the temperature profile across the entire diameter of the combustor. A traverse along each half of the

combustor was done from either side of the combustor. The temperature values at the same radial distances on either side of the combustor centerline differ by less than 3% of each other. Table 3.1 shows the axisymmetry of flow direction. (The θ values on opposite sides of the combustor are opposite in sign due to swirl). It can be seen from Table 3.1 that the asymmetries in the θ values are less than 1 degree. These results justify the assumption of axisymmetry at the measurement station. Hence all the results are presented for half the diameter of the combustor.

Measurements in this study were made over a period of approximately one year. Hence reproducibility of results is important to ensure consistency. Figure 3-2 shows the reproducibility of a temperature profile. The two profiles were measured 4 months apart. The local differences in temperatures are less than 3%. Table 3.1 also shows reproducibility of flow direction measurements to within 1^{o}.

3.3 Calculation of Average Values and Efficiencies

3.3.1 Composition on a Wet Basis

At each radial location the amount of water vapor present in the exhaust is determined from a local carbon atom balance with the assumption that all H from the burnt fuel is oxidized to H_2O. For every mole of CO_2 or CO in the exhaust, 4/3 moles of water vapor for propane and 2 moles of water vapor for methane are present. Therefore, the amount of

water vapor in the exhaust for every mole of dry exhaust gas is given by

$$X'_{H2O} = (4/3)(X'_{CO2} + X'_{CO}) \qquad \text{(propane)}, \qquad (3.1a)$$

$$X'_{H2O} = 2 (X'_{CO2} + X'_{CO}) \qquad \text{(methane)}, \qquad (3.1b)$$

where X'_{CO2} and X'_{CO} are local mole fractions of CO_2 and CO on a dry basis. The mole fraction of species i on a wet basis, denoted by X_i, is then given by

$$X_i = \frac{X'_i}{1 + X'_{H2O}} , \qquad (3.2)$$

where i refers to O_2, N_2, C_3H_8, CH_4, CO, CO_2 or H_2O.

3.3.2 Average Values

Average values of temperature and concentrations in the exhaust are obtained on a mass flux weighted basis. Average mass fractions are given by

$$\overline{Y_i} = \frac{\int_0^{R_o} \rho \, u \, Y_i \, 2\pi r \, dr}{\int_0^{R_o} \rho \, u \, 2\pi r \, dr} , \qquad (3.3)$$

where Y_i is the local time mean mass fraction of species i on a wet basis, ρ is the local density, and R_o ($=D_o/2$) is the radius of the combustor. Also $Y_i = X_i M_i / M_s$ where M_i is the molecular weight of the species i and M_s is the local molecular weight of the exhaust gas mixture. $\rho = (PM_s/RT)$ where P

and T are the local static pressure and temperature respectively and R is the universal gas constant. By substitution Equation 3.3 becomes

$$\overline{Y_i} = \overline{X_i}\frac{M_i}{M_s} = \frac{\int_0^{R_o} (PM_s/RT)uX_i(M_i/M_s)2\pi r\, dr}{\int_0^{R_o} (PM_s/RT)u2\pi r\, dr} . \qquad (3.4)$$

The static pressure inside the combustor is very nearly atmospheric and changes only slightly (by less than 5 cm of water column, i.e. 7.4×10^3 N/m^2) across the combustor as seen from the pressure readings for velocity measurements. Further, the major component of the exhaust gas is air and the local molecular weight is approximately equal to that of air. For example, at the location where maximum combustion products are encountered in this entire study, namely the centerline for the high co-swirl propane case (Table 3.2), the difference between the molecular weights of the local gas mixture and that of air is only 1.6%. Hence P and M_s are assumed constant for the integration in Equation 3.4, which then reduces to

$$\overline{Y_i} = \overline{X_i}\frac{M_i}{M_s} = \frac{M_i}{M_s}\frac{\int_0^{R_o} (u/T)\, X_i\, r\, dr}{\int_0^{R_o} (u/T)\, r\, dr} . \qquad (3.5)$$

Hence the average (mass flux weighted) mole fraction in the exhaust is calculated by

$$\overline{X_i} = \frac{\int_0^{R_o} (u/T)\, X_i\, r\, dr}{\int_0^{R_o} (u/T)\, r\, dr} \quad . \tag{3.6}$$

Based on Equation 3.6 the mass flux weighted average exhaust temperature is calculated by

$$\overline{T} = \frac{\int_0^{R_o} (u/T)\, T\, r\, dr}{\int_0^{R_o} (u/T)\, r\, dr} \quad . \tag{3.7}$$

Simpson's rule is used for integration from r=0 to r=5.0 cm, with a step size of 0.5 cm. The velocity at the wall ($r=R_o=5.1$ cm) is assumed to be zero. The trapezoidal rule for integration is used between r=5.0 and r=5.1 cm and the value is added to the integral obtained from the Simpson's rule. An error analysis of the integration shows that Simpson's rule gives the value of the integral to better than 0.5% accuracy. The reason for this accuracy is that the profiles of the integrands are quite smooth and Simpson's rule which uses a second order polynomial fit is sufficient to evaluate the integral accurately.

3.3.3 Efficiencies

Combustion efficiencies are calculated by three methods. In the first method, a chemical efficiency, η_c', is calculated based on the amount of unburnt fuel in the exhaust;

$$\eta_c' = 1 - \frac{\overline{X_f}}{[F]} \quad , \tag{3.8}$$

where $\overline{X_f}$ is the average mole fraction of fuel (propane or methane) in the exhaust calculatd by Equation 3.6 and [F] is the average mole fraction of the fuel entering the combustor, determined from calibrated rotameter settings.

The second method is an improvement on the first one. It relates chemical efficiency, η_c, to CO in the exhaust as well as unburnt fuel since CO not going to CO_2 is lost sensible energy.

$$\eta_c = 1 - \frac{\overline{X_f} + \overline{X_{CO}}(q_{CO}/q_f)}{[F]} \quad , \tag{3.9}$$

where q_{CO} is the heat release per mole of CO going to CO_2 at the inlet temperature, T_{in}, and q_f is the lower heating value per mole of fuel at T_{in}. For ease in the actual calculations the values of q_{CO} and q_f at STP (67.63 and 484.22 (propane) or 189.76 (methane) Kcal/gm mole respectively) are used since the difference between the inlet temperature and the standard temerature is only about 20°K and the values of q_{CO} and q_f at T_{in} are not significantly different from those at STP.

In the third method the exit sensible enthalpy flux is compared with the lower heating value of the fuel to define a thermal efficiency, η_T

$$\eta_T = \frac{\left(\begin{array}{c}\text{measured increase in sensible enthalpy} \\ \text{flux in the working fluid.}\end{array}\right)}{(\text{ lower heating value of the fuel }) \times \dot{m}_f} \qquad (3.10)$$

$$= \dot{H}_e / \dot{m}_f q'_f \ ,$$

where

$$\dot{H}_e = \int_0^{R_o} \rho \ u \ (\sum_i Y_i h_i) \ 2\pi r \ dr \qquad (3.11)$$

and

$$h_i = \int_{T_{in}}^{T} c_{pi} \ dT \ .$$

h_i is the increase in sensible enthalpy per unit mass of the species i in going from temperature T_{in} to the local temperature T, c_{pi} is the specific heat capacity of the species i, $\dot{m}_f$ is the fuel mass flow rate into the combustor and q'_f is the low heating value per unit mass of the fuel at the inlet temperature, T_{in}. The kinetic energy terms $u^2/2$ are small compared to the species enthalpy changes, h_i, and therefore, are neglected. By substituting for Y_i and ρ as shown in Section 3.3.2, Equation 3.11 simplifies to

$$H_e = \int_0^{R_o} (P/RT) u (\sum_i X_i \int_{T_{in}}^{T} C_{pi} \ dT) 2\pi r \ dr \qquad (3.12)$$

where C_{pi} is the molar heat capacity of the species i. The values of C_{pi} as a function of temperature are obtained from

sixth order polynomials fitted by Prothero[78] for various species.

All calculations were performed with a Digital Equipment Corporation PDP-11/34 computer. A listing of the program AVG.FTN is given in Appendix B. The program calculates the amount of water, mole fractions on a wet basis in ppm, the average values and the chemical efficiencies. The programs EFF.FTN and EFFM.FTN which calculate the thermal efficiencies for propane and methane firing respectively are also listed in Appendix B.

3.3.4 Atom Balance

As a check on the composition measurements, an atom balance was attempted. The amount of water in the exhaust at any radial location can be calculated from the dry gas composition at that location by two methods. The amounts of water calculated by the two methods are compared to check the accuracy of the composition measurements. The first method of calculation invokes a carbon atom balance. Based on this method the number of moles of water present per mole of dry exhaust gas is given by Equations 3.1a and 3.1b.

The second method is based on an oxygen atom balance and the relative percentage of oxygen and nitrogen in air. For this method

$$X'_{H2O} = 2[(X_{N2}/3.77) - (X_{O2}+X_{CO2}+X_{CO}/2)] \qquad (3.13)$$

for both propane and methane. Since Equation 3.13 involves a difference between two large and nearly equal numbers, small errors in composition measurements result in large variations in the amounts of water calculated by this method. A statistical error analysis for Equation 3.13 based on the uncertainties listed in Table 2.2 yields values of uncertainties, for the amount of water calculated, as high as 200% or more especially at large radial distances where small amounts of water are present. Similar analyses of Equations 3.1a and 3.1b yield uncertainties of less than 4%. Hence only the first method gives reliable values for X'_{H2O} and is used for the calculations. Due to the large uncertainties in the second method a meaningful atom balance cannot be obtained.

Though a check on the composition measurements cannot be made at every radial location an overall check on the measurements can be made by comparing the measured mass fluxes of carbon at the exhaust as fuel, CO_2 and CO with the inlet carbon mass flux. Such a comparison shows that the mass fluxes of carbon at the exhaust are lower than at the inlet by less than 10%. The lower value for the exit mass flux of carbon, calculated from the exhaust gas composition profile, may, in part, be due to air leakage into the sample train or syringes during composition measurements.

3.4 Phase 1: Propane Results

3.4.1 Visual Features

Visual features of the flame are the same as reported by Martin[38] and Yetter[42]. Photographs of the combustor operating under the four different test conditions in the present study are presented in Figures 3-3 to 3-6. The visible flame is small in diameter but very long, extending even past the sampling station, for the high co-swirl (55^{o}) case. The flame diameter remains almost constant along its length and hence appears as a long, cylindrical, luminous core in the combustor. For the moderate co-swirl case (30^{o}) the visible flame has similar features as for the high co-swirl case except that for 30^{o} co-swirl the flame is shorter and the diameter of the flame near the entrance to the combustor is larger and gets smaller downstream. The flame looks like an extended bubble. In both the co-swirl cases the flames are smooth and appear to be less turbulent than in the counter-swirl cases.

The counter-swirl cases are characterized by greater noise and appear more turbulent. The flame surface is not smooth but is broken and shows rapid fluctuations indicating higher levels of turbulence. The flames are much larger in diameter, shorter in length and appear as luminous bubbles. The luminous bubbles are indicative of the recirculation zones.

3.4.2 Temperature and Velocity

The temperature and velocity profiles for the four test conditions listed in Table 2.3 are presented in Figures 3-7 through 3-10.

Profiles for the co-swirl cases (Figures 3-7 and 3-8) show steep temperature and velocity gradients. The high co-swirl case has a slightly higher centerline temperature and shows steeper gradients than the 30° co-swirl case. The axial velocity profile for the 55° co-swirl case (Figure 3-7) shows almost a step change in axial velocity in the region of r/R_o=0.5 indicating a hot and fast moving core of fluid confined to the center of the combustor and bears out the visual observation of a long cylindrical core of hot gases. The profiles for the 30° co-swirl case show gradients which are spread over a slightly larger radial thickness and are less steep (than for the 55° co-swirl case) indicating a greater mixing of the hot, high velocity central core with the outer annular jet. In each case the axial velocity gradient is confined to a narrow annular region (the shear layer). This shear layer is caused by the accelaration of the inner core due to reaction. The fact that there is such a shear layer which is confined to a narrow sheet in each of the co-swirl cases indicates that turbulent mixing across the combustor is poor. Turbulent mixing would smooth out the steep velocity and temperature gradients. The tangential velocity profiles

show high tangential velocities for the 55° case and moderate velocities for the 30° case as expected.

The counter-swirl cases show more gradual radial variations in temperature and velocities (Figures 3-9 and 3-10). Gradients are spread out across the entire radius indicating a high degree of trubulent mixing of the outer air with hot combustion products. As a result, the temperatures near the centerline are much lower than in the co-swirl cases and the temperatures near the wall are higher than in the co-swirl cases. The axial velocities vary gradually across the whole radius of the combustor. A pronounced shear layer is not seen in the counter-swirl cases. In both the counter-swirl cases the outer swirl completely overpowers the inner swirl and hence the tangential veocities near the centerline are in the same direction as the tangential velocities in the outer flow. Lee's[44] cold flow measurements also demonstrate the dominance of outer swirl by the time the flow approaches 2 diameters downstream of the inlet.

It is seen from the temperature and velocity profiles (as well as from the composition profiles discussed in the next sub-section) that in going from co-swirl to counter-swirl, turbulent mixing is enhanced. Two mechanisms may account for this increase: first, the tangential slip velocities across the inter-jet shear layer are increased in going from co-swirl to counter-swirl increasing turbulence generation in the shear layer; and second, swirl in the presence of a

strong positive radial density gradient, as in the co-swirl cases, suppresses turbulence production which in turn dampens the turbulent exchange of mass and momentum between the two jets.

A comparison of Figures 3-9 and 3-10 shows that the axial velocity and temperature profiles are flatter and the center-line temperature is lower in the 30° counter-swirl case than in the 55° counter-swirl case indicating a greater mixing in the former case. This fact may be attributed to the greater suppression of trubulent mixing in the presence of density gradients due to the larger swirl in the high counter-swirl case.

3.4.3 Exhaust Gas Composition

Composition profiles on a dry basis are presented in Figures 3-11 through 3-14. Composition results are also presented on a wet basis in Tables 3.2 through 3.5 along with the mass flux weighted average values for each case. The average values for all the cases are listed in Table 3.6 for comparison. Figures 3-11 through 3-14 also show the profiles of the local equivalence ratio ϕ treated as a conserved scalar. ϕ is calculated from the local ratio of the total carbon atoms in the product species to the total oxygen atoms in the product species relative to the stoichiometric carbon to oxygen ratio. At the inlet $\phi=0.8$ in the inner jet and $\phi=0$ in the outer jet. Therefore, the profile of ϕ at the exit gives an indication of the extent of mixing between the inner

and outer jets. The values of the overall equivalence ratio ϕ_{oa} are also shown for each case.

A significant feature of the exhaust gas composition data is that no intemediate lower hydrocarbons are present in detectable quantities. Lower hydrocarbons and alcohols are typically present in substantial amounts in the low temperature oxidation or pyrolysis of hydrocarbons[79,80,81]. Results of the present study, however, indicate that once the propane molcule is broken to initiate reaction, the reaction proceeds quickly to form CO or CO_2. Reaction quenching rates in the combustor are not high enough to freeze the reactions of intermediate hydrocarbon species.

Composition profiles also show turbulent mixing trends similar to those shown by the temperature and velocity profiles. Inspection of the Φ profiles (Figures 3-11 and 3-12) shows that the value of Φ is close to 0.8 near the center and falls steeply near r/R_o=0.4 in the co-swirl cases showing that there is little mixing between the inner and outer jets. For the 55° co-swirl case the temperature and equivalence ratio fall steeply near r/R_o=0.3 and 0.7. This region defines the extent of mixing between the inner and outer jets and will be called the mixing layer. The mixing layer is thicker for the 30° co-swirl case and extends between r/R_o=0.2 and 0.7. The mixing layers are denoted by arrows in Figures 3-11 and 3-12. The Φ profiles for counter-swirl cases, Figures 3-13 and 3-14, are much flatter and the Φ

values are close to the ϕ_{oa} value across the entire radius of the combustor. Hence the mixing layer extends from the centerline to almost the wall of the combustor in the counter-swirl cases. The ϕ profiles also show a slightly better mixing in the 30^{o} counter-swirl case compared to the 55^{o} counter-swirl case.

The co-swirl composition profiles (Figures 3-11 and 3-12) have steep concentration gradients with little evidence of mixing with the high co-swirl case showing the steepest gradients. These gradients occur within the mixing layer between the hot inner jet of combustion products and the cold outer air jet as is to be expected. There is little or no fuel in the central hot core indicating combustion. Correspondingly, low concentrations of oxygen and large amounts of combustion products namely CO and CO_2 are seen in the central core. The concentrations of CO and CO_2 fall steeply while the concentrations of fuel and oxygen increase steeply across the mixing layer. CO concentration decreases less rapidly than the CO_2 concentration in the mixing layer due to the quenching of CO oxidation reactions in the mixing layer as a result of dilution, as demonstrated by Fenimore and Moore[17]. Outside the mixing layer, negligible amounts of CO and CO_2 are found. The unburnt fuel in the exhaust comes from the outer edges of the inner inlet jet (mechanism is discussed in Section 3.8). Hence the maximum unburnt fuel concentration is expected in the mixing layer between the inner and outer jets. As a result of poor mixing in the co-

swirl cases, most of the unburnt fuel is confined within the narrow mixing layer. The steep decline in fuel concentration near the wall (r/R_o=0.7) indicates the edge of the mixing layer. The steep decrease in fuel concentration towards the centerline is a result of combustion.

The counter-swirl composition profiles are more uniform, with smaller gradients, and they show evidence of a greater degree of mixing. Substantial amounts of oxygen and unburnt fuel can be seen on the centerline as a result of greater mixing. The unburnt fuel in the counter-swirl cases also comes from the outer edges of the inner inlet jet, but it is distributed across the entire diameter at the exit as a result of mixing in the post combustion zone. The mixing, however, is not sufficient to produce very uniform concentration profiles across the entire diameter of the combustor. The concentration of CO and of CO_2 decrease towards the wall but some amount of CO and CO_2 can be found close to the wall unlike the co-swirl cases. Fuel concentration decreases near the wall but not as steeply as in the co-swirl cases.

The composition profiles also point to a slightly greater mixing in the moderate counter-swirl case than in the high counter-swirl case; oxygen and propane concentrations are higher on the centerline and their profils are much flatter for the moderate counter-swirl case.

3.4.4 $NO-NO_x$

Radial distributions of NO, NO_x and NO_2 for the four test conditions are presented in Figure 3-15 through 3-18 as well as listed in Tables 3.2 through 3.5. The overall NO and NO_x values (Table 3.6) are quite low in agreement with previous results[26,33,40,42] for lean premixed combustion.

The NO_x values follow the temperture values closely. Maximum local values of NO_x occur in the co-swirl cases for which the maximum temperatures are observed, with high centerline NO_x values decreasing rapidly to nearly zero in the mixing layer where temperatures are lower. NO_x values on the centerline in the counter-swirl cases are nearly 10 times lower than in co-swirl cases due to the lower centerline temperatures in counter-swirl as well as due to the increased mixing in counter-swirl cases which causes the NO_x to be distributed across the entire diameter of the combustor.

The importance of quenching in the NO to NO_2 conversion (discussed in Section 1.2.3) is clearly demonstrated by the profiles. In the co-swirl cases NO_x is predominantly NO in the central core where quenching is minimal. Maximum amounts of NO are found in this region due to the high temperatures and reduced quenching. NO_2, however, predominates in the mixing layer. The NO_2 profiles peak in the mixing layer, with the peak being more pronounced in the 55° co-swirl case indicating a thinner mixing layer, than in the 30° case.

The NO_x in the counter-swirl cases is predominantly NO_2 over the entire radius at the exit. The large fractions of NO_2/NO_x can be attributed to quenching across the combustor in the post-combustion zone (see Section 1.2.3) by the mixing of the hot combustion products and unburnt fuel with the outer air.

Since large HO_2 concentrations are required for large NO_2/NO_x fractions (Equation 1.2), the reduced levels of oxygen, which may limit HO_2 formation (Equation 1.3), may also be a factor in the reduced NO_2 values on the centerline in the co-swirl cases.

Table 3.6 shows that inspite of locally high values of NO_x in the co-swirl cases the mass flux weighted average of NO_x values in the exhaust is of the same order for all the swirl conditions with slightly higher values for co-swirl cases. But, a larger fraction of NO_x is NO_2 in the counter-swirl cases.

It is believed that the use of cooled probes for sample withdrawl especially near reaction zones can result in the measurement of erronously high values for NO_2 concentration due to the reaction of NO with radicals in the sample probe druing the quenching process[30]. In the present study it can be concluded that the large fractions of NO_2/NO_x measured in the counter-swirl cases are real and not a result of quenching in the probe since large NO_2/NO_x fractions are not measured in co-swirl cases under the same probe quenching

conditions. Moreover, probe formed NO_2 is expected to be low in the present study since sampling is done well downstream of the combustion zone at a location where radical concentrations are expected to be low.

3.4.5 Efficiencies

Figure 3-19 shows the efficiencies obtained under the various swirl conditions. The chemical efficiencies plotted in the figure are based on unburnt fuel with correction for CO in the exhaust. Efficiencies are also listed in Tabls 3.2 through 3.6.

Efficiencies are quite low since a lot of fuel is trapped in the mixing layer and in the outer flow and remains unburnt due to dilution and the resultant quenching. An important observation is that the efficiencies do not change significantly in going from counter-swirl to co-swirl though discussion in the preceding subsections suggested decreased mixing and therefore decreased quenching in the co-swirl cases. The almost constant efficiency seen in the present study is in contradiction to the trend observed by Yetter[42] where the efficiency increased in going from counter to co-swirl. Hence additional results are required to explain the constant efficiencies observed in the present study. The additional experiments and their results are discussed in the following sections.

It can be seen from Figure 3-19 that the thermal effi-

ciency is much lower than the chemical efficiency for each case. Since the thermal efficiency is calculated based on the sensible enthalpy flux at the exit, the heat loss from the uninsulated combustor test section can account for the difference in chemical and thermal efficiencies. It is possible to estimate the heat loss required to account for the difference as

$$\dot{Q}_l = \dot{m}_f q'_f (\eta_C - \eta_T) \qquad (3.14)$$

It is seen that a heat loss of about 5 Kcal/s in each case can completely account for the difference in the efficiencies.

Heat can be lost from the hot gases by convection and gas radiation to the test section wall. This heat is transported by conduction across the wall thickness and is lost to the ambient. For the co-swirl cases the temperature profiles, Figures 3-7 and 3-8, suggest that convection to the wall is negligible (temperature profiles are flat near the wall; in fact the wall seems to be slightly hotter than the gas near the wall). However, due to the long luminous flame and high temperatures in the core, heat loss through radiation to the wall can be significant. In the counter-swirl cases the flames are shorter and the centerline temperatures are not very high near the exit. Hence radiation is important only near the inlet. The temperature profiles, Figures 3-9 and 3-10, show gradients near the walls suggesting that convective heat loss is important in the counter-swirl cases. Sim-

plified heat transfer analyses are done to estimate the magnitudes of the convective and radiative heat losses to ascertain whether a heat loss of 5 Kcal/s from the combustor is possible for each of the swirl conditions.

Co-swirl: Heat loss is almost entirely due to radiation. Combustion products, especially CO_2 and water vapor, emit at infrared wavelengths[82,83]. Visible and ultraviolet band spectra of flames arise from electronic transitions of free radicals like OH, CH, C_2, CN and HCO in hydrocarbon flames. The reaction zone also emits continuous spectra, produced by recombination of dissociated molecules. For a first approximation in calculations, the flame is often considered as a black body, and the fact that this is not entirely true is corrected for by an empirical factor smaller than 1[84].

The flame in the co-swirl cases is approximated by a cylinder of radius 2.5 cm (from Figures 3-7 and 3-8) and length 61 cm (upto the measurement station) and an average temperature of 1800°K. The wall temperature is 340°K. Since the flame is a clean hydrocarbon flame the emissivity will be considerably lower than 1 and hence a value of 0.3 for the emissivity is reasonable to assume. The Stefan-Boltzman law is used to calculate the radiative loss, with the surface area obtained from the flame dimensions mentioned above. The heat loss is found to be 4.1 Kcal/s. It should be noted that the flame temperatures near the inlet are much higher and the heat loss can be greater than the 4.1 Kcal/s calculated

above. Therefore, it is possible to account for the heat loss of approximately 5 Kcal/s for the co-swirl cases.

Counter-swirl: Heat transfer is primarily through convection. An estimate for the turbulent thermal conductivity of the gas near the wall, k', is obtained from $k' = \rho c_p u' l$, with turbulent Prandtl number=1, where u' and l are the turbulent velocity and length scales respectively. Measurements of mean velocities made by Depsky[71] show that u' is of the order of 3 m/s. l is taken to be 0.005 m which is approximately the thickness of the boundary layer as seen from the mean axial velocity profiles for the different swirl conditions. The values of c_p and ρ at 350°K are 0.24 Kcal/kg °K and 0.998 kg/m^3 respectively[84], which give a value of $k' = 3.6 \times 10^{-3}$ Kcal/s m °K. Heat loss by convection to the wall is given by $Q_c = k' A (dT/dr)$, where A is the inner surface area of the test section. (dT/dr) is estimated to be 7.4×10^3 °K/m from Figure 3-9 and Q_c is found to be 5.22 Kcal/s. It should be noted that the temperature gradient at the wall near the inlet will be lower and the convective loss will be lower. But the radiation losses are higher near the inlet. Hence it is reasonable to expect a heat loss of about 5 Kcal/s in the counter-swirl cases also.

As an additional check, the average temperature difference across the thickness of the quartz test section required to lose 5 Kcal/s of heat is found to be 28°C (Thermal conductivity of quartz = 2.2×10^{-3} Kcal/s m°K, wall thickness =

0.0025 m). It is reasonable to expect this temperature difference in actuality since the outside of the test section is exposed to the ambient air (295°K) while the inner wall is exposed to a temperature of about 340°K at the exit. However, actual measurements have not been made to determine the exact temperature difference across the wall thickness. (The ambient temperature is marked in the Figures 3-7 to 3-10 along with the temperature profiles).

It should also be noted that the estimate of 5 Kcal/s heat loss to account for the difference in the chemical and thermal efficiencies is based on the assumption that the chemical efficiency is the correct efficiency. However, air leakage into the samples during composition measurements results in a lower value for the mean unburnt fuel fraction and hence the chemical efficiency are overestimated. Therefore, the actual heat loss required is less than 5 Kcal/s. It is also to be noted that the thermal efficiencies would be about 2% higher than what are shown in Figure 3-19 if the temperature profiles are corrected for radiation losses from the thermocouple.

It is concluded that the difference between the calculated chemical and thermal efficiencies is due to the heat loss from the combustor. It is seen, based on the chemical efficiency, that the heat loss of 5 Kcal/s is about 25% of the heat generated in the combustion process. It is possible

that this heat loss by itself could partly account for the low efficiencies observed in the present study.

3.5 Comparison with Previous Results for Methane in the Combustor

Yetter's[42] and Oven's[40] results with methane fuel in the combustor are compared in this section.

Temperature and velocity results in the present study are qualitatively similar to Yetter's results which also show steep gradients for co-swirl cases (Figures 3-4a and 3-5a in [42]). The maximum (centerline) temperatures in the co-swirl cases in the present study, after the addition of radiation correction of approximately 90°K, are within 1.5% of the maximum temperatures observed by Yetter. The absolute values of the velocities in Yetter's study are much higher than in the present study (See Figure 3-26). Since the same probe was used in both the studies and the calibration done by Yetter was also in a jet of low turbulent intensity, his velocity data need to be corrected as described in Section 2.3.

Yetter's results (Figures 3-1a and 3-2a in [42]) also show a slightly lower centerline temperature and flatter temperature and velocity profiles for 30° counter-swirl case than the 55° counter-swirl case indicating better mixing in the 30° case. The 55° counter-swirl centerline temperature in the present study is significantly higher than in Yetter's results, but the wall temperatures in the present study espe-

cially in the counter-swirl cases are lower.

A significant observation is that the maximum temperature and velocity gradients in Yetter's results are found at larger radial distances than in the present study at corresponding axial stations, indicating that the central hot core is larger in diameter in Yetter's tests.

Though a number of similarities in composition profiles can be seen between Yetter's and the present results, there are some significant differences. Yetter's composition results show that the fuel concentrations do not peak near $r/R_o=0.5$, rather they peak at the combustor wall. This fact seems to imply a significant difference between the way the fuel is mixed and burnt under his test conditions and the present test conditions. Yetter's results also show pronounced CO peaks in the mixing layer indicating quenching of the CO oxidation reactions in the mixing layer. The relative locations of CO gradients in the two studies also indicates that the mixing layers in Yetter's study are at larger radial distances and hence the central hot core is larger in diameter.

There are no significant differences in the NO-NO_x results between the present study and Oven's results. Oven's results for high co-swirl (Figure 16 in [40]) also show low NO_2/NO_x ratios in the central core and an NO_2 peak in the mixing layer while almost all of the NO_x is NO_2 in the counter-swirl case (Figure 18 in [40]). Average NO_2 values in the exhaust

are not available from previous results[40,42] for comparison. Though Oven[40] has not made velocity measurements, the radial measurements of temperature and composition at various axial locations upto $6D_o$ downstream from the combustor inlet show trends which are consistent with observations at $6D_o$ made in this study.

The largest differences between results of the present study and Yetter's results are found in the efficiency values. Firstly, the efficiencies in Yetter's study are, in general, higher and secondly they increase significantly in going from counter-swirl to co-swirl (Figure 3-19). This trend is a serious deviation from the nearly contant efficiencies seen in the present study. The only significant differences in the operating conditions between the two studies are in the inner swirl number and axial velocity ratio. Yetter used $S_i=0.523$ and $U_i/U_o=1.5$ for his study. The slightly lower axial velocity ratio (=1.3) in the present study should, if anything, increase the efficiency according to the study of the effect of axial velocity ratio conducted by Yetter[42]. Effects of changes in inner swirl on combustor performance have not been studied so far.

The chemical and thermal efficiencies in Yetter's study are in good agreement with each other indicating a lower heat loss than in the present study. It is possible that the erronous high values for the velocities reported in Yetter's study, which contribute to an increase in the sensible

enthalpy flux, have caused overestimates of the thermal efficiencies, thereby underestimating the heat loss.

3.6 Phase 2: Cold Flow Measurements

Differences in the fuel distribution in the exhaust plane between Yetter's results and the present study suggest differences in the way the fuel is mixed and burnt in the combustion zone. Oven[40] has performed measurements at the inlet under cold flow conditions to test the efficacy of fuel-air premixing in the inner jet. His results indicated that the maximum fuel concentration occurs on the centerline and concentrations at the edge of the inner jet are 35% lower than the maximum (Figure 28 in [40]). One of the causes for such a distribution was thought to be the centrifugal forces in the swirling jet differentially forcing the air, which has a higher molecular weight than methane, towards the outer edge of the jet. Such a distribution was considered beneficial to the combustor efficiency since less methane would be diluted at the outer fringes of the inner jet in the inlet region of the combustor.

As a first step in the cold flow measurements, in the present study, the fuel distribution at the exit was measured for one of the operating conditions. Figure 3-20 shows the radial distribution of propane at the exit plane ($6D_o$) in cold flow under the 30^o counter-swirl condition. The figure shows that the extent of mixing is not sufficient to produce a uniform concentration of propane across the exit. Propane

concentration at the wall is 50% lower than the maximum concentration occuring on the centerline. The profile reinforces the observations in the hot flow of decreasing fuel concentrations near the combustor wall.

Possible differences in the injection mechanism and premixing in the inner jet due to different molecular weights of propane and methane were examined by inlet plane measurements. Results of these measurements, presented in Figure 3-21, show that the mixing of propane and methane in the inner jet are not significantly different. The inlet distribution of the fuels in slightly different from that observed by Oven in that the concentration at the edge of the inner jet is only 20% lower than on the centerline in the present study, in comparison to 35% in Oven's study. This may mean that more fuel could be diluted at the outer fringes of the inner jet causing lower efficiencies in the present study. But the differences in the variation of efficiency with outer swirl still remains to be explained.

The cold flow measurements suggest that the differences between the efficiencies observed by Yetter and in the present study are not likely to be due to differences in the premixing of the fuels propane and methane. Measurements were therefore performed with methane fuel in the combustor for similar test conditions as for propane in order to compare directly with Yetter's results and to determine if the differences in the efficiencies between the two studies are

due to the differences in the chemistry of combustion of propane and methane.

Phase 2: Methane Results

Results are presented for the two test conditions listed in Table 2.3. Temperature and velocity profiles are presented in Figures 3-22 and 3-23. Composition profiles are presented in Figures 3-24 and 3-25. Concentrations in ppm on a wet basis, the average values and the efficiencies are listed in Tables 3.7 and 3.8. Average values are compared in Table 3.6. $NO-NO_x$ measurements were not performed for methane.

The temperature and velocity profiles are almost identical to the profiles for propane for corresponding swirl conditions (Figures 3-7 and 3-9). The maximum temperature and velocity gradients occur at identical radial locations.

Composition profiles for methane are qualitatively identical to the profiles for propane. Steep concentration gradients (especially CO gradients) occur at the same radial locations for propane and methane for the respective swirl conditions. Hence all the remarks in the discussion of propane results in Section 3.4 are pertinent to methane results also, with the exception that the CO peaks are more pronounced in the methane results.

Efficiencies for the methane case (Figure 3-19) are approximately 5% higher, but as in the case of propane the

efficiencies do not change significantly in going from counter to co-swirl. The temperature profile corrected for radiation losses from the thermocouple for the high co-swirl methane case is shown and compared with the uncorrected temperature profile in Figure 3-22. Only the high temperatures close to the centerline are altered by the radiation correction. The value of the thermal efficiency goes up by only 2% when the corrected temperatures are used for the calculation. This increase no doubt brings the value of thermal efficiency closer to the respective chemical efficiency, but does not alter the conclusion that efficiency is not significantly changed by variation of outer swirl for the test conditions studied.

A comparison of temperature and velocity profiles reported by Yetter and in the present study is shown in Figure 3-26. It is apparent from Figure 3-26 that for Yetter's operating condition, the central core is hotter and larger in diameter which strengthens the same observation made in Section 3.5.

The value of inner swirl number for Yetter (S_i=0.523) is only slightly different from S_i=0.495 used in this study. However, even a small change in S_i seems to affect the combustor operation substantially.

3.8 Proposed Mechanism for the Combustor Operation

The following mechanism for the combustion operation is proposed which will consistently explain the observations in

the present study as well as Yetter's study.

It is proposed that most of the fuel burnt is burnt in front and on the sides of the recirculation zone, in a region very close to the combustor inlet. Fuel from the inner regions of the inner jet is burnt in this region of low to moderate velocities, thus forming the intense reaction zone (shown in Figure 1-1) which will be referred to as the 'flame' in the ensuing discussion. (It has been established[47,71] that the role of the recirculation zone is to stabilize the flame by providing a region of low velocity flow in front of the recirculation zone). Inefficiency in the combustor is caused by the inability to burn the fuel flowing at the edges of the inner jet which flows around and at large radial distances from the recirculation zone and is lost to the combustion process. High efficiencies result from the ability of the flame to propagate radially outward in order to burn the fuel flowing in the outer edges of the inner jet.

The following four characteristics are considered important in determining how much fuel is burnt in front of the recirculation zone and the ability of the flame to propagate radially: 1) The size of the recirculation zone, 2) inlet turbulence, 3) velocities around the sides of the recirculation zone and 4) the local equivalence ratio on the sides of the recirculation zone.

Beyler's[47] mean CH radiant emission data are plotted, with the reverse flow region as measured by Depsky[71], in Figure 3-27. The elliptical arc represents the reverse flow region (the other symbols in the Figure are explained later in this section). The extent of the recirculation zone is about the same as that of the region of reversed flow[71]. It is seen from Figure 3-27 that the recirculation zone is larger for the counter-swirl case than for the co-swirl case. Since a larger recirculation zone has a larger region of reduced velocity in front of it, it is proposed that a larger amount of fuel is burnt in front of the recirculation zone in the counter-swirl case than in the co-swirl case. The above hypothesis is necessary to explain the constant efficiencies observed in the present study as will be seen later in this section. A rigorous check on this hypothesis would be to clearly delineate the reaction zone in front of the recirculation zone, draw streamtubes from the inlet jet and determine what mass of fuel-air mixture enters the reaction zone for each of the outer swirl conditions. Unfortunately, sufficient data near the inlet is not available at present to make this check.

A recent study by Moreau and Borghi[85] of a turbulent premixed flame shows large changes in combustion efficiency for small changes in inlet turbulence. Lee's[44] measurements in the present combustor for cold flow show large r.m.s values for axial and tangential velocities near the inlet for counter-swirl compared to the co-swirl case, which might also

contribute to a larger amount of fuel being burnt in front of the recirculation zone in the counter-swirl case than in the co-swirl case. It should be noted that in Lee's[44] cold flow measurements there is no recirculation zone for the co-swirl case, whereas under combusting conditions there is a recirculation zone for the co-swirl case also. Depsky's[71] measurements under combusting conditions show large values of r.m.s axial and tangential velocities at the inlet for co-swirl also. It is worthwhile to make more detailed measurements of the inlet turbulence (in front of the recirculation zone) to characterize its effect on the flame.

The ability of the flame to propagate radially outward depends greatly on the local velocity and equivalence ratio on the sides of the recirculation zone. In Figure 3-27 the circles represent the peaks in the mean CH radiant emission profiles and the squares represent the half maximum points from Reference 47. The triangles represent the location of the axial velocity peaks and the vertical bars represent the region of steep radial gradients of axial velocity from Reference 71 for nearly the same operating conditions including the same inner swirl number as in Reference 47 and in the present study. The peaks in the axial velocity (Figure 3-27) are, in part, a result of the acceleration of the flow around the recirculation zone as opposed to combustion induced acceleration and are seen in Lee's[44] cold flow measurements as well. Chemiluminescent emission from CH has been established as a signature of the reaction zone in the combus-

tor[47]. Figure 3-27 shows that the maxima of mean CH emissions occur outside the recirculation zone but well interior to the region of peak axial velocity. This implies that the flame is not able to propagate across the region of high velocities. The peaks in the axial velocities are as high as $1.25U_i$ where U_i is the average axial velocity in the inner jet. The flame is able to propagate radially until the steep gradients in velocity are encountered. Then the radial propagation is slower since the flame is almost parallel to the flow direction due to the high flow velocities. This slower radial propagation as the flow moves downstream is possible only if the local equivalence ratios are above the local inflammability limits determined by the local turbulence, temperature and velocity conditions. For both the co- and counter-swirl cases the peak velocities are nearly the same ($1.25U_i$) near the inlet but the peak value is slightly lower and the peak is broader by the time the flow reaches $1D_o$ downstream as a result of increased momentum transport due to greater mixing in the counter-swirl case (Figures 7 and 11 in [71]). In the co-swirl cases, however, the local equivalence ratios in the region of the steep gradients of axial velocity are expected to be higher than the local inflammability limits due to reduced mixing with the outer jet. Therefore, the flame can propagate radially outward though it does so very gradually on account of the high axial velocities and the flame being almost parallel to the flow. In counter-swirl, in addition to the velocities on the sides of the recircula-

tion zone being high, the local equivalence ratios in that region are expected to decrease rapidly as we go downstream due to increased mixing with the outer air. Hence the flame cannot propagate radially outward as the flow moves downstream. Figure 3-27 shows that the flame as denoted by the peaks of mean CH emissions does not propagate radially outward to the extent it does in the co-swirl case. The greater the radial propagation of the flame, the larger the number of streamtubes it is likely to cut, thereby burning more fuel.

Based on the mechanism discussed above, a smaller amount of fuel is burnt in front of the smaller recirculation zone in the co-swirl case than in the counter-swirl case. But more fuel is burnt on the sides of the recirculation zone in the co-swirl case than in the counter-swirl case.

In the present study, it so happens that the amounts of fuel burnt in front and on the sides of the recirculation zone add up to approximately the same amount in the co- and counter-swirl cases resulting in the same efficiency. As seen from the discussions above, this insensitivity of the efficiency to outer swirl does not imply that the combustion mechanism is unaffected by outer swirl. It could be considered fortuitious that the operating conditions set in the present study resulted in a constant efficiency with varying outer swirl. On the other hand, with flow conditions resulting in a smaller recirculation zone in co-swirl than in the present study, one can possibly achieve higher efficiencies

for counter-swirl than for co-swirl though there is more dilution from the outer air in the counter-swirl than in the co-swirl case. There are also operating conditions for which the efficiencies for co-swirl are greater than those for counter-swirl.

Yetter's[42] observation of a higher efficiency for co-swirl than for counter-swirl may be explained as follows. A study of the size of the recirculation zone formed from a single jet for varying swirl numbers made by Syred and Beer[2] shows that the recirculation zone increases in size with increasing swirl numbers. This suggests that for operating conditions in [42], the recirculation zones were probably bigger than in the present study due to the larger inner swirl in [42]. This means that in co-swirl cases in [42], a larger amount of fuel is burnt in front of the recirculation zone as well as that the flame propagates farther radially than in the present study since the high velocity peaks occur at larger radial distances due to the larger recirculation zone resulting in much higher efficiencies (Figure 3-19) and a larger central hot core (Figure 3-26) than in the present study. The increase in efficiency in the counter-swirl cases is not much (Figure 3-19). There seems to be an upper limit to the efficiency in the counter-swirl cases as a result of dilution from the outer air. Beyond a certain size, an increase in the size of the recirculation zone in the counter-swirl cases is of no use, since, eventhough the flow conditions are suitable for

more combustion, the local equivalence ratios are too low as a result of dilution.

Therefore, it appears that even small changes in inner swirl can cause large changes in efficiency. Exploratory measurements performed by the author, the results of which are not presented here for want of systematic data, show that minor adjustments of the butterfly valve controlling the inner swirl causes changes in centerline temperature at the exit of the order of 150°K. The experiment done for the moderate co-swirl case demonstrates that the combustor is very sensitive to inner swirl.

The oxidation of CO and NO in the combustor to CO_2 and NO_2 respectively is explained as follows. The CO to CO_2 and NO to NO_2 conversions being slower reactions are determined by conditions downstream of the combustion zone in the post-combustion zone. Inspection of the time mean isotherms in the combustor measured by Oven, et al.[41] (Figure 3-28) shows that cooling rates on the centerline for the counter-swirl case can be as high as 250°K per millisecond (an axial velocity of 50 m/s is assumed). This cooling rate is much higher than the minimum cooling rate of 70°K per millisecond at 1270°K specified by Fenimore and Moore[17] for CO remaining permanently quenched. There is little or no cooling of the hot core in the co-swirl case (Figure 3-28). Hence large amounts of CO are found at the exit in the counter-swirl cases compared to the co-swirl cases. Inspection of the time

mean isopleths of CO measured by Oven, et al.[41] and presented in Figure 3-29 shows CO being rapidly converted to CO_2 in the central core of the post-combustion zone for the co-swirl case whereas large amounts of CO are quenched in this zone and mixed across the combustor for the counter-swirl cases. Large fractions of NO_2/NO_x in the counter-swirl cases are a result of the increased quenching in the post-combustion zone in the counter-swirl cases promoting the formation of HO_2 which oxidizes NO to NO_2.

CHAPTER 4

CONCLUSIONS

The measurements reported in this work in combination with results from previous measurements in the swirl combustor lead to the following major conclusions and suggest future experiments designed to understand specific aspects of the combustor operation.

The exhaust from the combustion of propane in the combustor is free from lower hydrocarbons like ethane, ethylene and methane.

There is no difference in the combustor operation for the fuels propane and methane. The use of either of the fuels results in nearly the same temperature and velocity profiles and the same efficiency for a given operating condition suggesting that differences in the chemistry of combustion between propane and methane do not affect the overall combustor operation.

Practically all the combustion occurs in the region close to the combustor inlet upto about $1.5D_o$ from the inlet, called the combustion zone. The CO to CO_2 and NO to NO_2 conversions occur in a region downstream of the combustion zone called the post-combustion zone.

Turbulent mixing in the combustor is enhanced in going from high co-swirl to counter-swirl with the 30^o counter-

swirl showing the greatest degree of mixing. The mixing trends are a result of interactions between tangential shear between inner and outer jets and swirl in the presence of positive radial density gradients.

The NO_x levels in the exhaust are low as a result of lean premixed combustion. Large fractions of NO_2/NO_x are found as a result of quenching in the post-combustion zone due to dilution from the outer air jet especially in the counter-swirl cases. Quenching of CO oxidation reactions in the post-combustion zone is the cause for the large amounts of CO in the counter-swirl cases.

Combustion efficiencies in the present study are low and remain constant with varying outer swirl. A mechanism for the combustor operation is proposed which explains the constant efficiencies in the present study as well as the increase in efficiency in going from counter to co-swirl observed by Yetter[42]. The flame (intense reaction zone) is stabilized in front of the recirculation zone. Inefficiency in the combustor stems from the inability of the flame to propagate radially outward and burn the fuel from the outer edges of the inner jet. The following four fluid-mechanical characteristics are considered important in determining the efficiency of the combustor:

1) The size of the recirculation zone
2) Inlet turbulence
3) Velocities around the recirculation zone

4) Local equivalence ratio on the sides of the recirculation zone.

It is apparent that these flow characteristics should be investigated in detail and related to the operating parameters of the combustor as a viable means to control combustion.

It is evident that the combustor operation is very sensitive to even small changes in the inner swirl number. It is therefore necessary to study the effect which the inner swirl has on the above mentioned four flow characteristics for different outer swirl conditions.

A few measurements are suggested for the future aimed at achieving the objectives mentioned above. It is necessary to delineate the flame precisely and draw streamtubes for the flow in the combustion zone to determine how much of fuel is burnt where in the combustion zone. It is important to use non-intrusive optical techniques for the measurements. Laser Doppler Velocimetry is suggested for making extensive mean and r.m.s velocity measurements especially in front of the recirculation zone. Temperature measurements using the Rayleigh scattering technique will provide information on the local densities. The local velocity and density information can be used to draw streamtubes based on mass flow. Measurements of CH emissions using Emission Spectroscopy can be used to delineate the flame. Measurement of major species concentrations in the combustion zone using techinques such as

Raman Spectroscopy provides information on the local equivalence ratios. These measurements should be performed for varying inner and outer swirl conditions. Effects of other operating conditions like inner jet equivalence ratio and inner to outer jet axial velocity ratio on the combustor performance can also be studied. There are, however, numerous problems in the practical utilization of the suggested techniques like signal processing, noise, biases in measurement, maintaining uniform scattering cross-sections for Rayleigh scattering measurements, spatial resolution, signal to noise ratio especially for low concentrations, laser beam quality and reliability, etc. Most of these problems are being overcome and the techniques are becoming available for accurate and reliable measurements. Optical access to the region of interest in the combustor is necessary. Figures 3-3 to 3-6 show that the combustion zones extend into the inner tube of the combustor posing the problem of optical access to that region. But in general, the configuration of the present combustor provides good optical access and is well suited for optical techniques.

Measurements similar to those suggested above can be performed in the post-combustion zone to study the dynamics of the CO to CO_2 and NO to NO_2 conversions. Conventional sampling and velocity probes are nevertheless still effective tools for analysis in regions far away from reaction zones like near the exit. New techniques using acousto-optic filters (SMART sensors)[86,87] for absorption spectroscopy are

being developed which may prove very valuable in combustion research on account of their speed and ruggedness of operation. The development and application of these techniques will help in understanding the combustor better.

Some modifications to the combustor design could be attempted. For example, a shield can be provided around the fuel injector so that fuel is injected only into the central region of the inner jet. This will improve the combustor efficiency since little or no fuel is diluted on the outer edges of the inner jet. Another modification could be to put a diffuser-like shield over the inner jet and the recirculation zone to delay the mixing of the outer jet with the inner jet. With a better understanding of the present combustor, suitable designs for practical applications of premixed prevaporized swirl combustors can be developed.

REFERENCES

1. Beer, J.M. and Chigier, N.A. Combustion Aerodynamics, Applied Science Publishers, London, 1972.

2. Syred, N. and Beer, J,M., "Combustion in Swirling Flows: A review", Combustion and Flame, Vol.23, 1974.

3. Syred, N., Chigier, N.A. and Beer, J.M., "Flame Stabilization in Recirculation Zones of Jets with Swirl", Thirteenth Symposium (International) on Combustion, Combustion Institute, Pittsburgh, PA, 1971.

4. Swithenbank, J. and Chigier, N.A., "Vortex Mixing for Supersonic Combustion", Twelfth Symposium (International) on Combustion, Combustion Institute, Pittsburgh, PA, 1969.

5. Drake, P.F. and Hubbard, E.F., Journal of Fuel, Vol.39, P.98, 1966.

6. Kerr, N.M. and Fraser, D., Journal of Institute of Fuel, Vol.38, p.519, 1965.

7. Mather, M.L. and Maccallum, Nr..R.L., J.Inst. of Fuel, Vol.40, p.214, 1967.

8. Afrosimova, V.N., Thermal Engineering, Vol.14, No.1, p.10, 1967.

9. Hall, M.G., "Vortex Breakdown", Annual Review of Fluid Mechanics, Vol.4, p.195, 1972.

10. Leibovich, S., "The Structure of Vortex Breakdown", Annual Review of Fluid Mechanics, Vol.10, p.221, 1978.

11. Faler, J.H. and Leibovich, S., "Disrupted States of Vortex Flow and Vortex Breakdown", Physics of Fluids, Vol.20, p.1385, 1977.

12. Panton, P.L. and Sweat, R.H., "Vortex Bursting with Combustion", Combustion and Flame, Vol.30, p.133, 1977.

13. Rice, I.G., "The Industrial Application of the Gas Turbine", Turbomachinery International, Vol.17, p.66, April 1978.

14. Stambler, I., "EPRI Gas Turbine Outlook", Combustion, Vol.47, P.9, April 1976.

15. "Problems and Progress in Developing the Automotive Gas Turbine", Mechanical Engineering, Vol.100, p.40, May 1978.

16. Rudy, R.A. and Reck, G.M., "Advanced Combustion Techniques for Controlling NO_x Emissions of High Altitude Cruise Aircraft", NASA TM-73473, 1976.

17. Fenimore, C.P. and Moore, J., "Quenched Carbon Monoxide in Fuel-Lean Flame Gas", Combustion and Flame, Vol.22, p.343, 1974.

18. Johnston, H.A., "Catalytic Reduction of Stratospheric Ozone by Nitrogen Oxides", Univ. of California, Lawrence Radiation Laboratory Report No. UCRl-20568, June, 1971.

19. Johnston, H.A., "Redcution of Stratospheric Ozone by Nitrogen Oxide Catalysts from Supersonic Transport Exhaust", Science, Vol.173, p.517, 6 August, 1971.

20. Johnson, R.H., Wilkes, C. and Holt, M., "Gas Turbine Environmental Factors", General Electric, Gas Turbine Reference Library, #GER-2486B, 1973.

21. Environmental Protection Agency, "Aircraft and Aircraft Engines, Proposed Standards for Control of Air Pollution", Federal Register 37, No.239, Part 2, 26488-26503, Dec., 1972.

22. "EPA Proposed Air Pollution rules for Stationary Gas Turbines", Journal of the Air Pollution Control Association, 27, 1210, Dec., 1977.

23. Sawyer, R.F., "Experimental Studies for Chemical Processes in a Model Gas Turbine Combustor", Emissions from Continous Combustion Systems, ed. Cornelius and Agnew, Plenum Press, New York, 1972.

24. Fristrom, R.M. and Westenberg, A.A, Flame Structure, McGraw Hill, New York, 1965.

25. Anderson, L.B., Meyer, J.W. and Mclean, W.J., "Turbojet Exhaust Reactions in Stratospheric Flight", AIAA Journal, Vol.12, p.56, 1974.

26. Schefer, R.W. and Sawyer, R.F., "Lean Premixed Recirculatory Flow Combustion for Control of Oxides of Nitrogen", Sixteenth Symposium (International) on Combustion, The Combustion Institute, PA, 1976.

27. Gouldin, F.C, "Controlling Emissions from Gas Turbines - The Importance of Chemical Kinetics and Turbulent Mixing", Combustion Science and Technology, Vol.7, p.33, 1973.

28. Takagi, T., Ogasawara, M., Daizo, M. and Tatsumi, T., "NO_x Formation from Nitrogen in Fuel and Air During Turbulent Diffusion Combustion", Sixteenth Symposium (International) on Combustion, The Combustion Institute, Pittsburgh, PA, 1976.

29. Fenimore, C.P., "Formation of Nitric Oxide in Premixed Hydrocarbon Flames", Thirteenth Symposium (International) on Combustion, The Combustion Institute, Pittsburgh, PA, 1970.

30. Allen, J.D., "Probe Sampling of Oxides of Nitrogen from Flames", Combustion and Flame, Vol.24, No.1, 1975.

31. Merryman, E.L., and Levy, A., "Nitrogen Oxide Formation in Flames: The Roles of NO_2 and Fuel Nitrogen", Fifteenth Symposium (International) on Combustion, The Combustion Institute, Pittsburgh, PA, 1975.

32. Fenimore, C.P., "The Ratio NO_2/NO in Fuel-Lean Flames", Combustion and Flame, Vol.25, p.85, 1975.

33. Oven, M.J., McLean, W.J. and Gouldin, F.C., "NO-NO_x Measurements in a Methane-Fuelled Swirl-Stabilized Combustor", Paper presented at the Central States Section, The Combustion Institute, Spring Techinal Meeting, NASA Lewis Research Center, 1977.

34. Ceransky, N.P., "Sampling and Measuring for NO and NO_2 in Combustion Systems", AIAA Paper No.76-139, Presented at the AIAA Fourteenth Aerospace Sciences Meeting, Washington, D.C., 1976.

35. Cernansky, N.P. and Sawyer, R.F., "NO and NO_2 Formation in Turbulent Hydrocarbon/Air Diffusion Flame", Fifteenth Symposium (International) on Combustion, The Combustion Institute, Pittsburgh, PA, 1975.

36. Chen, J.Y., McLean, W.J. and Gouldin, F.C., "The Oxidation of NO to NO_2 During Combustion Quenching Processes", Paper (No. 79-17) presented at the Western States Section/ The Combustion Institute, Spring Combustion Meeting, Brigham Young University, Provo, Utah, April, 1979.

37. Lefebvre, A., "Pollution Control in Continous Combustion Systems", Fifteenth Symposium (International) on Comustion, The Combustion Institute, Pittsburg, PA, 1975.

38. Martin, D.T., "Stability Limits of a Methane-Fueled Swirl-Combustor", M.S. Thesis, Cornell University, Ithaca, NY, 1975.

39. Martin, D.J., Gouldin, F.C. and Yetter, R.A., "Preliminary Evaluation of Vortex Breakdown Stabilized Combustor", Paper presented at the Fall Meeting, Eastern States Section, The Combustion Institute, Brookhaven National Laboratories, Long Island, NY, 1975. Also Coll. of Engr. Energy Program Rep. EPR-75-9, Cornell University, Ithaca, NY, Nov., 1975.

40. Oven, M.J., "Temperature and Species Concentration Measurements in Swirl-Stabilized Combustor", M.S. Thesis, Cornell Unversity, Ithaca, NY, 1979.

41. Oven, M.J., Gouldin, F.C. and McLean, W.J., "Temperature and Species Concentration. Measurements in Swirl-Stabilized Combustor", Seventeenth Sumposium (International) on Combustion, The Combustion Institute, Pittsburgh, PA, 1979.

42. Yetter, R.A.,"Experimental Study of Vortex Breakdown Stabilized Combustor: Analysis of Exhaust Emission and Combustor Efficiency", M.S. Thesis, Cornell University, Ithaca, NY, 1981.

43. Yetter, R.A. and Gouldin, F.C.,"Exhaust Gas Emissions of a Vortex Breakdown Stabilized Combustor", Paper presented at the Fall Meeting of the Western States Section, The Combustion Institute, LaJolla, CA, October, 1976.

44. Lee, Sun-Leung, "Laser Doppler Velocimetry Measurements in a Swirl-Stabilized Combustor", M.S. Thesis, Cornell University, Ithaca, NY, 1980.

45. Halthore, R.N., Private Communication, Cornell University, Ithaca, NY.

46. Beyler, C.L. "Flame Structure and Stabilization in Premixed Swirl-Stabilized Combustion", M.S. Thesis, Cornell University, Ithaca, NY, 1981.

47. Beyler, C.L. and Gouldin, F.C.,"Flame Structure in a Swirl-Stabilized Combustor Inferred by Radiant Emission Measurements", Eighteenth Symposium (International) on Combustion, The Combustion Institute, Pittsburgh, PA, 1980.

48. Bilger, R.W., "Probe Measurements in Turbulent Combustion", Combustion Measurements, p.333, R.Goulard edt., Academic Press, New York, 1976.

49. England, C., Houseman, J. and Teixeira, D.P., "Sampling Nitric Oxide from Combustion Gases", Combustion and Flame, Vol.20, p.439, 1973.

50. Gouldin, F.C., "Probe Measurements in Multi-Dimensional Reacting Flows", AGARD-Testing and Measurement Techniques in Heat Transfer and Combustion Conference Proceedings No.281, NATO Publication.

51. Samuelson, G.S and Harman, J.N., "Transformation of the Oxides of Nitrogen Composition while Sampling Combustion Products", Paper presented at the First Chemical Congress of the North American Continent, Mexico City, 1975.

52. Patterson, D.J. and Henein, N.A., "Emissions from Combustion Engines and their Control", Ann Arbor Science Publishers Inc., 1973.

53. Homan, H.S., "An Experimental Study of Reciprocating Internal Combustion Engines Operated on Hydrogen", PhD Thesis, Cornell University, Ithaca, NY, 1978.

54. Dimitriades, B., "Determination of Nitrogen Oxides in Auto Exhaust", Journal of Air Pollution Association, Vol.17, 1967.

55. Tuttle, J.H., Shisler, R.A. and Mellor, A.M., "Nitrogen dioxide Formation in Gas Turbine Engines: Measurements and Measurement Method", Combustion Science and Technology, Vol.9, Nos. 5 and 6, 1974.

56. Sigsby, J.E., Black, F.M., Bellar, T.A and Klosterman, D.L., "Chemiluminescent Method for Analysis of Nitrogen Compounds in Mobile Source Emissions (NO, NO_2, NH_3)", Environmental Science and Technology, Vol.7, 1973.

57. Siewert, R.M., "Hydrogen Influence in Chemiluminescent NO_x Analysis", Combustion and Flame, Vol.25, No.2, 1975.

58. Breitenbach, L.P. and Schelef, M., "Development of a Method for the Analysis of NO_2 and NH_3 by NO Measuring Instruments", APCA Journal, Vol.23, 1973.

59. Matthews, R.D., Sawyer, R.F. and Schefer, R.W., "Interferences in the Chemiluminescent Measurements of NO and NO_2 Emissions from Combustion Systems", Presented at the Fall Meeting of the Western States Section of the Combustion Institute, LaJolla, CA, 1976.

60. Oppegaard, A., "The Use of Septum/ Syringe/ Injector in Gas Chromatography. Problems and Improvements", Journal of Chromatographic Sciences, Vol.10, p.716, 1972.

61. Alltech Associates, "Everything for Chromatography", Catalog No.30, p.25, Arlington Heights, IL, 1979.

62. Kaiser, R., Chromatographia, Vol.2, p.453, 1969.

63. Kaiser, R., "Carbon Molecular Sieve", Chromatographia, Vol.3, p.38, 1970.

64. Zlatkis, A., Kaufman, H.R. and Durbin, D.E., "Carbon Molecular Sieve for Trace Analysis in Gas Chromatography", Journal of Chromatographic Science, Vol.8, p.416, 1970.

65. Bollman, D.H. and Mortimore, D.M., "Determination of Carbon Dioxide, Hydrogen Sulphide, Sulphur Dioxide, Ethane and Propane using a Carbon Molecular Sieve Column", Journal of Chromatographic Science, Vol.10, p.523, 1972.

66. Supleco Inc., "Chromatography Supplies", Catalog No.10, p.48, Bellefonte, PA, 1976.

67. Supleco Inc., "Carbosieve B and S - GSC Packing", Bulletin 712B, Bellefonte, PA, 1976.

68. Supleco Inc., "Chromatography Supplies", Catalog No.11, Bellefonte, PA, 1977 and onwards.

69. Schlichting, H., Boundary Layer Theory, McGraw Hill, 1966.

70. Bryer, D.W. and Pankhurst, R.C., Pressure Probe Methods for Determining Wind Speed and Flow Direction, Her Majesty's Stationery Office, London, 1971.

71. Depsky, J.S., "Laser Velocimetry Measurements in a Methane-Fueled Swirl Combustor", M.S. Thesis, Cornell University, Ithaca, NY, 1982.

72. Vu, B.T., "Experiments on Turbulent Co-axial Swirling Flows", PhD Thesis, Cornell University, Ithaca, NY (In preperation)

73. Vu, B.T., "A Flow Tunnel for Studies of Confined Co-axial Turbulent Swirling Flows and A Discussion on Turbulence Measurements in Such Flows", Coll. of Engineering, Energy Program Report, Cornell University, August 1974.

74. Fishenden, M. an Saunders, O.A., "The Errors in Gas Temperature Measurements and their Calculation", Journal of The Institute of Fuel, Vol.12, No.64, 1939.

75. Gubareff, G.G., Janssen, J.E. and Torborg, R.H., Thermal Radiation Properties Survey, Second Edition, Honeywell Research Center, Minneapolis, 1960.

76. Handbook of Chemistry and Physics, 53rd Edition, p.E3, CRC Press, 1972.

77. Frock, E.F., Olsen, L.O. and Freeze, P.D., "The Use of Thermocouples in Streaming Exhaust Gas", Third Symposium on Combustion, Flame and Explosion Phenomena, 1948.

78. Prothero, A., "Computing with Thermochemical Data", Combustion and Flame, Vol.13, p.399, 1969.

79. Ciavaldini, H., "The Slow Oxidation of Propane, n-Butane and Iso-Butane", PhD Thesis, University of London, 1975.

80. Griffiths, J.F., Gray, B.F. and Gray, P., "Multi-stage Ignition in Hydrocarbon Combustion: Temperature Effects and Theories of Nonisothermal Combustion", Thirteenth Symposium (International) on Combustion, The Combustion Institute, Pittsburgh, PA, 1971.

81. Walker, R.W., "A Critical Survey of Rate Constants for Reactions in Gas-Phase Hydrocarbon Oxidation", Specialist Periodical Report, Reaction Kinetics I, The Chemical Society of London.

82. Gaydon, A.G., Spectroscopy of Flames, Wiley, New York, 1957.

83. Tourin, R.H., Spectroscopic Gas Temperature Measurements, Elsevier Publishing Company, 1966.

84. Eckert, E.R.G. and Drake, R.M., Analysis of Mass and Heat Transfer, McGraw Hill Kogakusha Ltd., 1972.

85. Moreau, P. and Borghi, R., "Experimental and Theoretical Studies of Nitrogen Oxide Production in a Turbulent Premixed Flame", Journal of Energy, Vol.5, No.3, 1981.

86. Chang, I.C., "Tunable Acousto-Optic Filters: An Overview", SPIE, Vol.90, Acousto Optics, 1976.

87. Gouldin, F.C., Private Communication, College of Engineering, Cornell University, Ithaca, NY, 1981.

Table 2.1.

Compositions (in % by volume) of calibration gas mixtures

Mixture No.	1 (air)	2	3	4	5
O_2	20.9	5.0			
N_2	79.1	72.38	90.0	99.0	99.0
CO		7.02			
CO_2		15.6			
CH_4					1.0
C_3H_8			10.0	1.0	

Table 2.2.

Response factors and estimated errors.

Species	Response factor (b_i)	% error in b_i (σ_{bi}/b_i)	% error in species conc. (σ_{xi}/X_i)	Typical species conc. used in calculation (% by volume)
O_2	1.062	2.8	2.9	15
N_2	1.000	-	<1.0	80
CO	0.983	1.55	2.4	0.1
CO_2	0.526	0.6	0.8	3
C_3H_8	0.784	3.0	3.2	0.4
CH_4	0.9335	2.45	2.75	0.7

Table 2.3.

Test Conditions

Outer Swirl	S_o	U_i [m/s]	U_i/U_o	U_{oa} [m/s]	Φ_i	Φ_{oa}
PROPANE:						
55°Co -	+0.56	30.0	1.32	24.3	0.81	0.214
30°Co -	+0.20	30.3	1.25	25.6	0.80	0.210
30°Ct -	-0.20	30.1	1.26	25.3	0.80	0.210
55°Ct -	-0.56	30.2	1.37	23.9	0.80	0.224
METHANE:						
55°Co -	+0.56	31.5	1.33	25.4	0.81	0.218
30°Ct -	-0.20	31.6	1.28	26.2	0.80	0.213

$S_i = 0.495$ $\quad Q_f$ = 3.4 SCFM (Propane)

= 8.5 SCFM (Methane).

Table 3.1.

θ values on either side of the centerline
for the 55° co-swirl, propane case
showing axisymmetry at the measurement station
and reproducibility of combustor operation

r(cm)	θ(°)	θ(°) separate run
5.0	-19.5	
4.0	-22.5	-22.0
3.0	-21.0	-20.0
2.0	-16.0	-15.5
1.0	-10.5	-10.5
0.5	-6.0	-6.0
0.0	0.0	0.0
0.5	6.0	5.5
1.0	11.0	
2.0	16.5	
3.0	21.0	
4.0	23.0	
5.0	20.5	

Table 3.2.

Composition (wet basis), velocity, temperature, their average valves and efficiencies for the 55° co-swirl, propane case

55 CO-SWIRL PROPANE

R CM	U M/S	O2 PPM	N2 PPM	CO PPM	FUEL PPM	CO2 PPM	NO PPM	NOX PPM	T K	H2O PPM
0.0	50.48	41200.	755781.	1370.	0.	85664.	78.00	95.60	1942.	116046.
0.5	50.35	43517.	757172.	1194.	0.	84620.	84.20	103.80	1927.	114419.
1.0	50.46	48030.	759082.	1077.	0.	81728.	65.70	85.00	1899.	110406.
1.5	50.98	64649.	755434.	1034.	778.	72781.	33.40	56.30	1847.	98420.
2.0	50.22	109027.	766346.	1032.	1925.	51630.	3.85	29.70	1716.	70216.
2.5	49.34	171208.	786911.	998.	3383.	15450.	1.80	10.00	1335.	21930.
3.0	40.59	198004.	790778.	260.	7174.	1450.	1.68	2.50	546.	2280.
3.5	34.62	206588.	786242.	51.	6181.	291.	1.52	1.97	346.	456.
4.0	34.18	209343.	783731.	0.	4406.	291.	1.39	1.39	331.	387.
4.5	34.18	206629.	786397.	0.	3652.	194.	1.26	1.25	331.	258.
5.0	31.35	205548.	790569.	0.	3615.	291.	1.09	1.23	337.	387.
	AVG=	195211.	785005.	164.	4424.	5837.	3.66	5.86	513.	8001.

CHEMICAL EFFICIENCY (UNBURNT FUEL ONLY) = 51.158%
CHEMICAL EFFICIENCY (UNBURNT FUEL AND CO)= 50.905%

Table 3.3.

Composition (wet basis), velocity, temperature, their average valves and efficiencies for the 30^{o} co-swirl, propane case

30 CO-SWIRL PROPANE

R CM	U M/S	O2 PPM	N2 PPM	CO PPM	FUEL PPM	CO2 PPM	NO PPM	NOX PPM	T K	H2O PPM
0.0	51.35	47907.	749116.	2175.	0.	84813.	73.90	91.10	1935.	115983.
0.5	51.20	54150.	756974.	1787.	72.	78246.	65.00	81.00	1907.	106710.
1.0	50.70	72081.	757365.	1507.	308.	70038.	43.00	65.33	1842.	95393.
1.5	50.11	113738.	757498.	1324.	2094.	56082.	9.00	38.00	1735.	76541.
2.0	49.31	164359.	784411.	1234.	4819.	15661.	2.67	15.00	1520.	22526.
2.5	46.27	195724.	788613.	814.	5347.	4288.	1.00	5.00	1225.	6802.
3.0	40.65	202632.	787259.	344.	5389.	1245.	0.95	1.87	610.	2118.
3.5	37.18	207205.	787547.	125.	5002.	383.	0.54	1.33	391.	678.
4.0	35.51	211293.	784240.	49.	4247.	384.	0.46	1.35	340.	577.
4.5	34.73	212592.	783444.	0.	3794.	384.	0.00	1.33	335.	511.
5.0	33.11	209809.	790220.	0.	3438.	384.	0.50	1.33	339.	511.
	AVG=	202346.	784584.	208.	4209.	4049.	1.70	4.33	521.	5677.

CHEMICAL EFFICIENCY (UNBURNT FUEL ONLY) = 51.773%
CHEMICAL EFFICIENCY (UNBURNT FUEL AND CO)= 51.439%

Table 3.4.

Composition (wet basis), velocity, temperature, their average valves and efficiencies for the 30° counter-swirl, propane case

30 CT-SWIRL PROPANE

R CM	U M/S	O2 PPM	N2 PPM	CO PPM	FUEL PPM	CO2 PPM	NO PPM	NOX PPM	T K	H2O PPM
0.0	52.90	173247.	771480.	2537.	3936.	18468.	0.61	9.60	855.	28006.
0.5	52.64	174213.	774710.	2390.	4051.	17027.	0.61	8.11	825.	25890.
1.0	51.90	175747.	776286.	2260.	4205.	15671.	0.64	7.10	787.	23908.
1.5	51.21	177897.	777949.	2145.	4390.	14218.	0.75	6.48	740.	21817.
2.0	50.31	181831.	775777.	2062.	4436.	11933.	0.85	5.89	688.	18660.
2.5	48.81	187041.	779325.	1997.	4198.	9375.	0.86	4.97	626.	15163.
3.0	47.83	191030.	782637.	1694.	3975.	7284.	0.81	3.87	560.	11971.
3.5	46.66	193895.	785378.	1165.	3764.	5218.	0.70	3.05	500.	8510.
4.0	45.04	196745.	787194.	830.	3571.	3833.	0.61	2.34	449.	6217.
4.5	41.47	198096.	788587.	639.	3397.	2705.	0.44	1.86	407.	4459.
5.0	36.28	200697.	788562.	572.	3257.	2045.	0.40	1.53	370.	3489.
	AVG=	192789.	784617.	1206.	3742.	5970.	0.63	3.29	510.	9568.

CHEMICAL EFFICIENCY (UNBURNT FUEL ONLY) = 57.131%
CHEMICAL EFFICIENCY (UNBURNT FUEL AND CO)= 55.202%

Table 3.5.

Composition (wet basis), velocity, temperature, their average valves and efficiencies for the 55^{o} counter-swirl, propane case

55 CT-SWIRL PROPANE

R CM	U M/S	O2 PPM	N2 PPM	CO PPM	FUEL PPM	CO2 PPM	NO PPM	NOX PPM	T K	H2O PPM
0.0	51.60	147689.	778222.	3680.	1972.	31363.	0.56	8.55	1144.	46723.
0.5	51.22	148541.	772877.	3517.	2205.	29350.	0.57	8.52	1102.	43824.
1.0	50.66	149889.	774645.	3355.	2597.	27873.	0.64	8.39	1040.	41637.
1.5	49.42	158531.	769471.	3218.	3384.	26326.	0.86	7.73	944.	39393.
2.0	48.54	170612.	776104.	3159.	3907.	17969.	1.01	6.65	836.	28170.
2.5	46.45	181051.	774223.	3067.	5102.	13891.	1.07	5.17	711.	22612.
3.0	43.75	192906.	775786.	2297.	5449.	8656.	1.01	3.95	566.	14605.
3.5	41.65	196711.	783385.	1844.	4938.	4923.	0.80	2.91	475.	9022.
4.0	38.86	204780.	780720.	1341.	4189.	4148.	0.61	2.02	417.	7318.
4.5	37.03	209200.	778406.	806.	3836.	3826.	0.50	1.81	378.	6175.
5.0	32.58	207545.	780884.	806.	3748.	3760.	0.44	1.65	362.	6088.
	AVG=	195948.	778587.	1720.	4280.	7944.	0.70	3.24	517.	12886.

CHEMICAL EFFICIENCY (UNBURNT FUEL ONLY) = 54.002%
CHEMICAL EFFICIENCY (UNBURNT FUEL AND CO)= 51.419%

Table 3.6.

Mass flux weighted average composition (ppm), temperature (^{o}K) and efficiencies (%) for all the test conditions listed in Table 2.3.

	$T^{o}K$	$[O_2]$	$[N_2]$	[CO]	[FUEL]	$[CO_2]$	$[H_2O]$	[NO]	$[NO_x]$	η'_c	η_c	η_T
PROPANE:												
55^{o} Co-	513	195211	785005	164	4424	5837	8001	3.66	5.86	51.16	50.91	35.34
30^{o} Co-	521	202346	784584	208	4209	4049	5677	1.70	4.33	51.77	51.44	35.36
30^{o} Ct-	510	192789	784617	1206	3742	5970	9568	0.63	3.29	57.13	55.20	36.26
55^{o} Ct-	517	195948	778587	1720	4280	7944	12886	0.70	3.24	54.00	51.42	34.05
METHANE:												
55^{o} Co-	499	199642	770700	138	9343	6782	13840	-	-	58.27	58.05	41.37
30^{o} Ct-	517	199013	774983	671	9395	4889	11119	-	-	57.05	55.96	41.28

Table 3.7.

Composition (wet basis), velocity, temperature, their average valves and efficiencies for the 55° co-swirl, methane case (Oxides of nitrogen are not measured.)

55 CO-SWIRL METHANE

R CM	U M/S	O2 PPM	N2 PPM	CO PPM	FUEL PPM	CO2 PPM	NO PPM	NOX PPM	T K	H2O PPM
0.0	49.54	61954.	714038.	1318.	0.	73396.	0.00	0.00	1923.	149429.
0.5	49.57	53334.	709309.	1153.	0.	78491.	0.00	0.00	1906.	159288.
1.0	49.91	49928.	706853.	1039.	0.	80060.	0.00	0.00	1877.	162198.
1.5	50.05	72229.	702102.	1109.	454.	73011.	0.00	0.00	1820.	148239.
2.0	49.37	121145.	711380.	1220.	3718.	53602.	0.00	0.00	1684.	109644.
2.5	46.93	174076.	723313.	960.	14342.	28507.	0.00	0.00	1167.	58934.
3.0	37.25	197431.	779833.	0.	15148.	2529.	0.00	0.00	460.	5058.
3.5	34.98	207942.	779231.	0.	11413.	763.	0.00	0.00	345.	1527.
4.0	35.23	213478.	776602.	0.	9017.	287.	0.00	0.00	338.	573.
4.5	34.88	213600.	779579.	0.	7772.	0.	0.00	0.00	337.	0.
5.0	31.78.	212532.	780423.	0.	6934.	0.	0.00	0.00	340.	0.
	AVG=	199642.	770700.	138.	9343.	6782.	0.00	0.00	499.	13840.

CHEMICAL EFFICIENCY (UNBURNT FUEL ONLY) = 58.267%
CHEMICAL EFFICIENCY (UNBURNT FUEL AND CO)= 58.047%

Table 3.8.

Composition (wet basis), velocity, temperature, their average valves and efficiencies for the 30^{o} counter-swirl, methance case (Oxides of nitrogen are not measured.)

30 CT-SWIRL METHANE

R CM	U M/S	O2 PPM	N2 PPM	CO PPM	FUEL PPM	CO2 PPM	NO PPM	NOX PPM	T K	H2O PPM
0.0	48.59	172953.	777586.	1488.	7978.	12339.	0.00	0.00	845.	27654.
0.5	48.16	175500.	772492.	1348.	9432.	12258.	0.00	0.00	815.	27213.
1.0	48.10	177394.	771122.	1265.	10804.	12224.	0.00	0.00	776.	26979.
1.5	47.98	181153.	770869.	1354.	11596.	10324.	0.00	0.00	730.	23355.
2.0	48.13	185866.	770080.	1439.	11773.	9252.	0.00	0.00	678.	21382.
2.5	47.70	189524.	774880.	1080.	10934.	6560.	0.00	0.00	625.	15281.
3.0	46.47	194254.	777140.	790.	10039.	5414.	0.00	0.00	566.	12409.
3.5	45.19	199272.	777999.	634.	9680.	4521.	0.00	0.00	509.	10312.
4.0	43.44	201061.	776083.	496.	9385.	3862.	0.00	0.00	460.	8716.
4.5	41.13	210246.	772702.	289.	7976.	2674.	0.00	0.00	420.	5927.
5.0	33.99	206204.	778879.	388.	7552.	2184.	0.00	0.00	383.	5144.
	AVG=	199013.	774983.	671.	9395.	4889.	0.00	0.00	517.	11119.

CHEMICAL EFFICIENCY (UNBURNT FUEL ONLY) = 57.050%
CHEMICAL EFFICIENCY (UNBURNT FUEL AND CO)= 55.957%

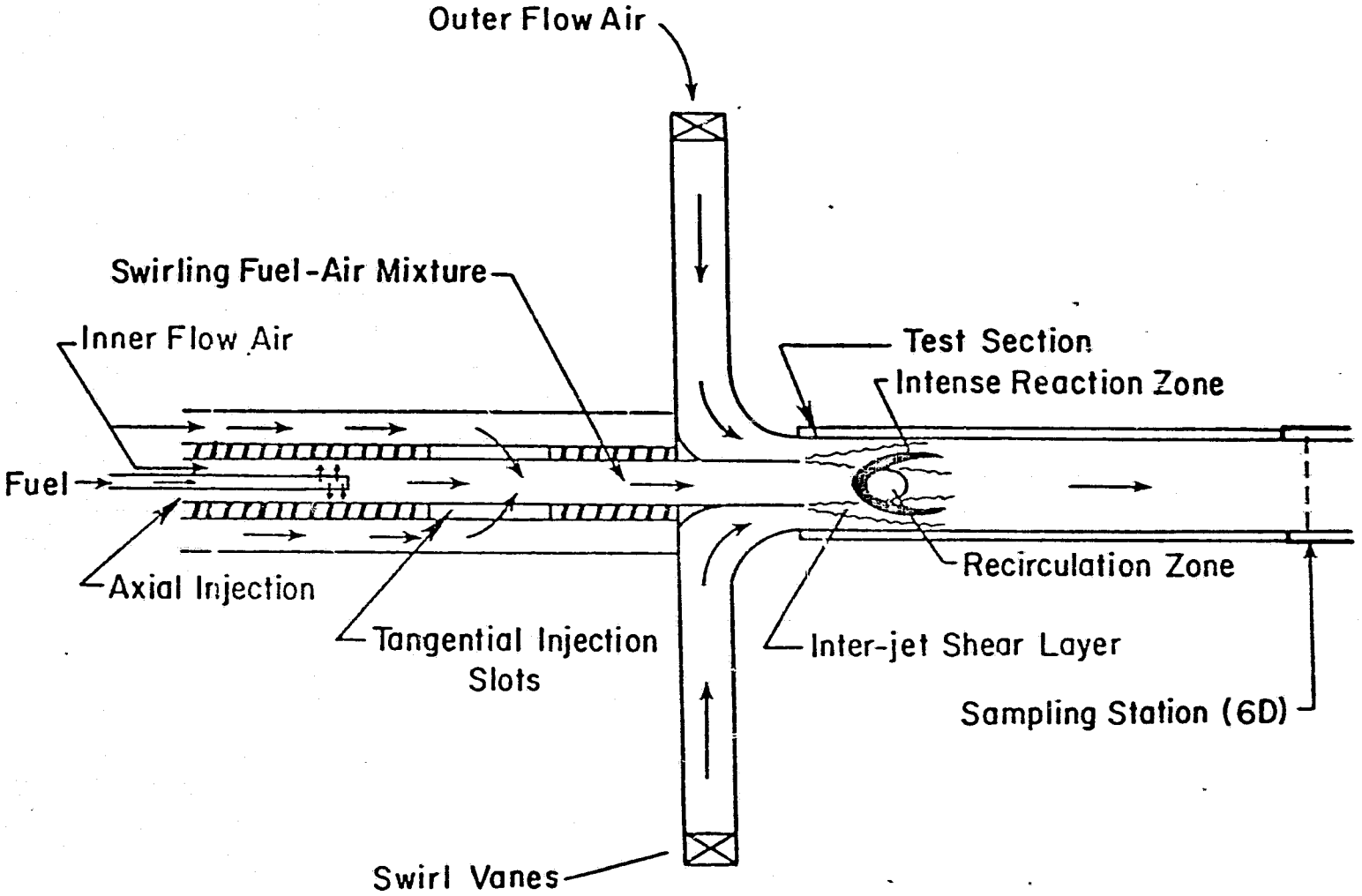

Figure 1-1: Schematic diagram of the swirl combustor.

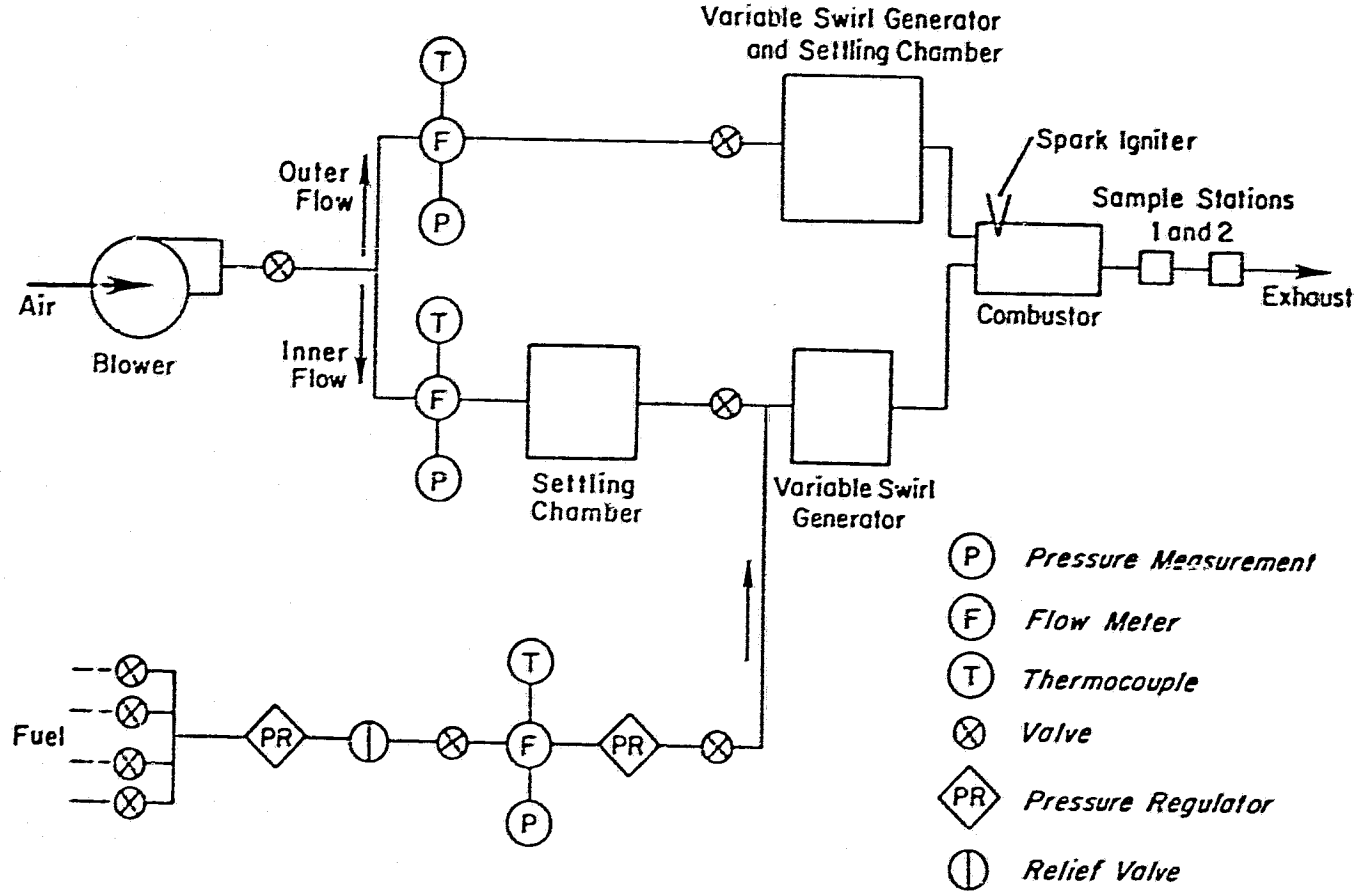

Figure 2-1: Schematic diagram of the swirl combustor test facility.

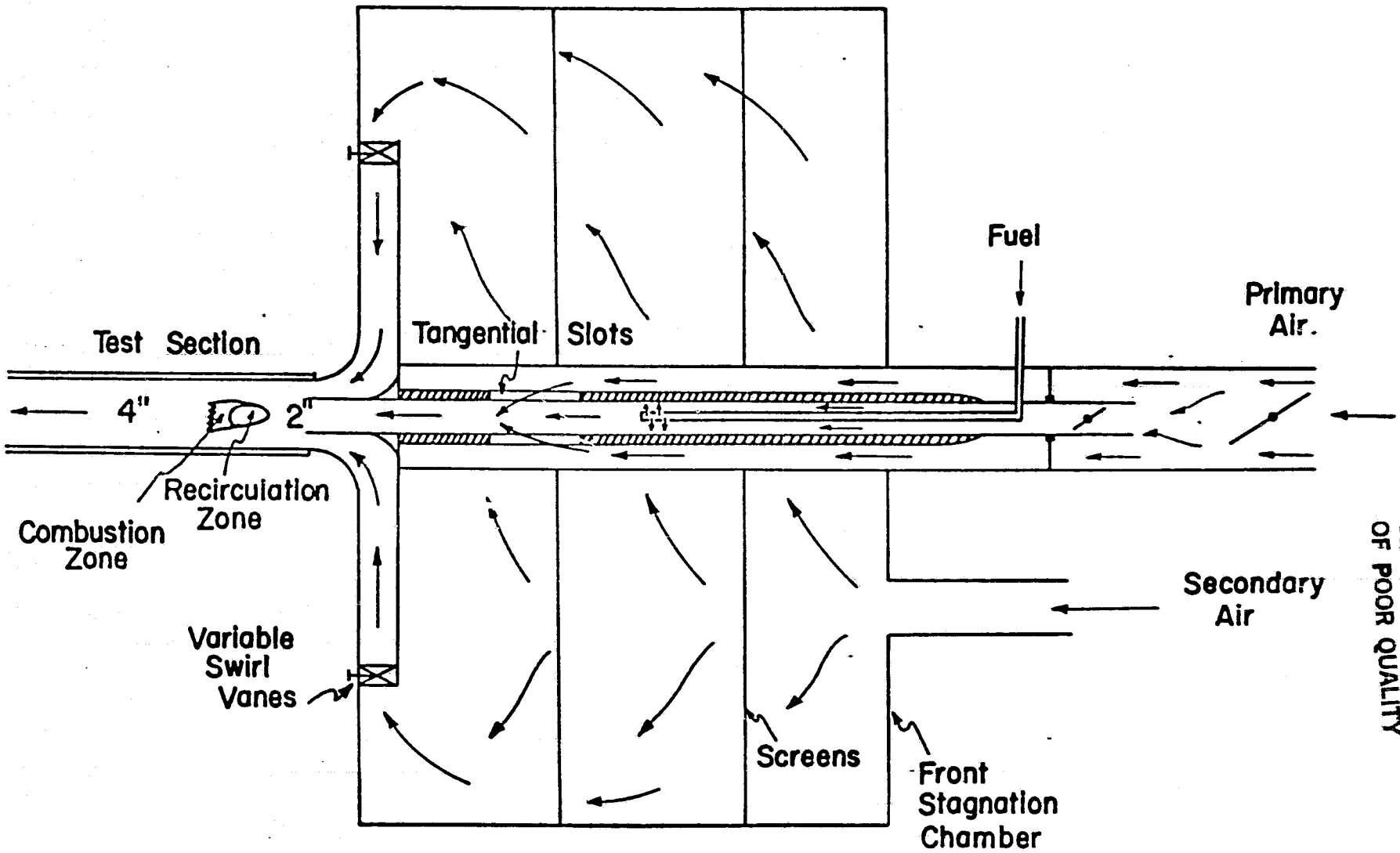

Figure 2-2: Variable swirl generators.

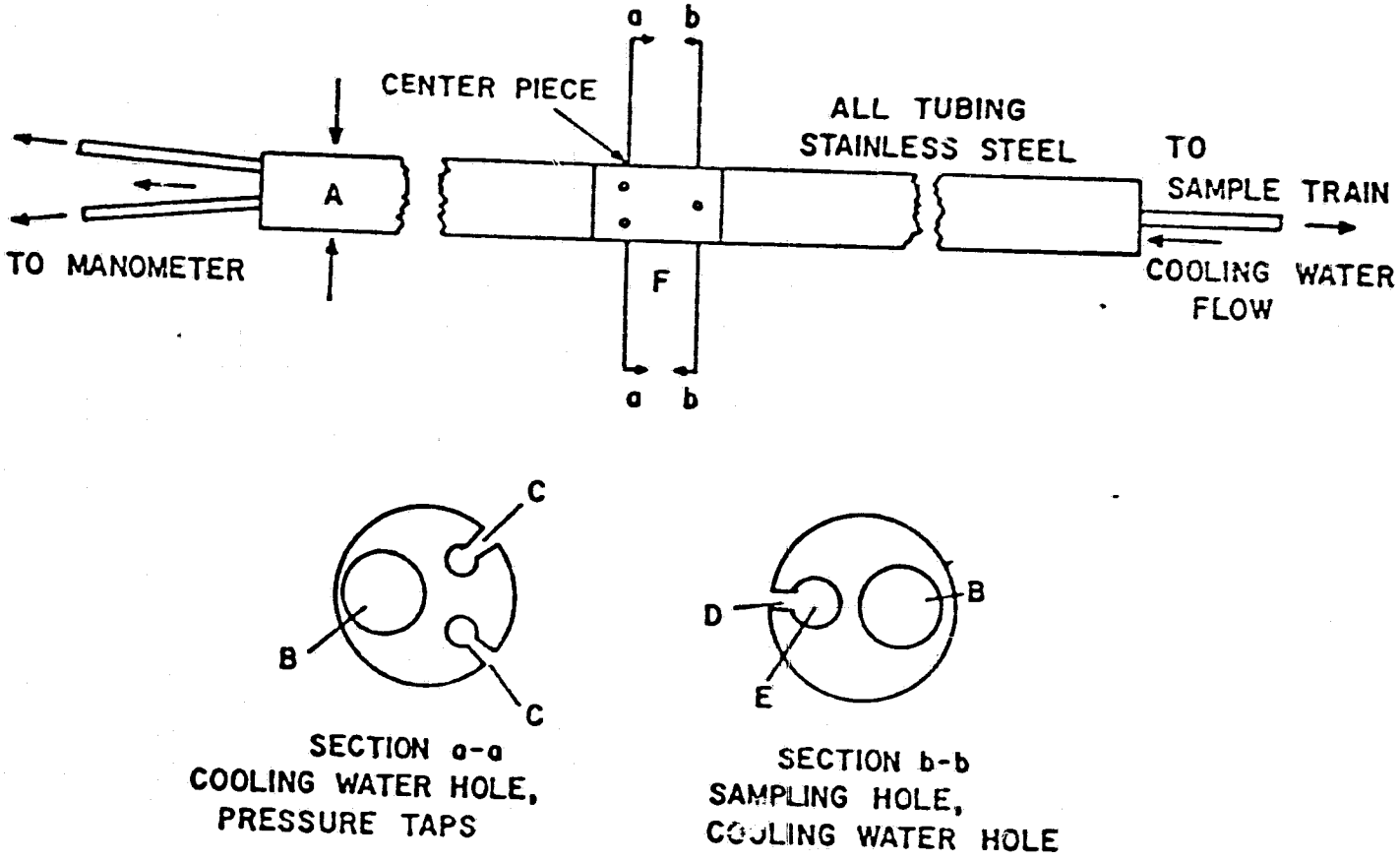

Dimensions: A = 7.9 mm O.D., B = 2.5 mm dia, C = 0.9 mm dia,
D = 1.6 mm dia, E = 1.8 mm dia, F = 7.9 mm

Figure 2-3: Cylindrical probe for sampling and velocity measurements.

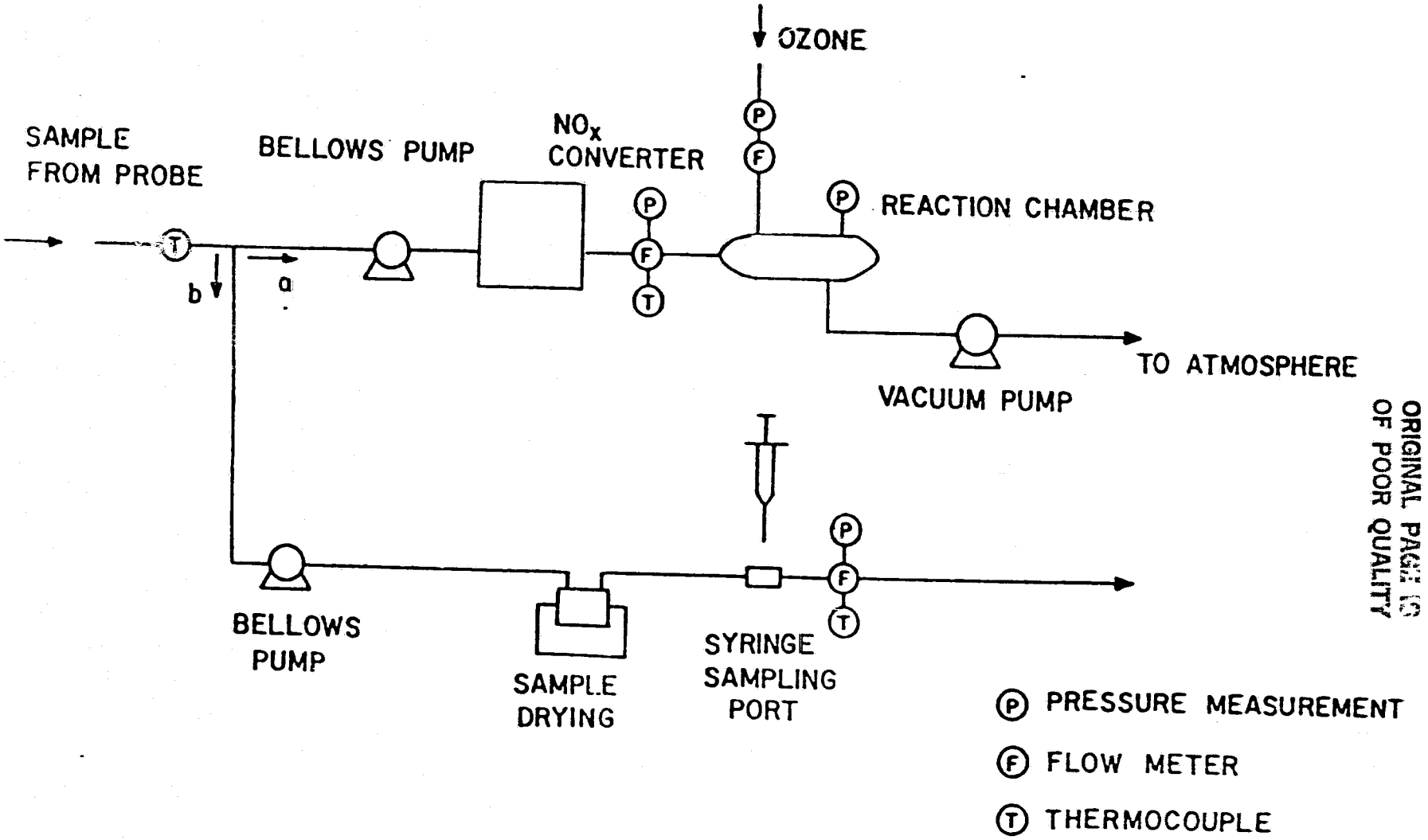

Figure 2-4: Sample train and analysis system.

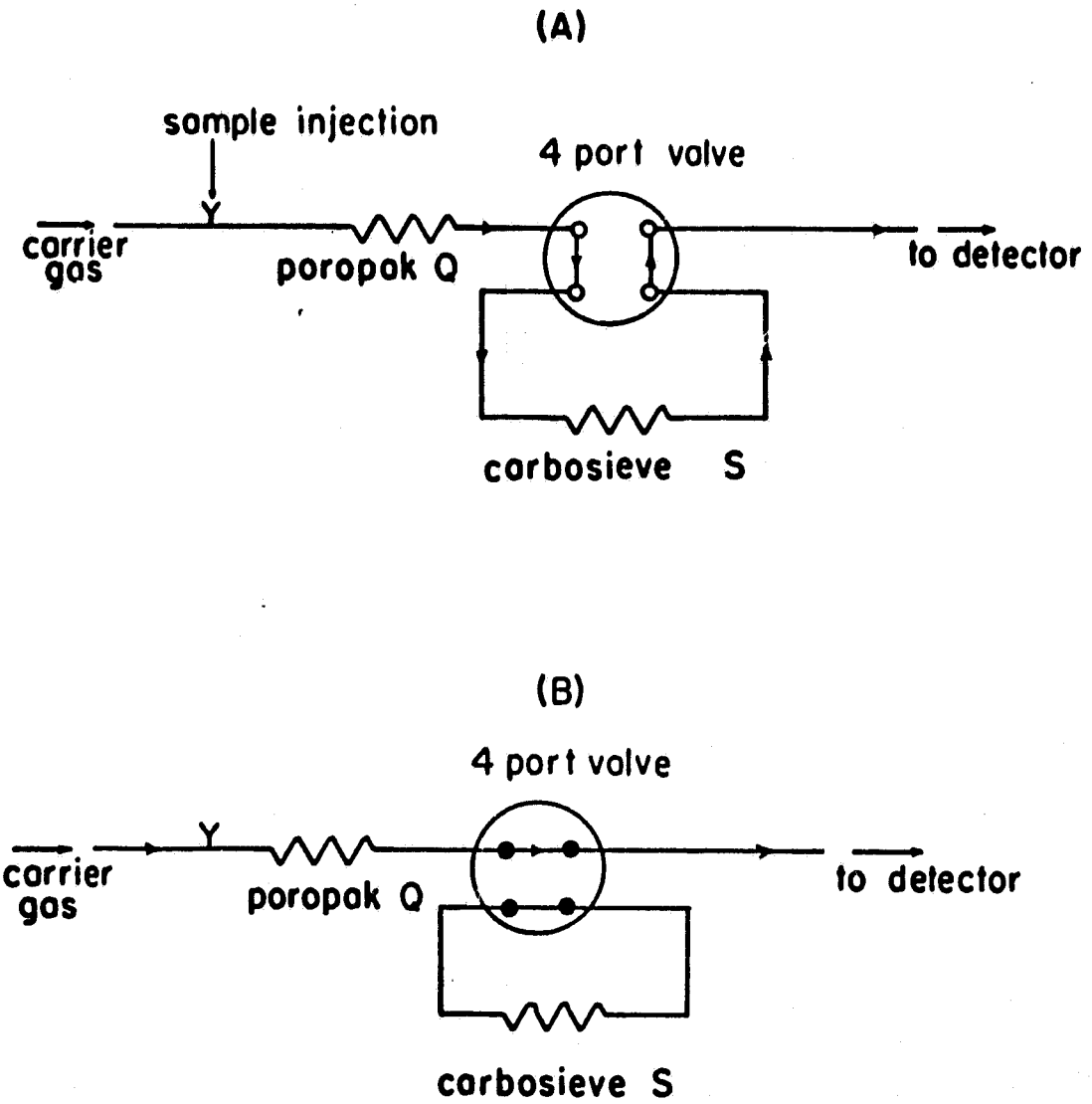

Figure 2-5: Schematic diagram of column arrangement and flow paths in the gas chromatograph for valve positions A and B.

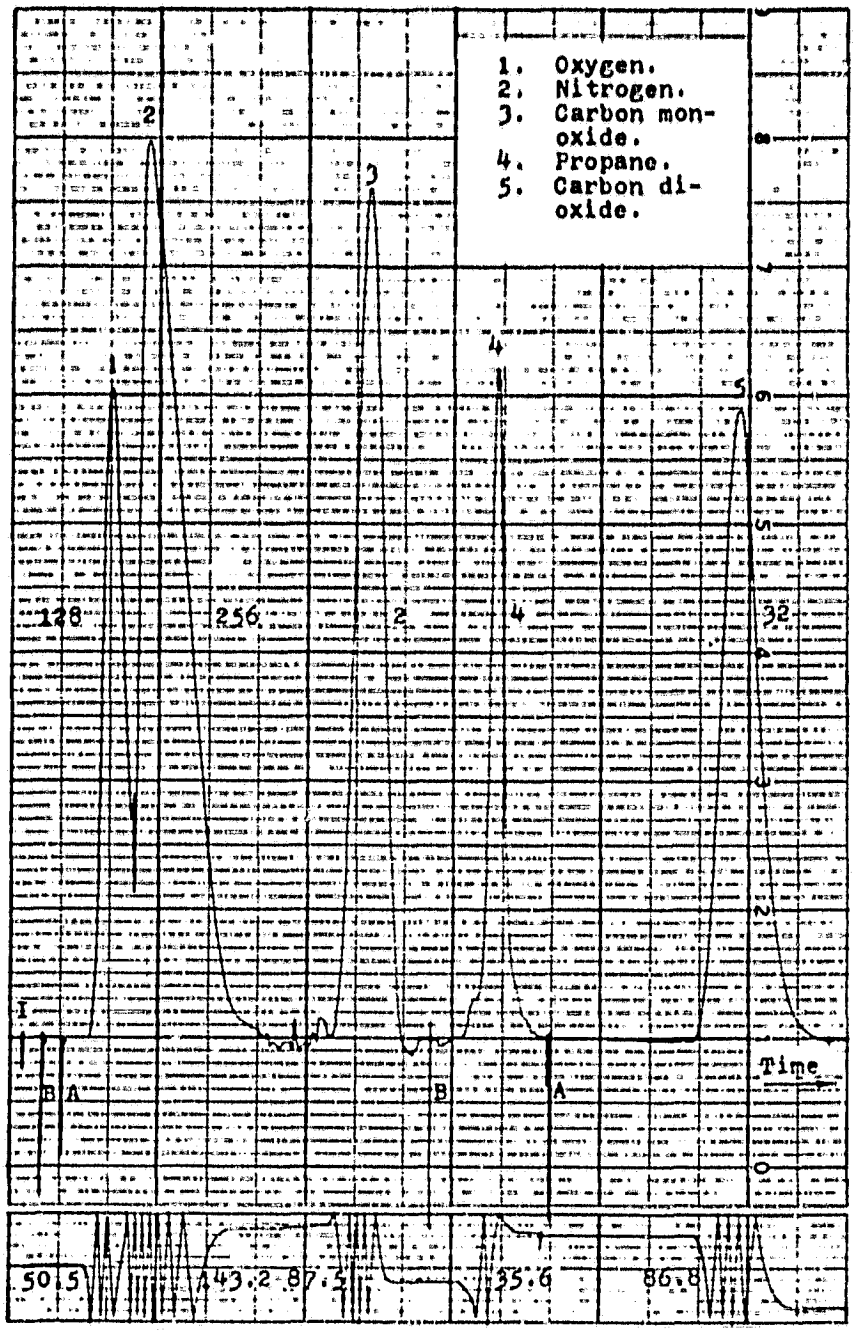

Figure 2-6. Sample chromatogram. (The numbers on the sides of the peaks indicate detector attenuation. The sample injection point (I) and points of valve switching to positions A and B are indicated. The time axis is compressed between peaks. The integrator trace at the bottom shows the number of line crossings).

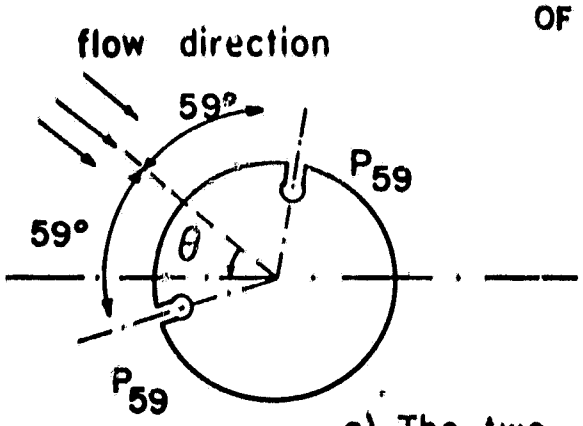

a) The two pressures are balanced to obtain θ.

b) One of the pressure taps is disconnected to measure $P_{59} - P_{atm}$

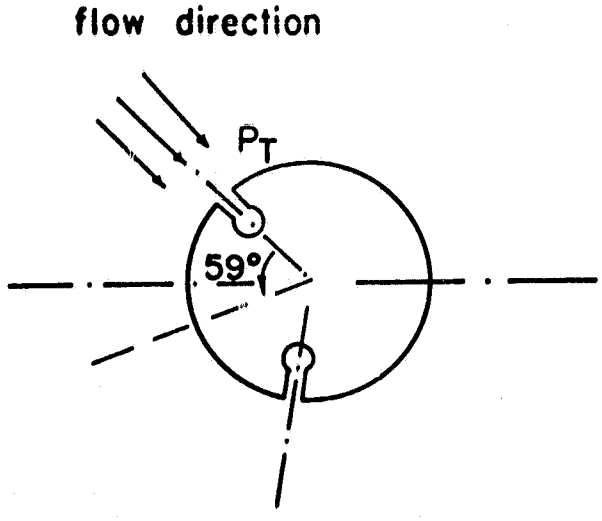

c) The probe is rotated by 59° to measure $P_T - P_{atm}$

The difference between (b) and (c) gives $P_T - P_{59}$

Figure 2-7: Velocity measurement scheme.

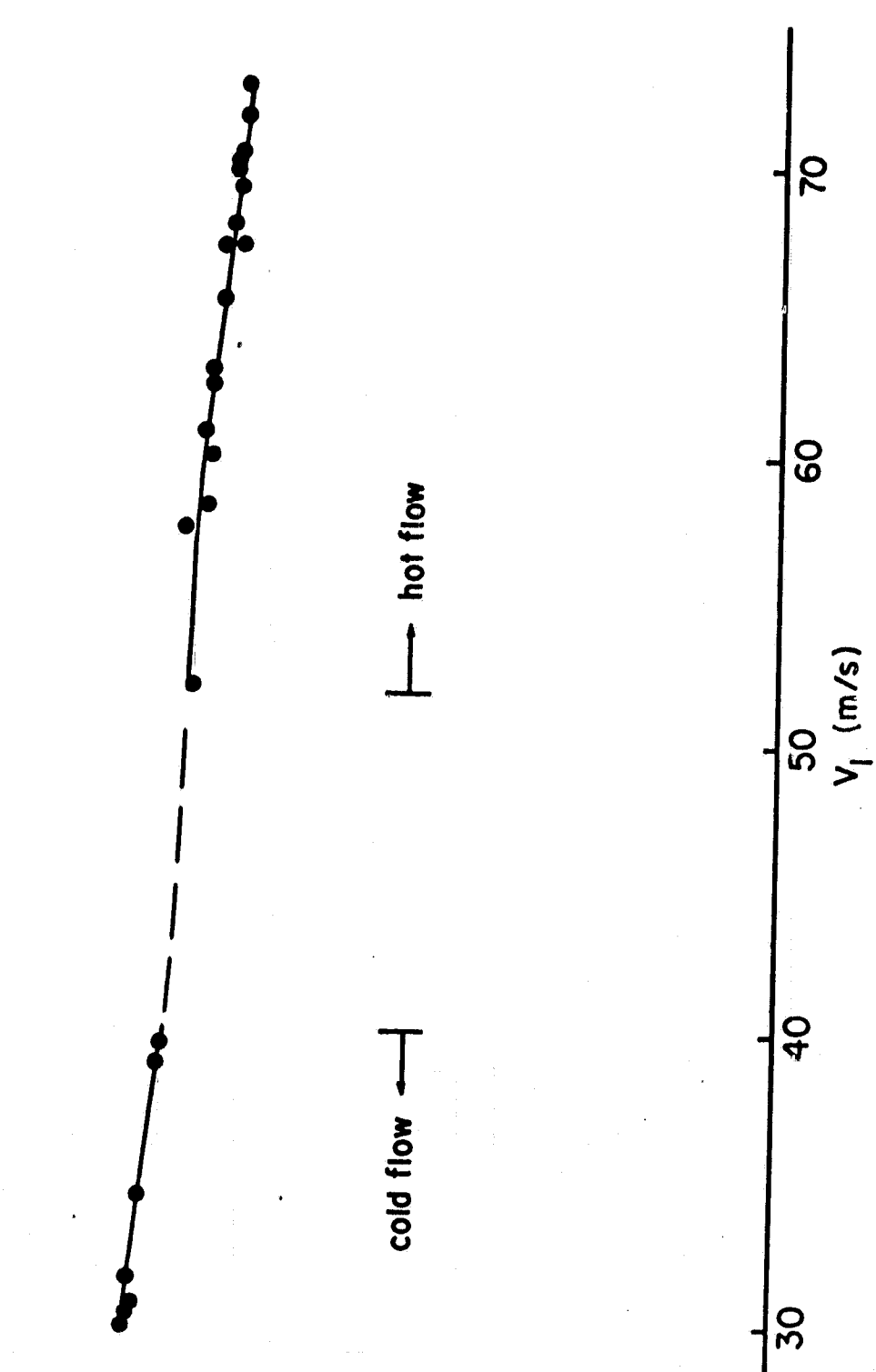

Figure 2-8: Velocity correction factor (f_c) plotted against the mean total velocity (V_I).

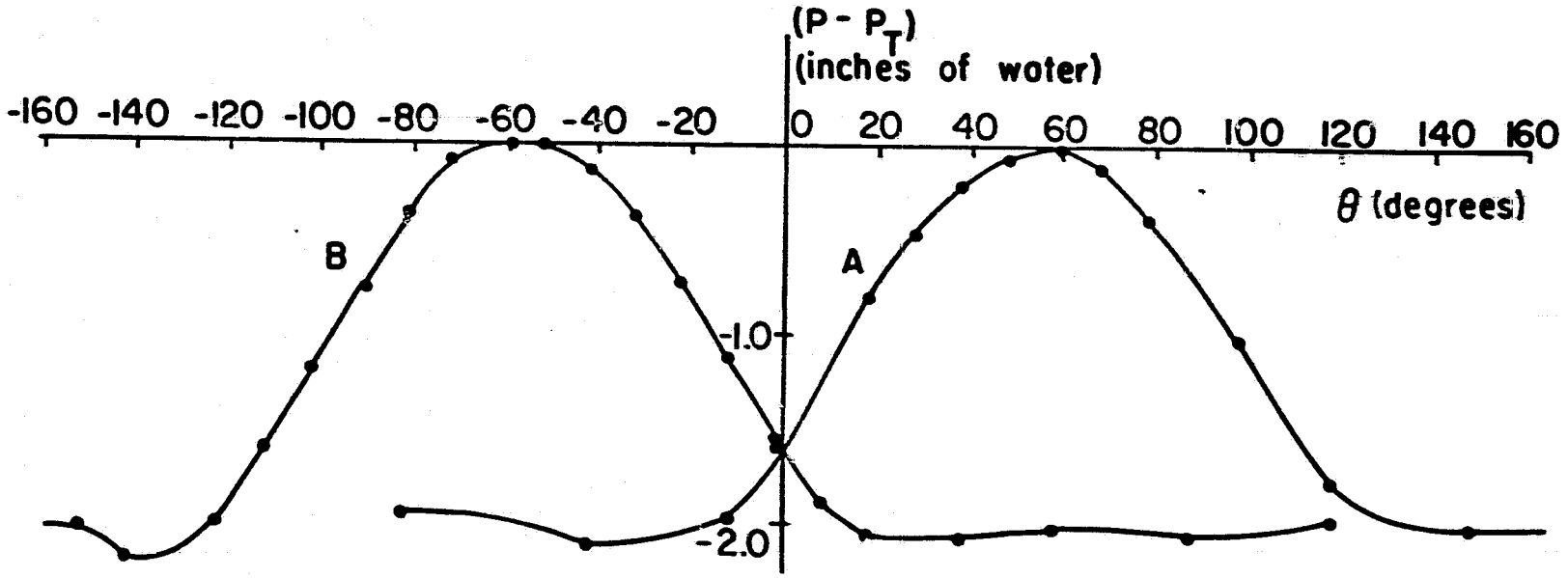

Figure 2-9: Pressure distribution around the surface of the cylindrical probe.

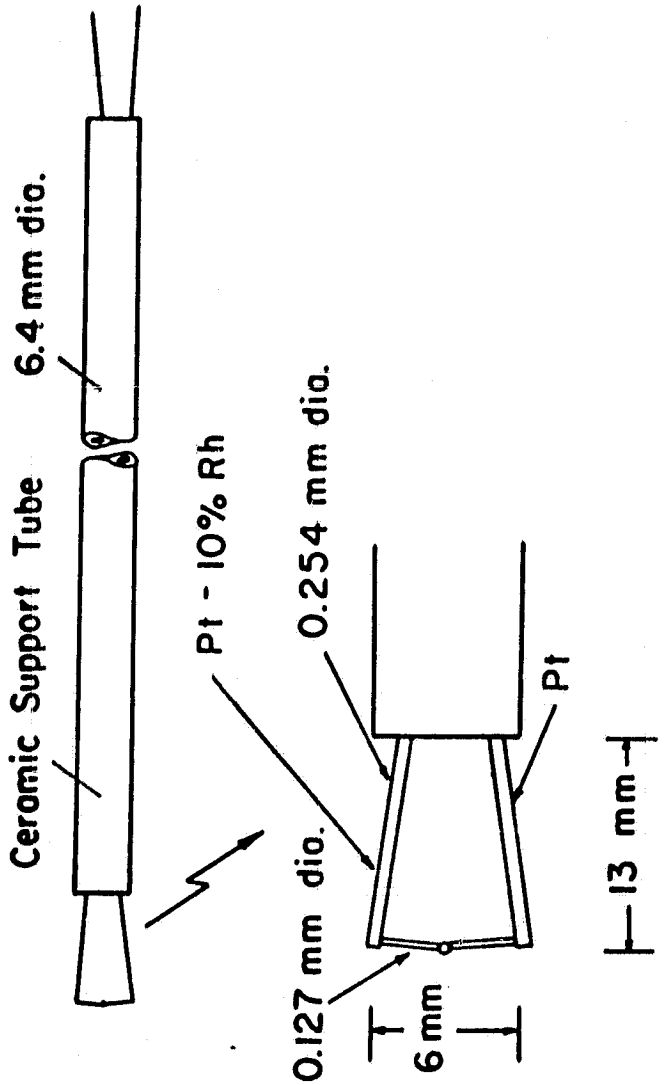

Figure 2-10: Schematic diagram of the thermocouple probe.

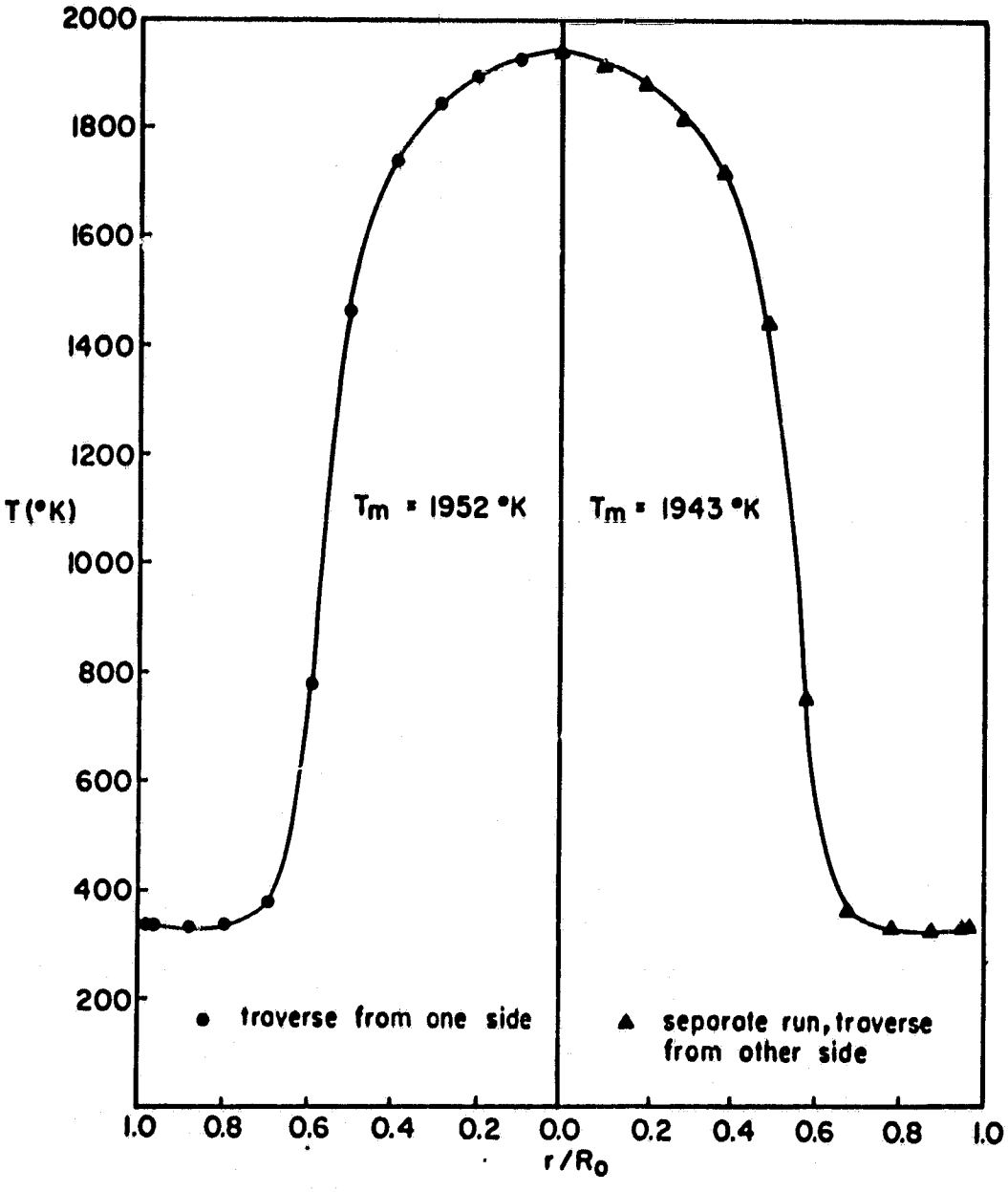

Figure 3-1: Mean temperature profiles for the 55° co-swirl, propane case showing axisymmetry in the combustor.

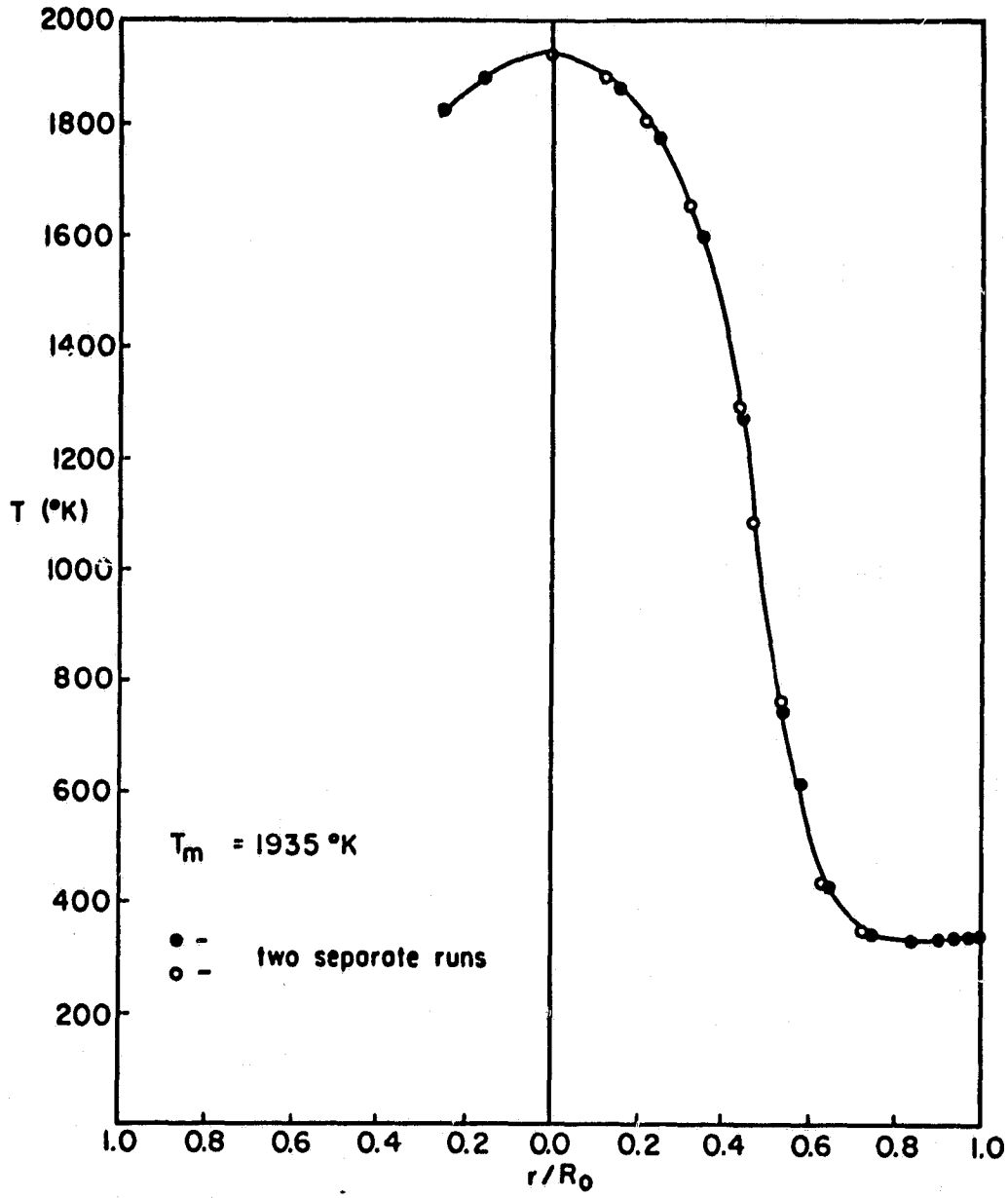

Figure 3-2: Mean temperature profiles for two separate runs of the 30° co-swirl case showing reproducibility of combustor operator.

Figure 3-3: Photograph of the combustor in operation under 55^{0} co-swirl, propane firing.

Figure 3-4: Photograph of the combustor in operation under 30^{0} co-swirl, propane firing.

Figure 3-5: Photograph of the combustor in operation under 30° counter-swirl, propane firing.

Figure 3-6: Photograph of the combustor in operation under 55° counter-swirl, propane firing.

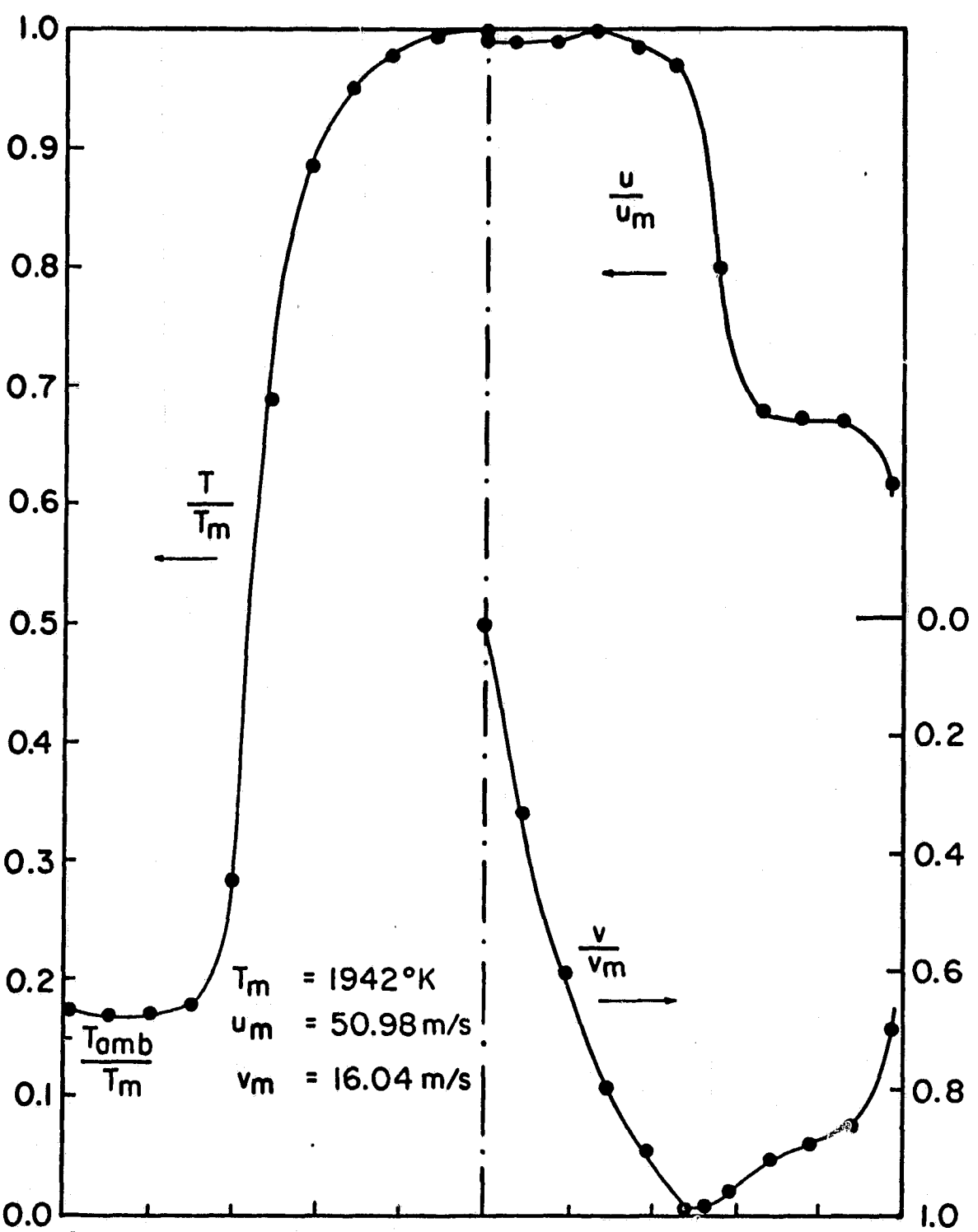

Figure 3-7: Mean temperature and velocity profiles for the 55° co-swirl, propane case.

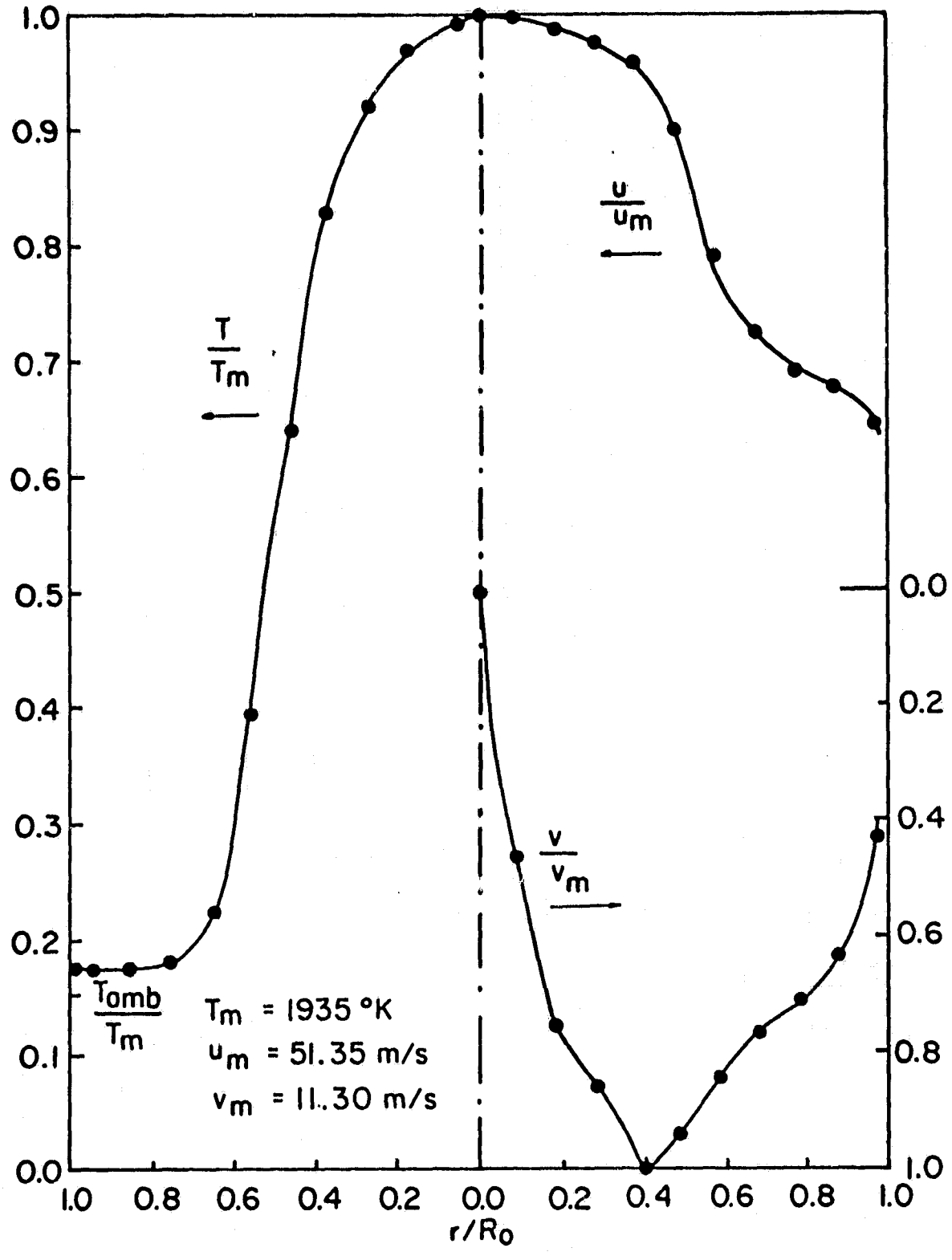

Figure 3-8: Mean temperature and velocity profiles for the 30° co-swirl, propane case.

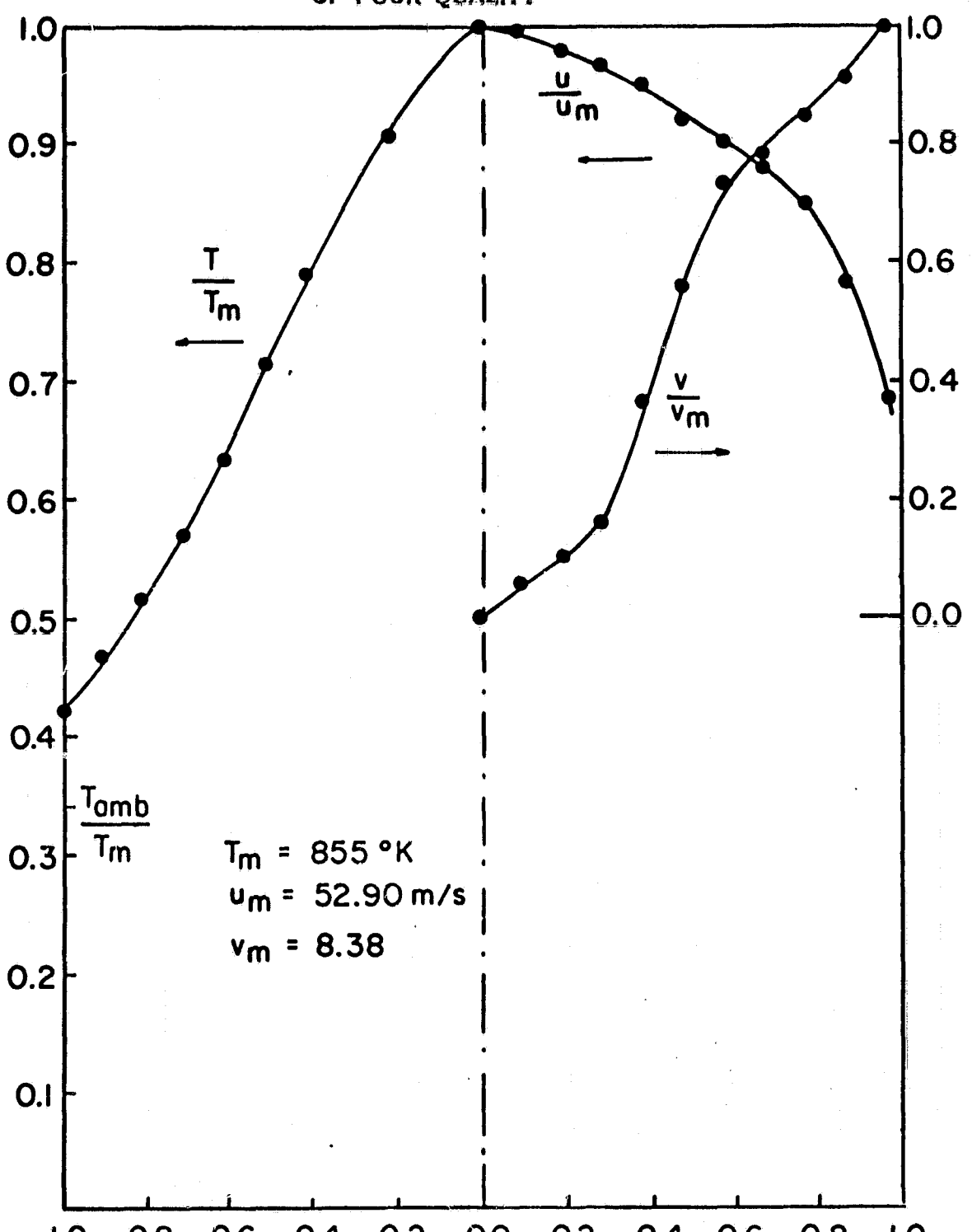

Figure 3-9: Mean temperature and velocity profiles for the 30° counter swirl, propane case.

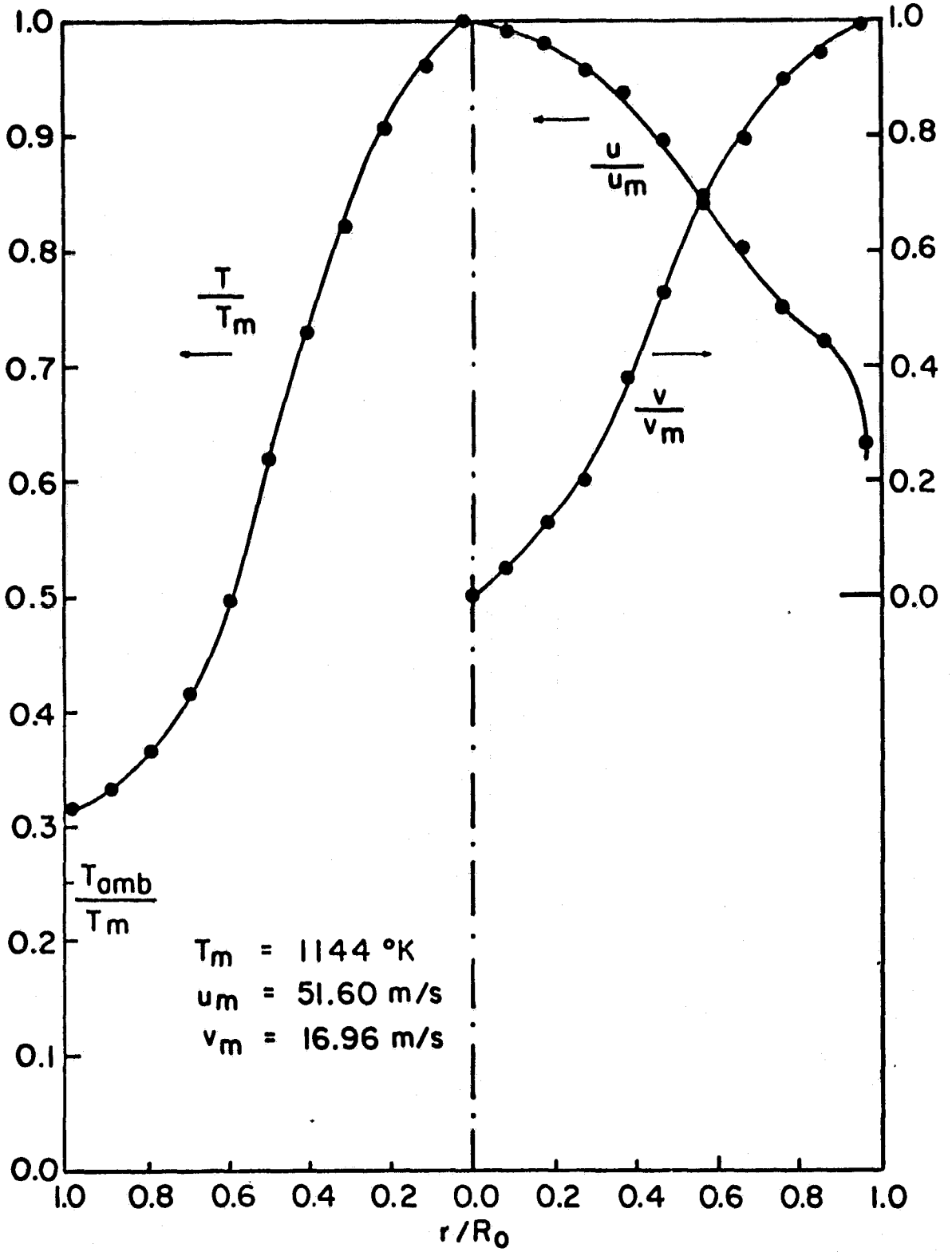

Figure 3-10: Mean temperature and velocity profiles for the 55° counter-swirl, propane case.

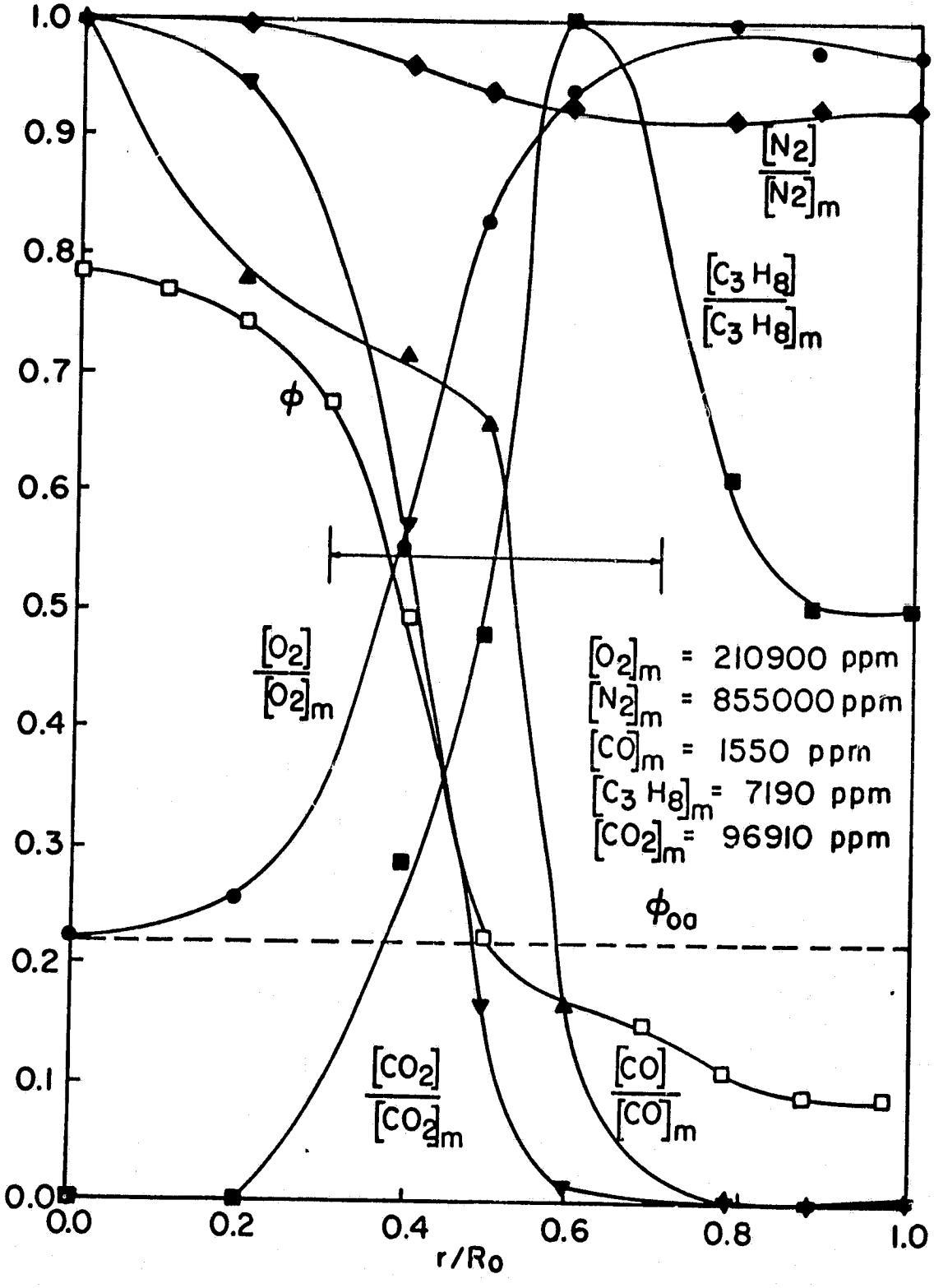

Figure 3-11: Mean composition and equivalence ratio profiles for the 55° co-swirl, propane case.

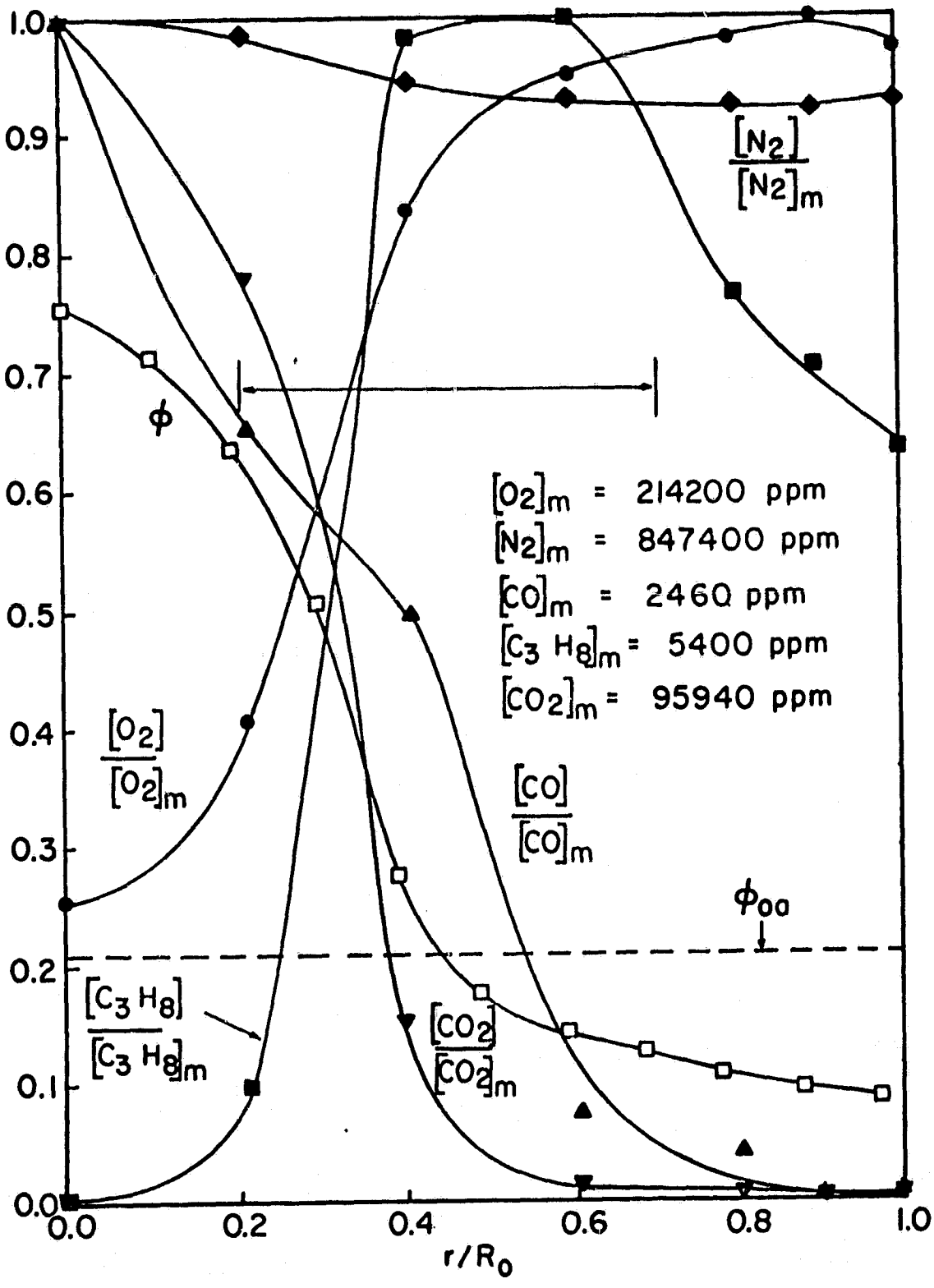

Figure 3-12: Mean composition and equivalence ratio profiles for the 30° co-swirl, propane case.

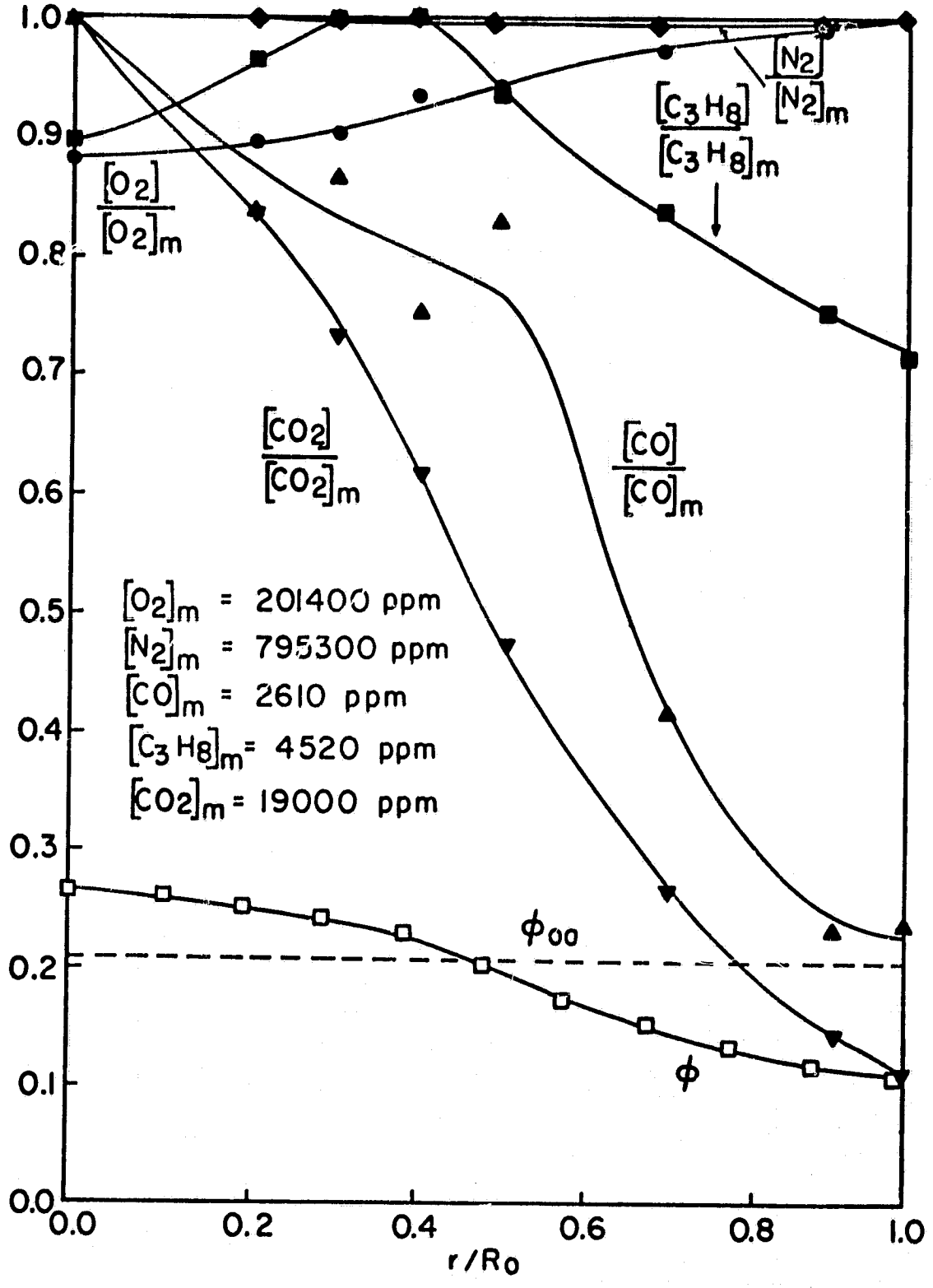

Figure 3-13: Mean composition and equivalence ratio profiles for the 30° counter-swirl, propane case.

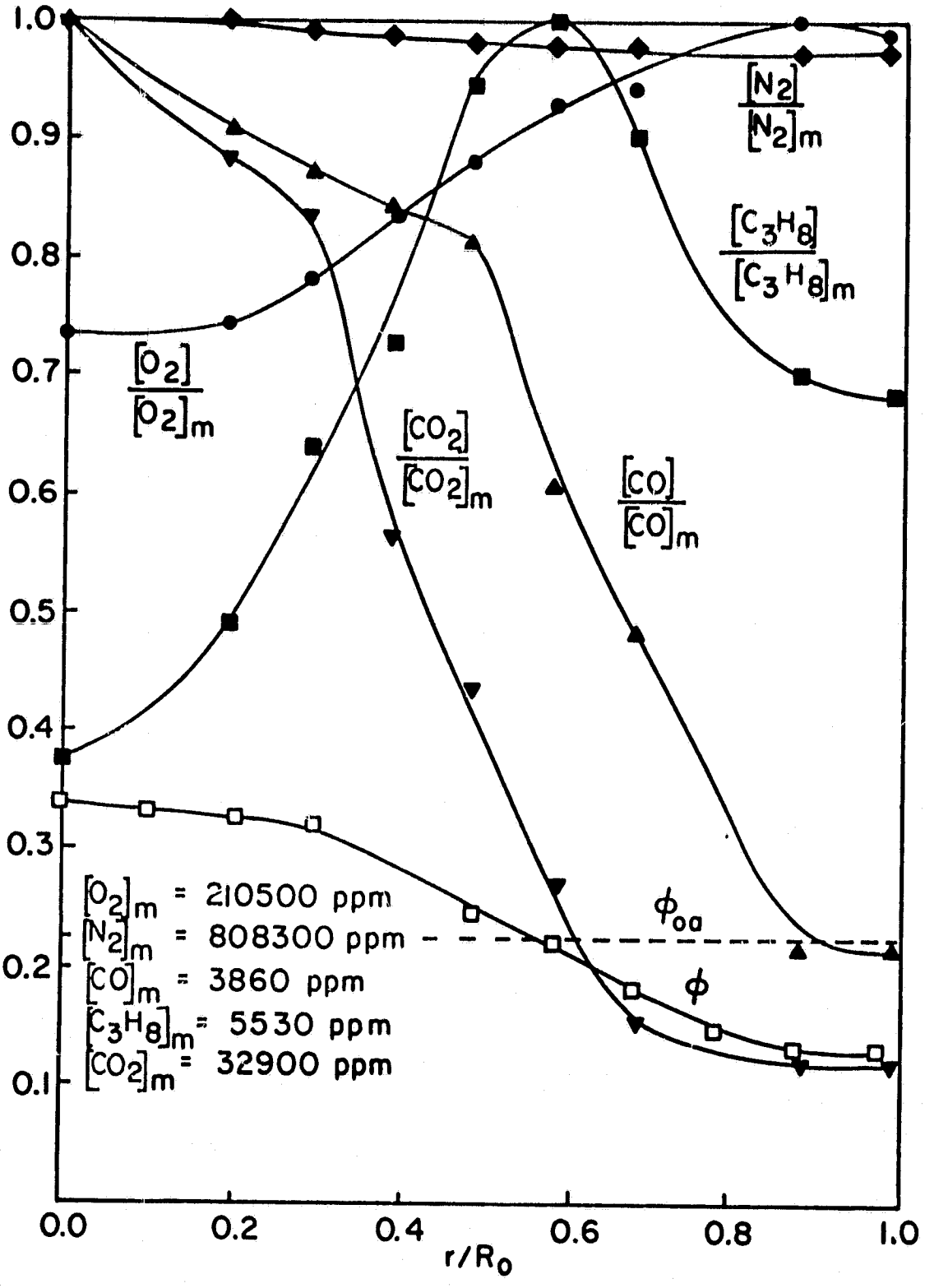

Figure 3-14: Mean composition and equivalence ratio profiles for the 55° counter-swirl, propane case.

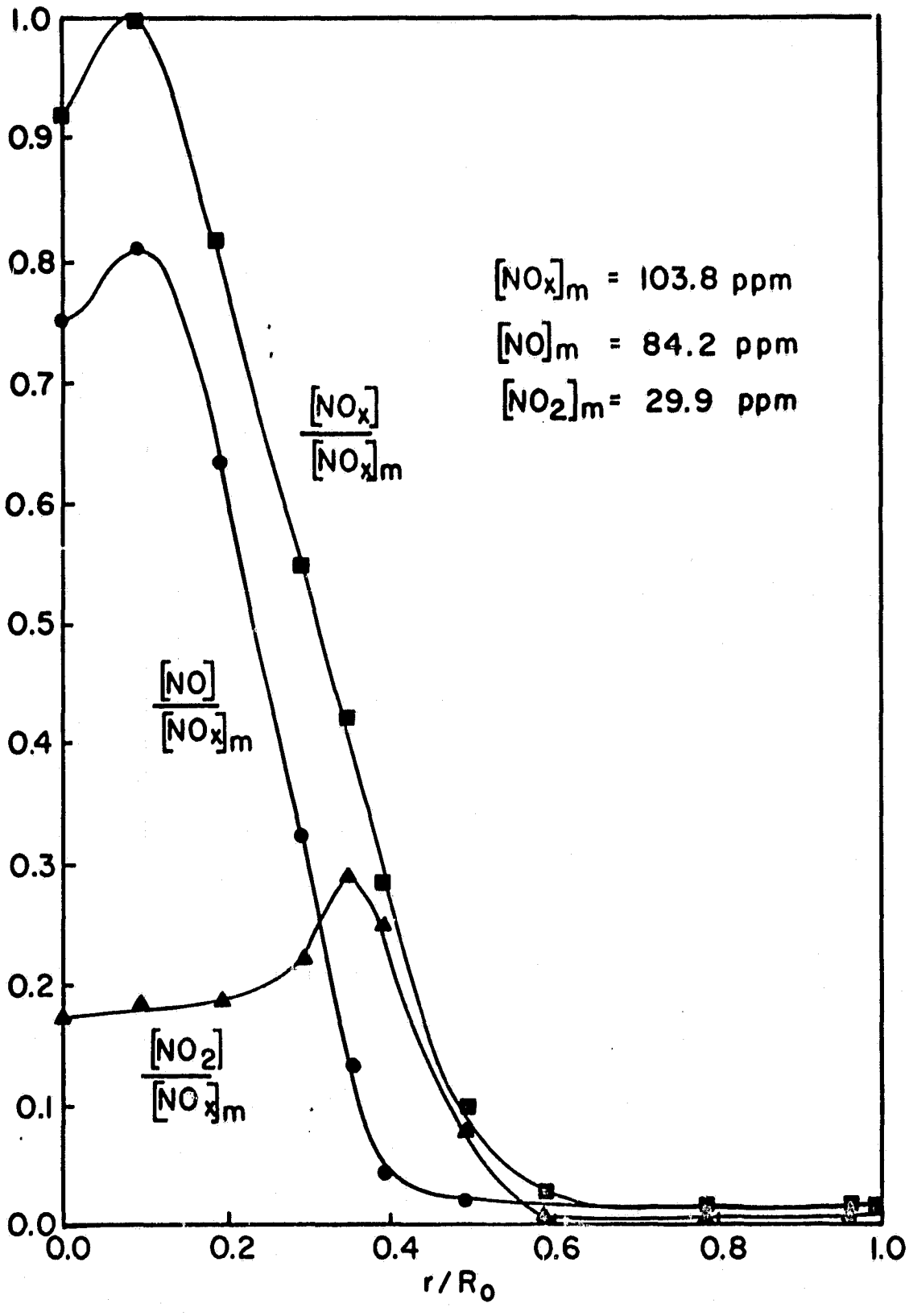

Figure 3-15: Mean concentration profiles of oxides of nitrogen for the 55^{0} co-swirl, propane case.

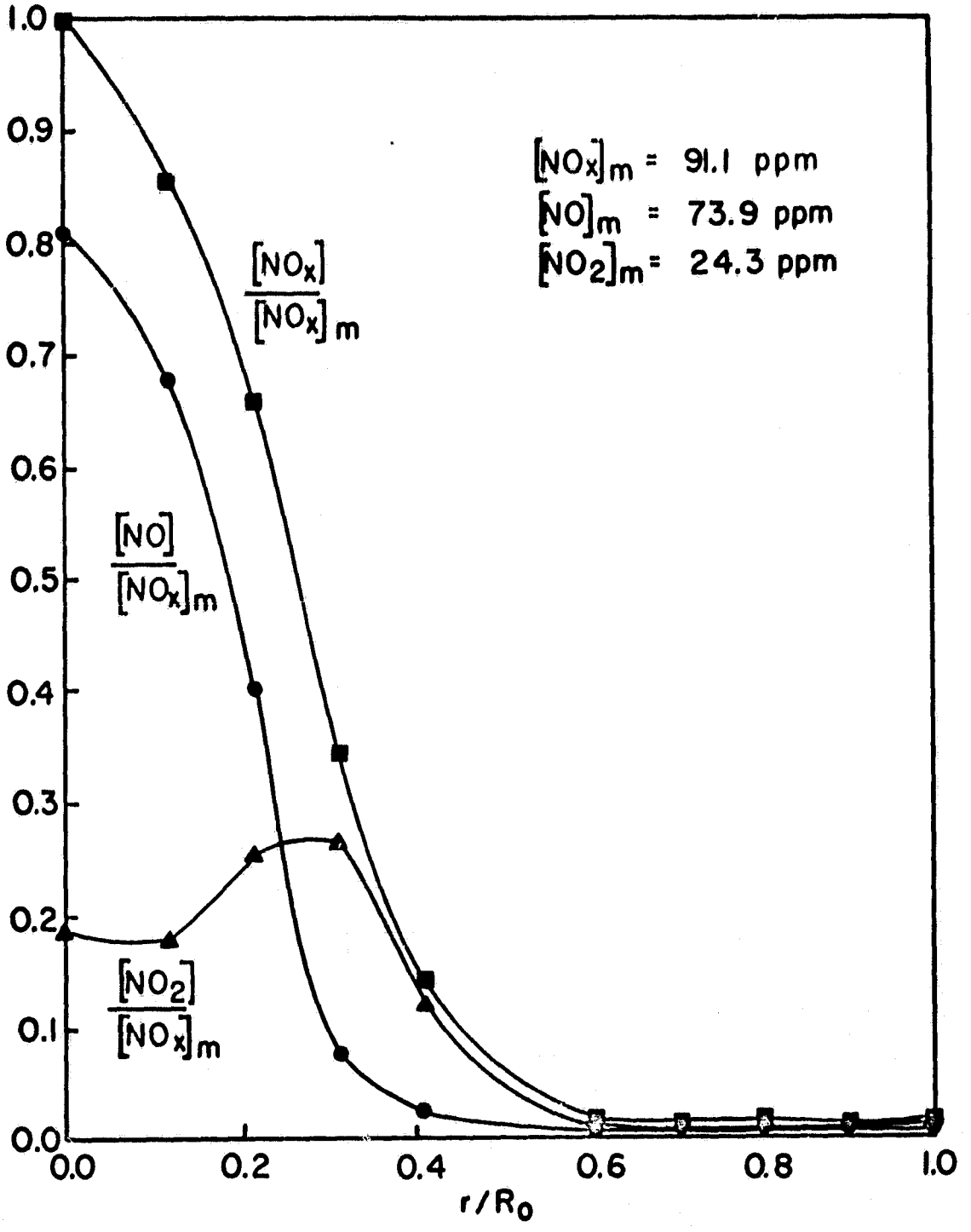

Figure 3-16: Mean concentration profiles of oxides of nitrogen for the 30° co-swirl, propane case.

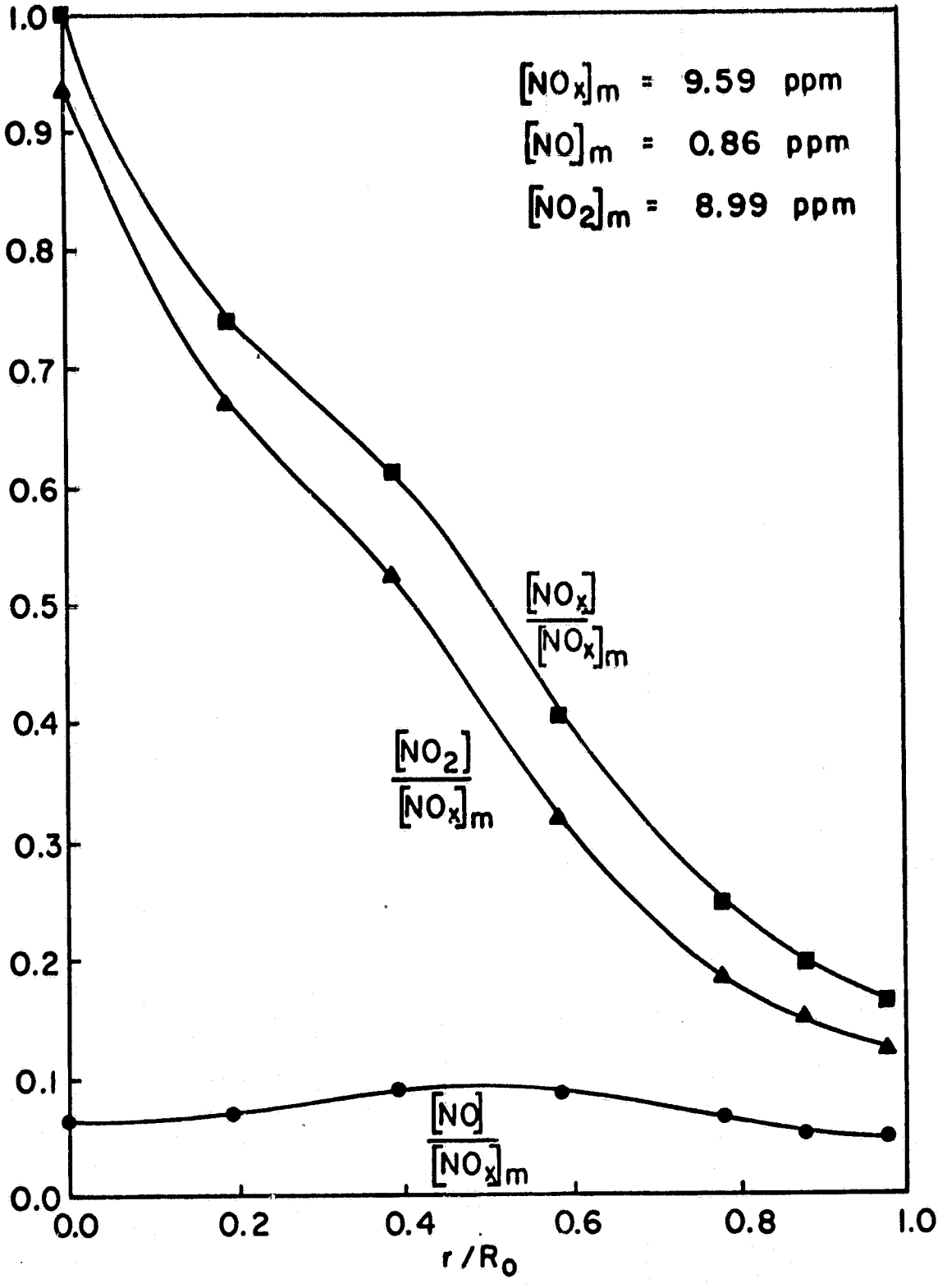

Figure 3-17: Mean concentration profiles of oxides of nitrogen for the 30^o counter-swirl case.

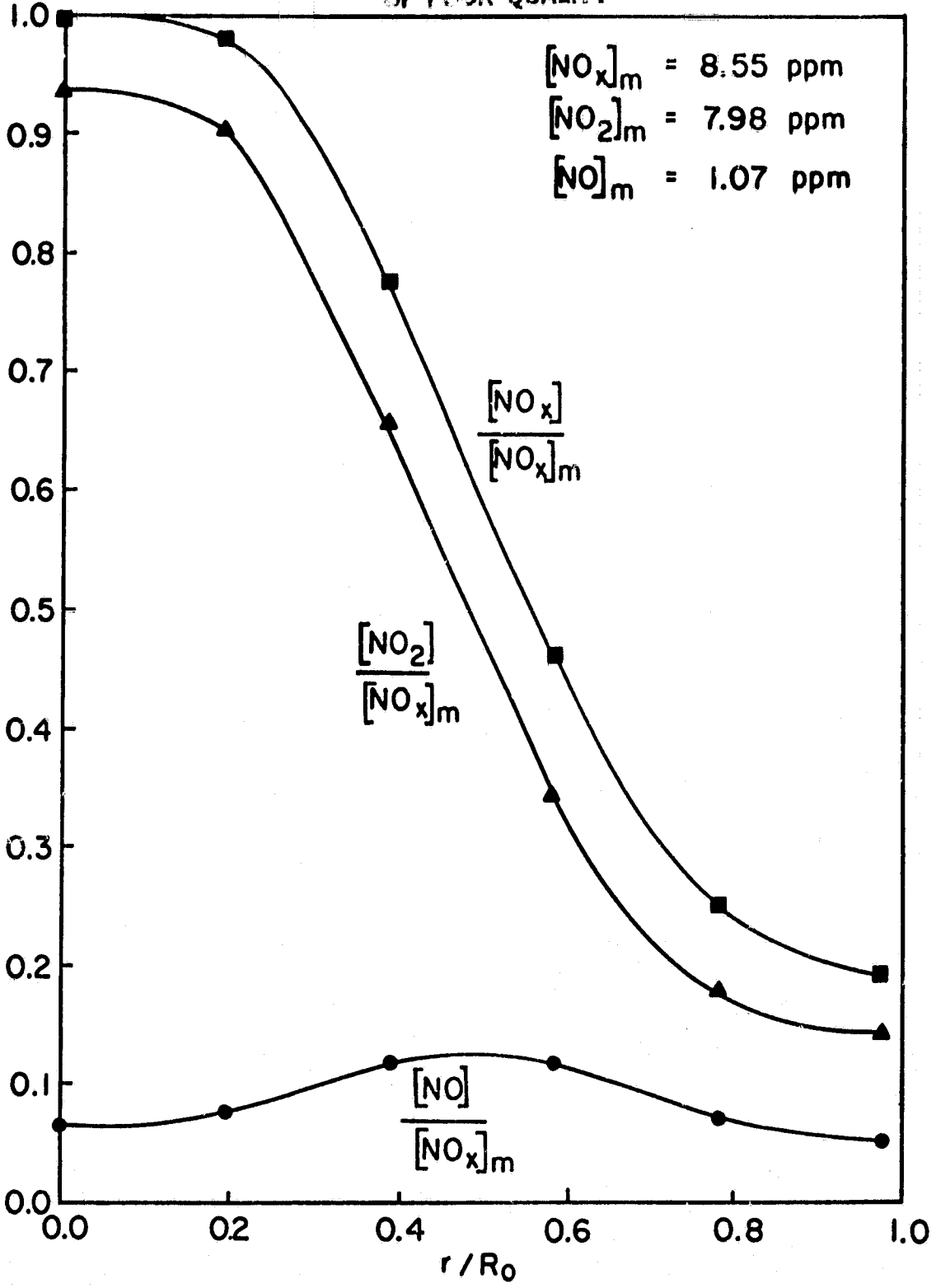

Figure 3-18: Mean concentration profiles of oxides of nitrogen for the 55° counter-swirl case.

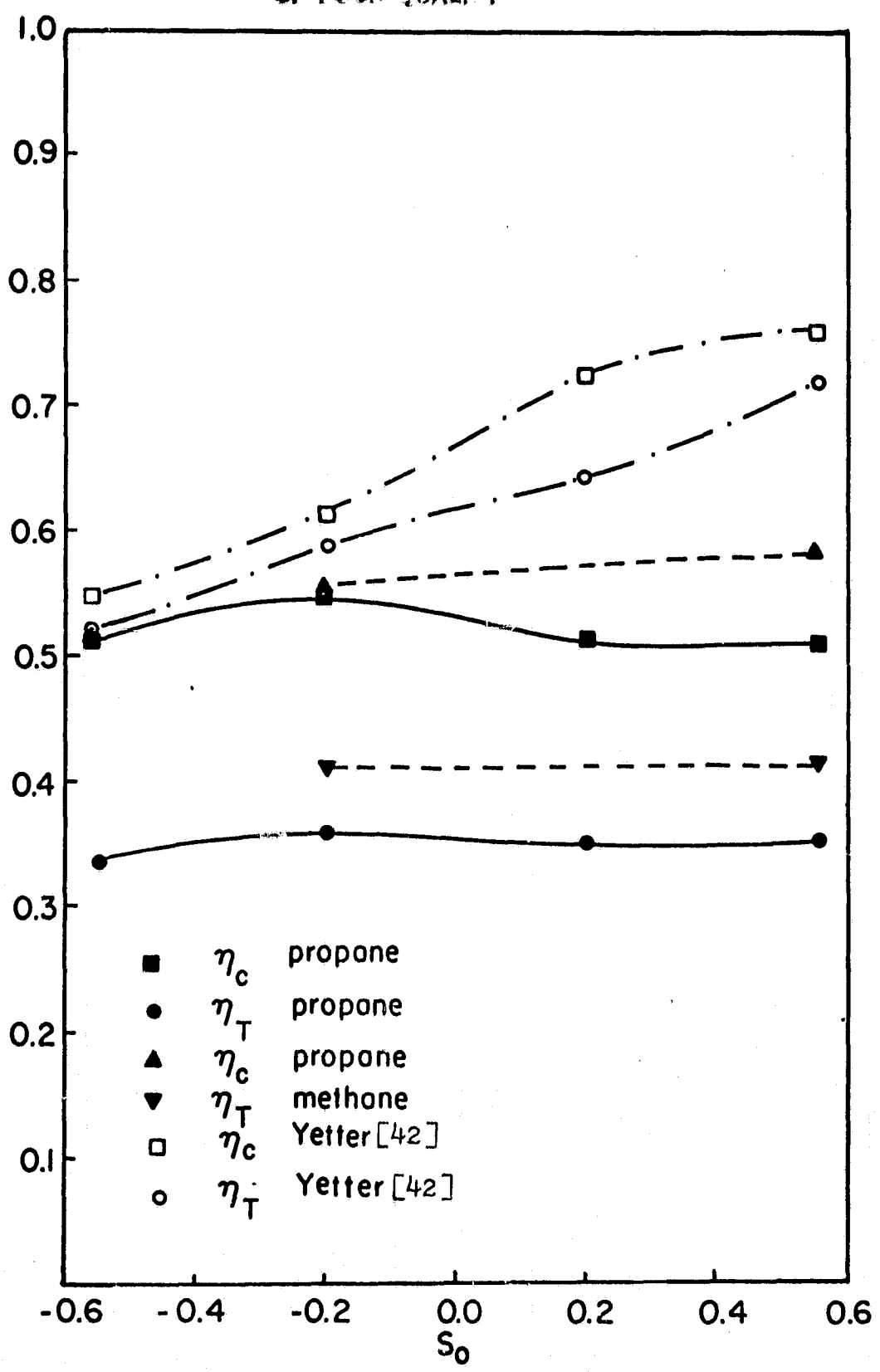

Figure 3-19: Chemical and thermal efficiencies for the different outer swirl conditions under propane and methane firing in the present study compared with those in Yetter's [42] study.

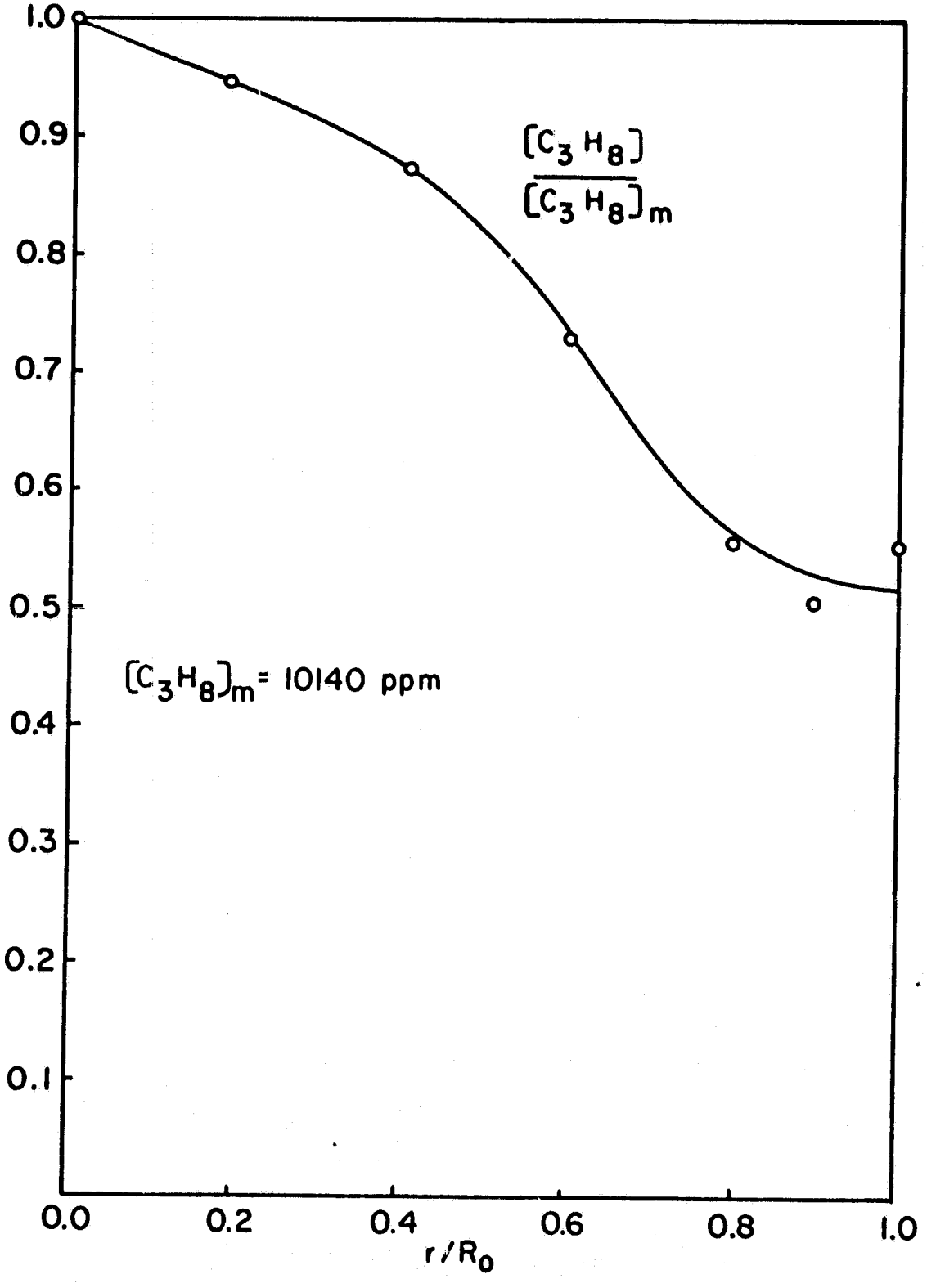

Figure 3-20: Mean concentration profile for propane for the 30° counter-swirl case under cold flow conditions.

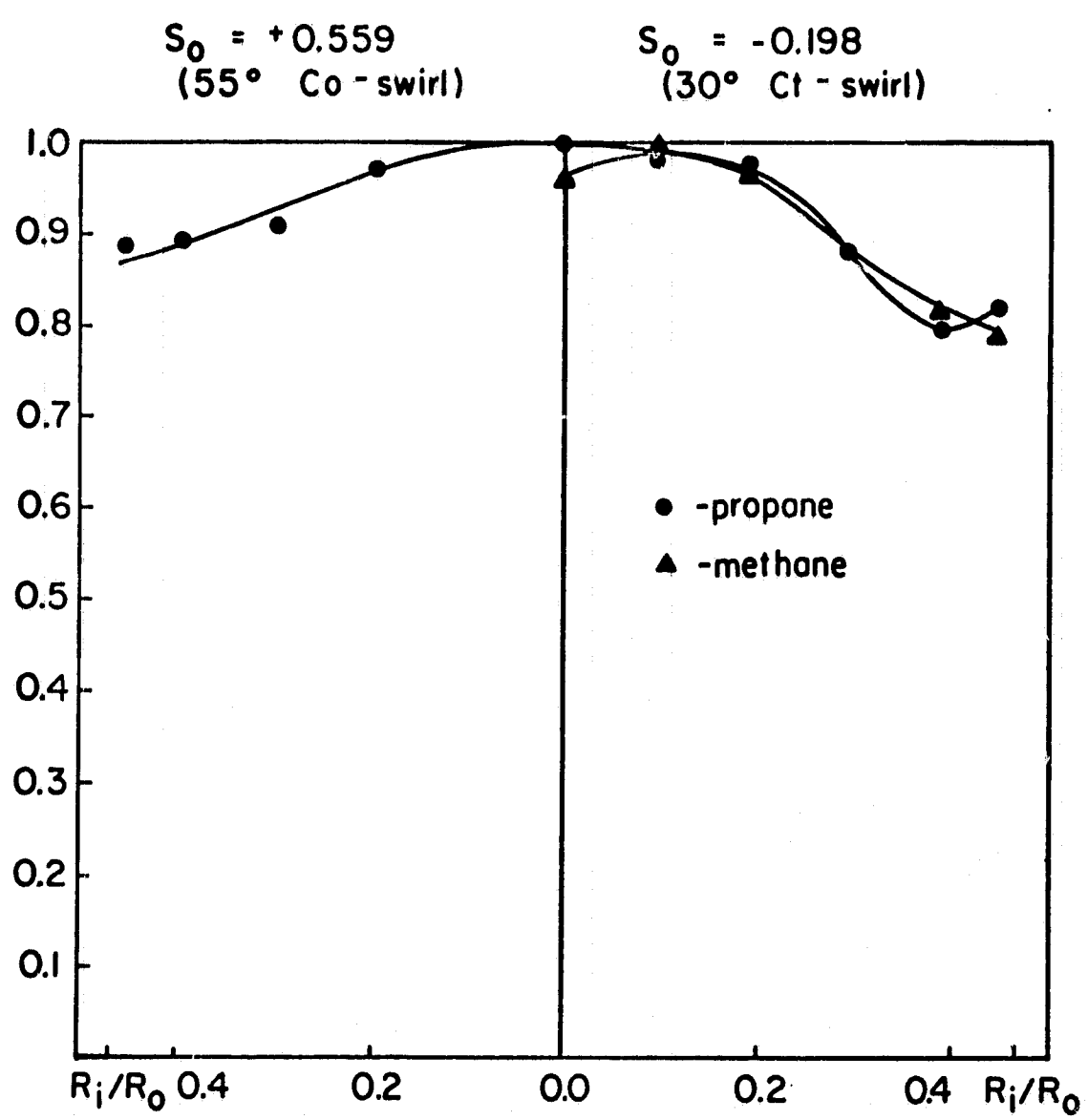

Figure 3-21: Fuel distribution in the inner jet at the inlet. Molefractions plotted are non-dimensionalized by their maximum values in each case.

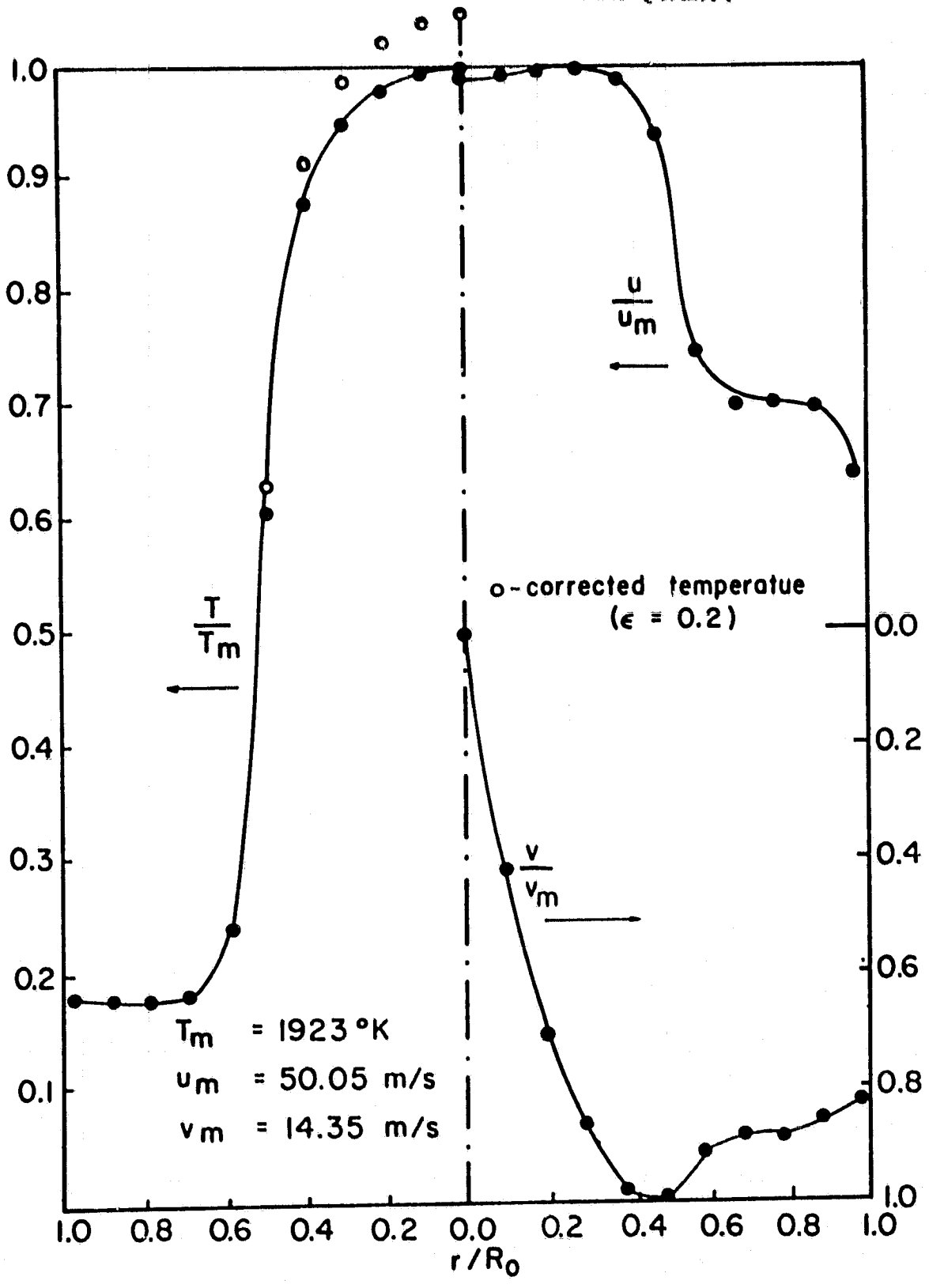

Figure 3-22: Mean temperature and velocity profiles for the 55° co-swirl, methane case. Temperature values after radiation correction are also shown.

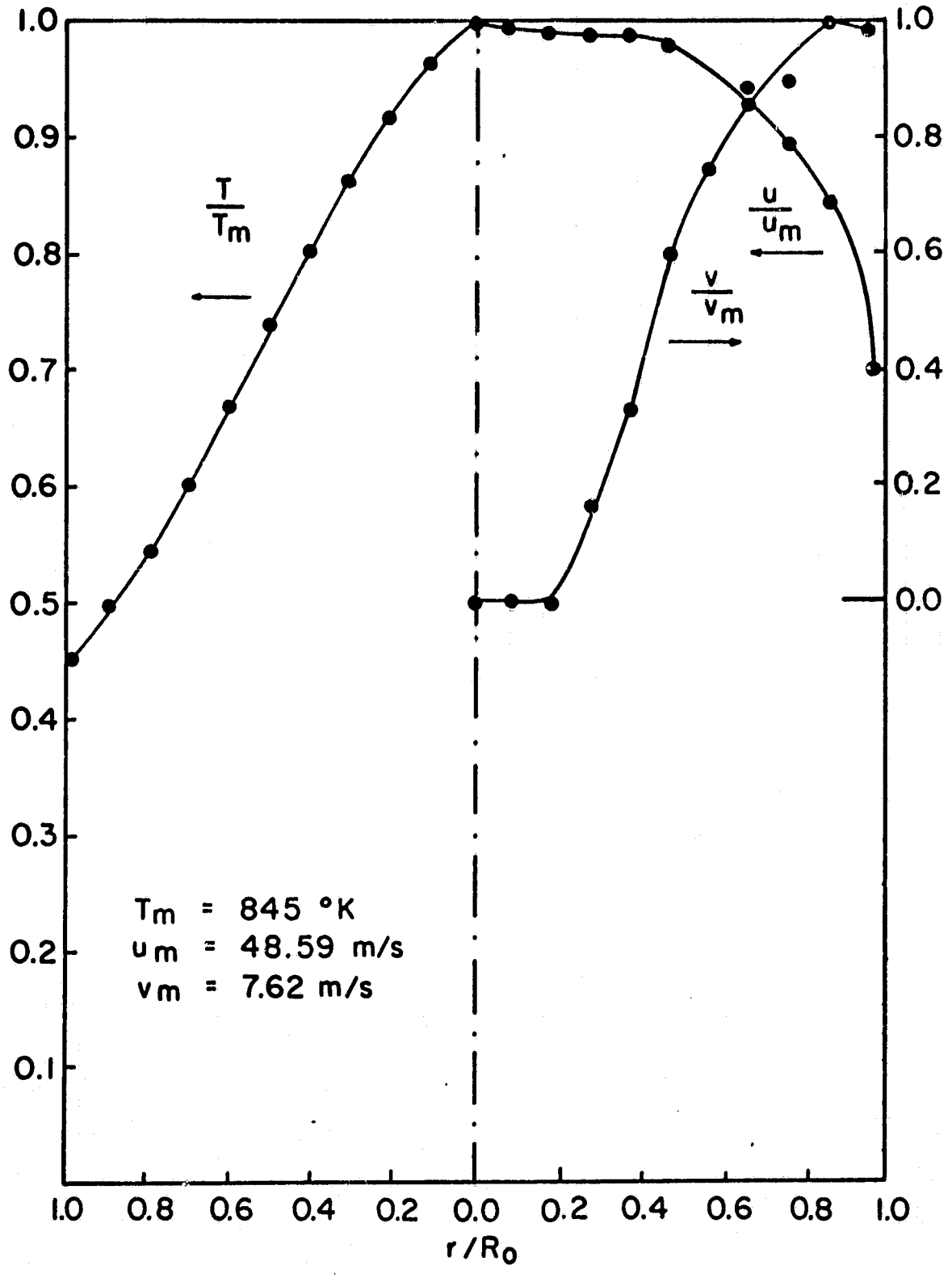

Figure 3-23: Mean temperature and velocity profiles for the 30° counter swirl, methane case.

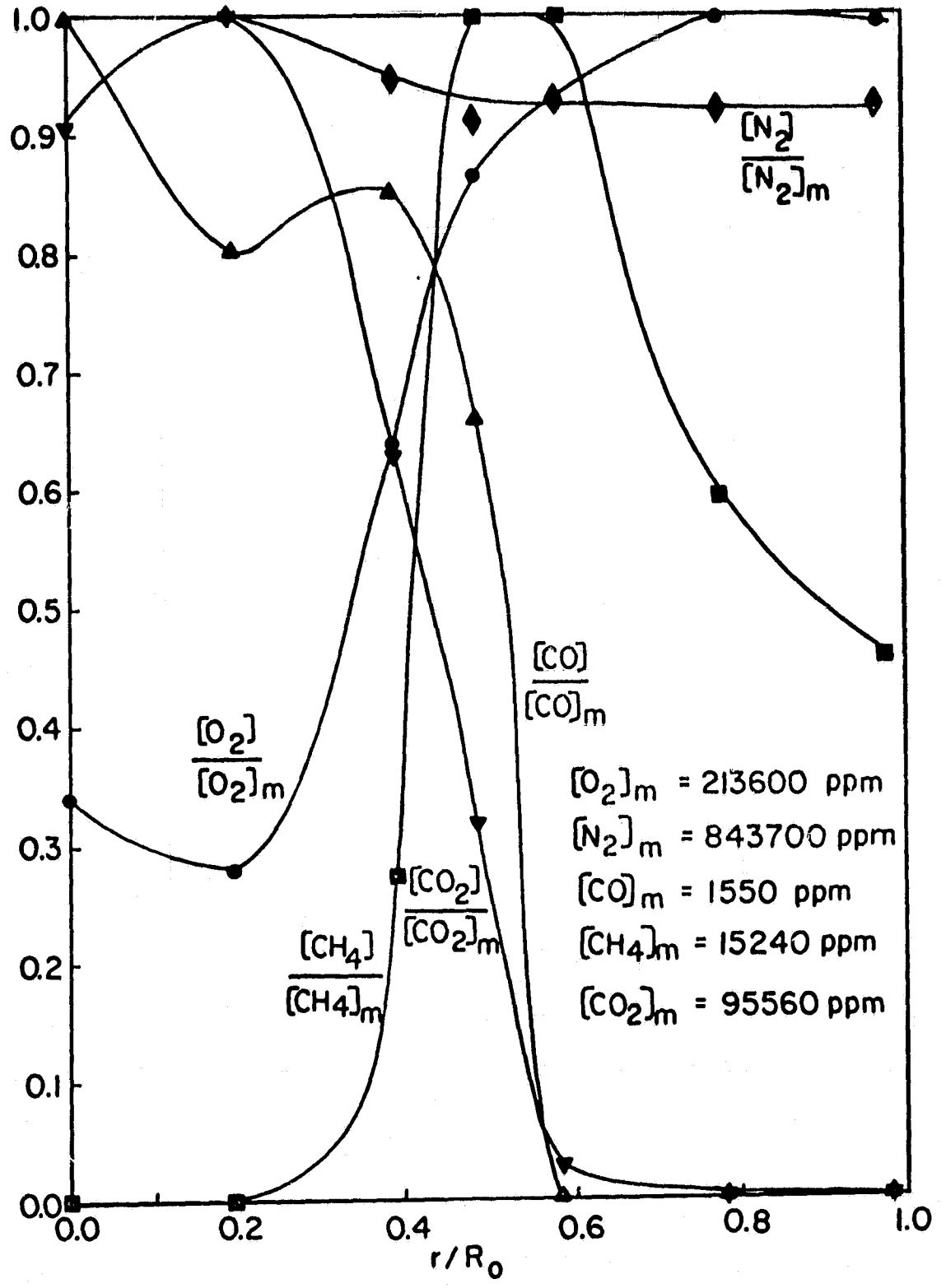

Figure 3-24: Mean composition profiles for the 55° co-swirl, methane case.

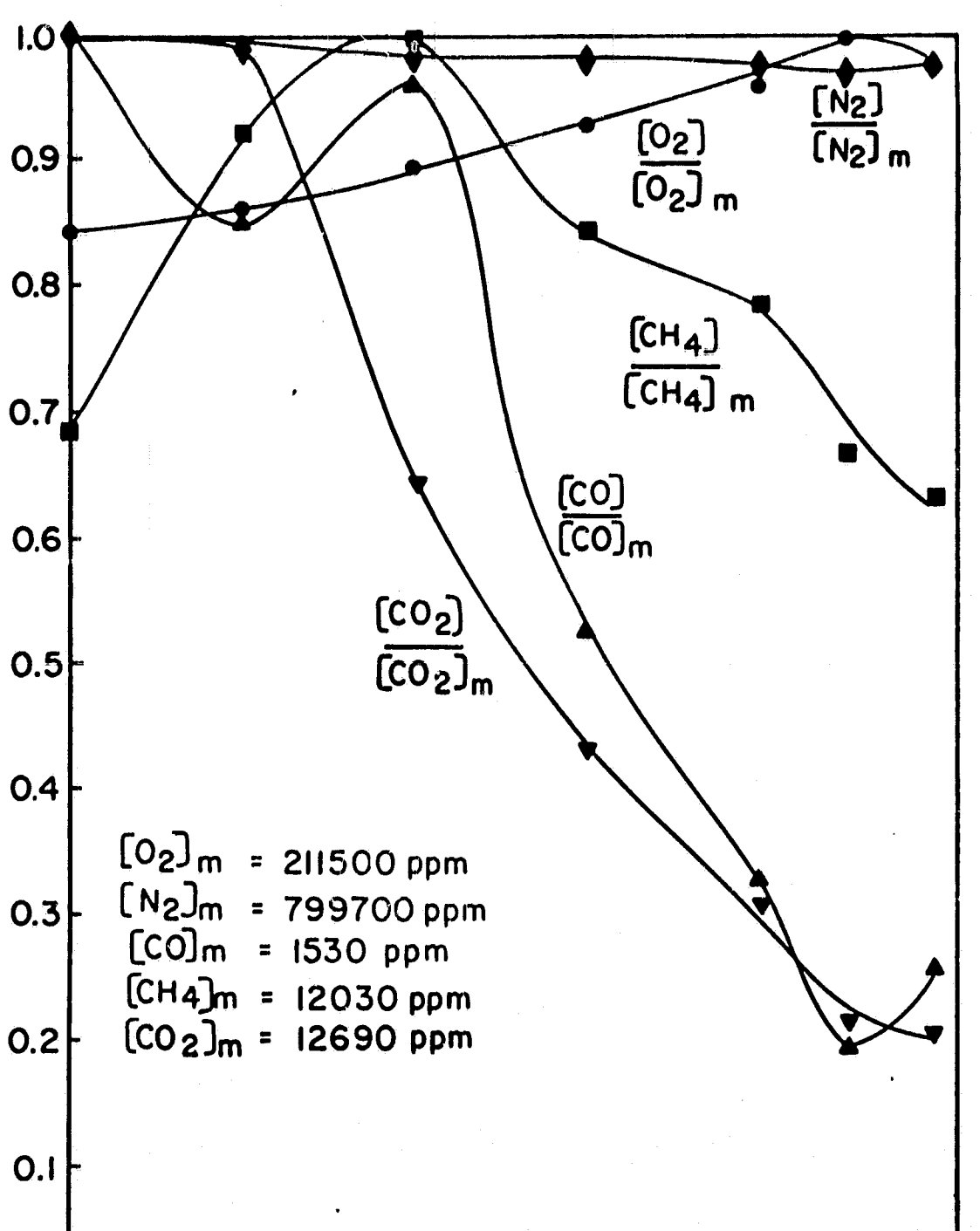

Figure 3-25: Mean composition profiles for the 30° counter-swirl, methane case.

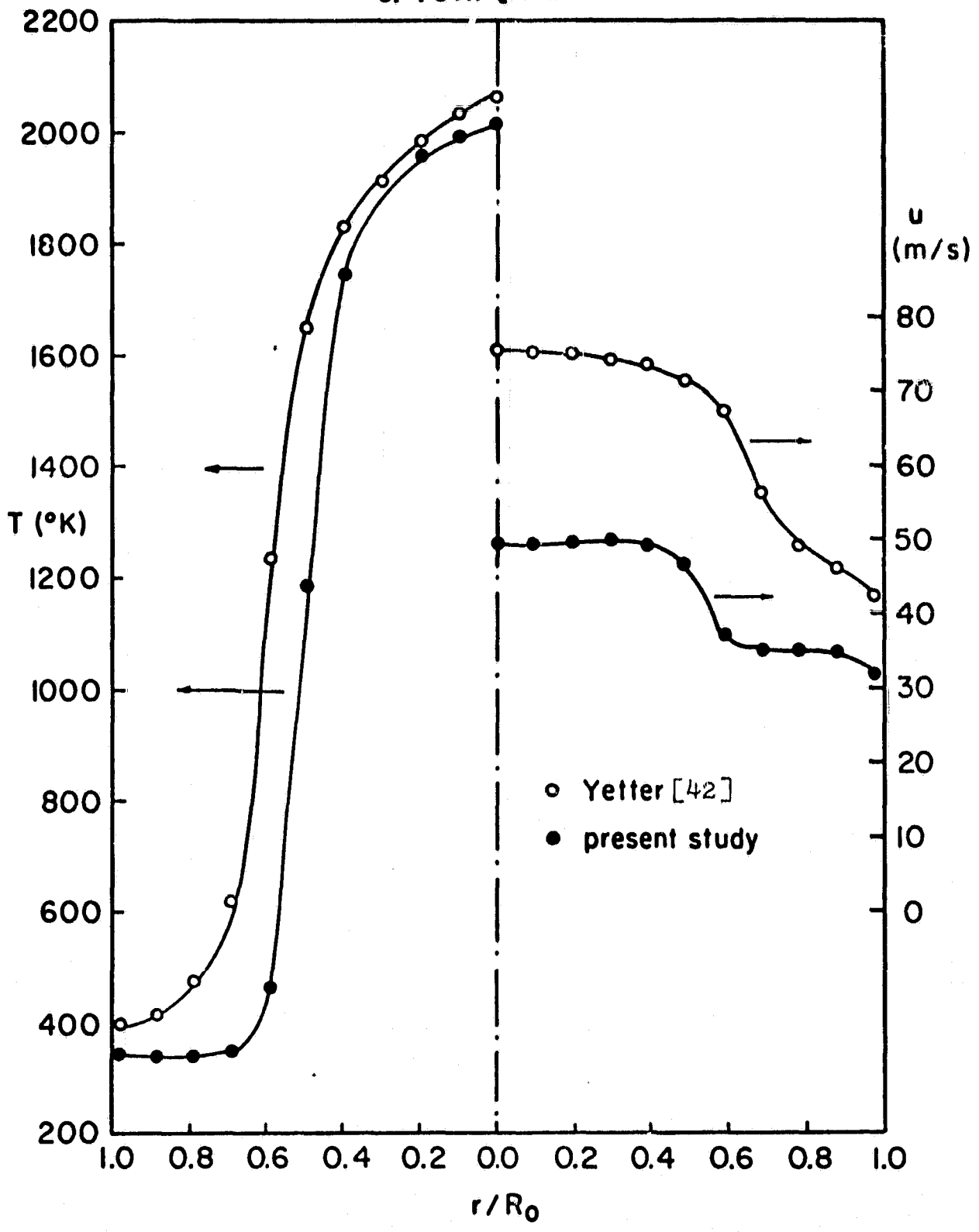

Figure 3-26: Mean temperature and axial velocity profiles for the 55° co-swirl, methane case in the present study compared with the corresponding profiles in Yetter's [42] study.

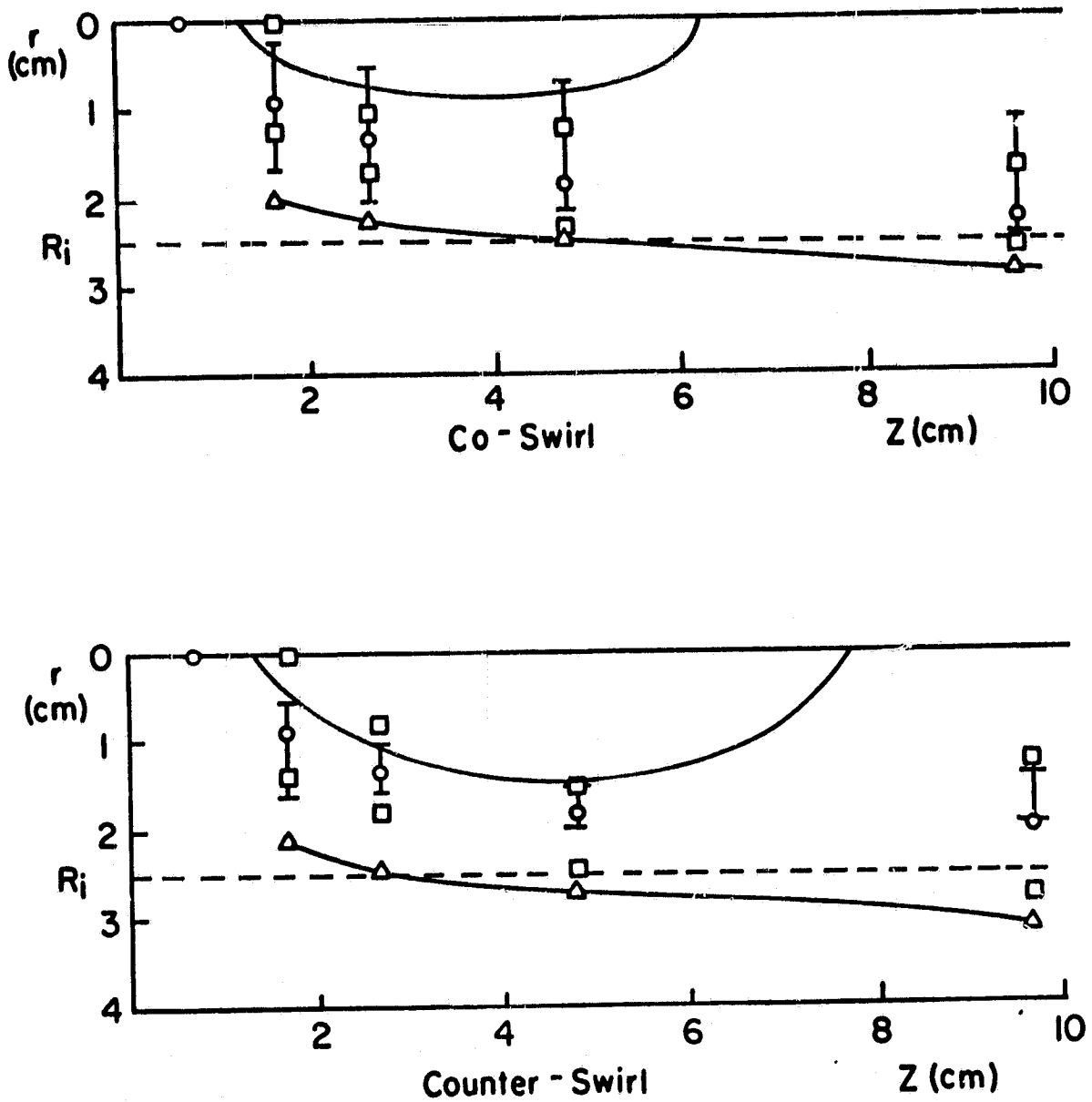

Figure 3-27: Reverse flow zones, mean CH radiant emissions maxima and peak axial velocity regions near the inlet for the high co- and counter-swirl cases.

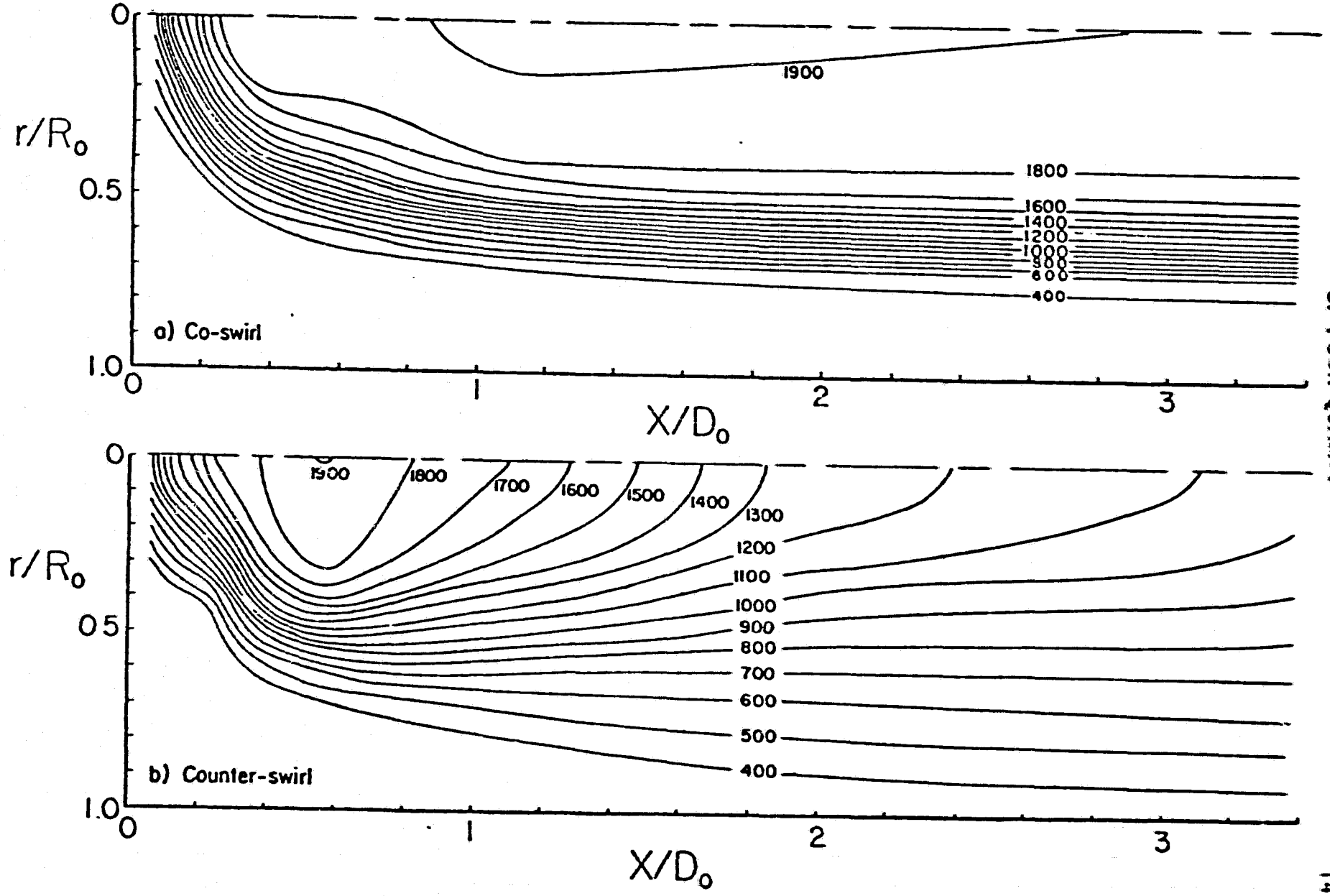

Figure 3-28: Mean isotherms (^{o}K) in the combustor (from Reference 41).

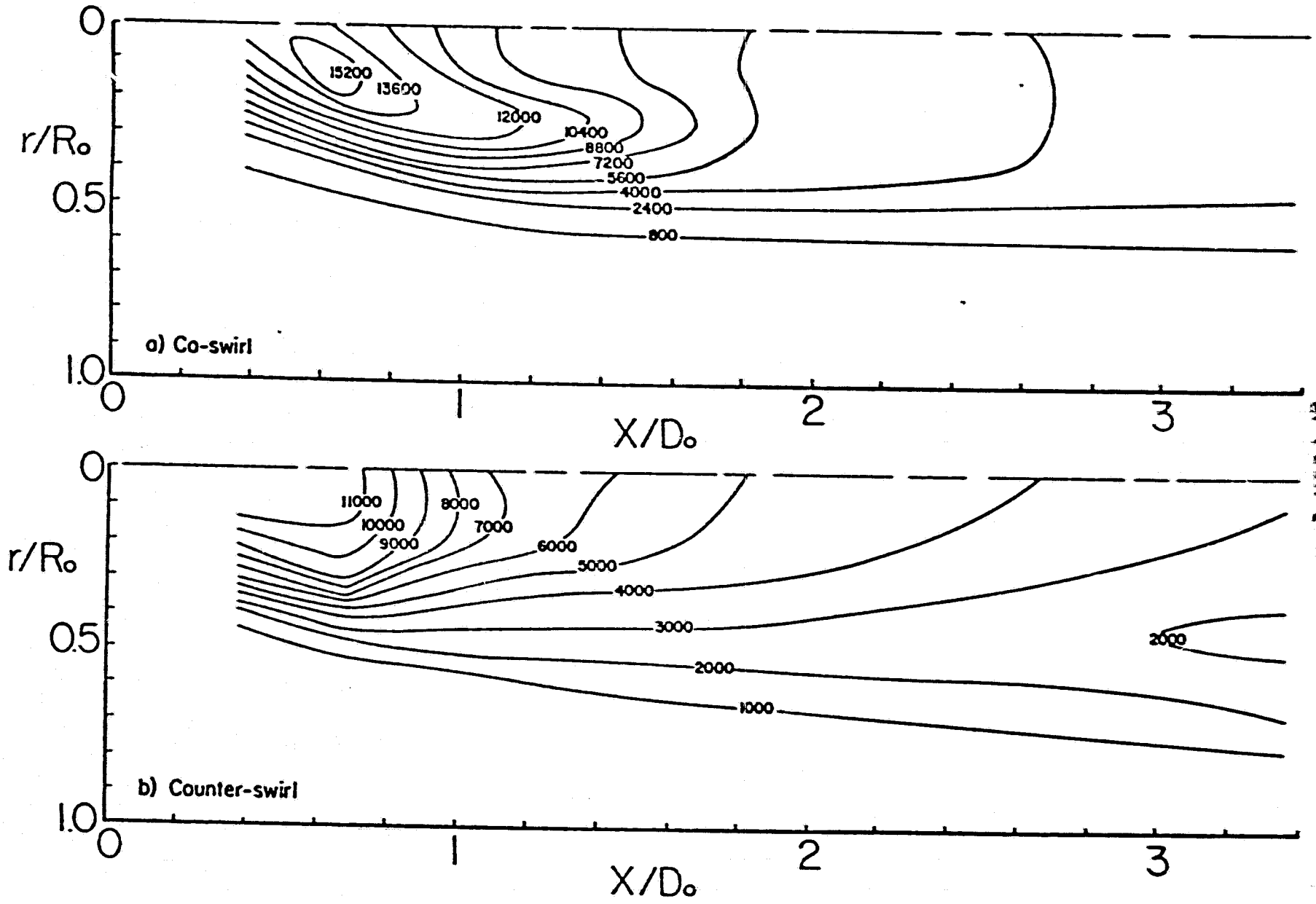

Figure 3-29: Mean isopleths of CO (ppm on a dry basis) in the combustor (from Reference 41).

APPENDIX A

Equations for Determining Combustor Operating Conditions

Subscripts:

i - inner jet

o - outer jet

oa - overall

f - fuel

1. Inner Jet Mass Flow Rate (lbm/min)

$$\dot{m}_i = A_i \left(\sqrt{hP/T}\right)_i \qquad \text{(A.1)}$$

Where A_i = Constant = 24.1285 (determined from pitot tube measurements)

h = differential pressure across the annubar (inches of water column)

p = static pressure at the annubar (psia)

T = temperature at the annubar ($^{\circ}R$)

2. Outer Jet Mass Flow Rate (lbm/min)

$$\dot{m}_o = A_2 \left(\sqrt{hP/T}\right)_o \qquad \text{(A.2)}$$

Where A_2 = constant = 59.5491 (determined from pitot tube measurements)

3. Volumetric Air Flow Rate (CFM)

$$Q = \dot{m}/\rho \qquad \text{(A.3)}$$

Where ρ = density in the corresponding jet (lbm/ft^3)

4. Inner Jet Mean Axial Velocity (ft/sec)

$$U_i = (Q_i + Q_f)/A_i$$

$$= 0.8692\ [8.916(\sqrt{hT/P})_i + Q_f] \qquad (A.4)$$

Where A_i = inner jet area = 0.8789π in^2

Q_f = fuel flow rate from rotameter readings (CFM)

5. Outer Jet Mean Axial Velocity (ft/sec)

$$U_o\ Q_o/A_o = 5.602(\sqrt{hT/P})_o \qquad (A.5)$$

Where A_o = outer jet area = 3π in^2

6. Overall Combustor Mean Axial Velocity (ft/sec)

$$U_{oa} = (Q_i + Q_o + Q_f)/A_c$$

$$= .1910(Q_i + Q_o + Q_f) \qquad (A.6)$$

Where A_c = area of the combustor = 4π in^2

7. Inner Jet Equivalence Ratio

$$\phi_i = [(Q_f)_{scfm}/(Q_i)_{scfm}]/(F/A)_{st}$$

$$= 0.07501(Q_f/\dot{m}_i)/(F/A)_{st} \qquad (A.7)$$

Where $(F/A)_{st}$ is the stoichiometric fuel-air ratio = 0.105 for methane

= 0.042 for propane

ρ = 0.07501 (lbm/ft^3) for air at STP

8. Overall Equivalence Ratio

$$\phi_{oa} = 0.07501\ [Q_f/(\dot{m}_i + \dot{m}_o)]/(F/A)_{st} \qquad (A.8)$$

APPENDIX B

Listings of Programs AVG.FTN, EFF.FTN and EFFM.FTN

```
C     PROGRAM AVG FIN
C     ***************
C
C     THIS PROGRAM CALCULATES THE MASS FLUX WEIGHTED AVERAGES
C     FOR THE X(I,J) VALUES FOR AN OPERATING CONDITION
C     X CORRESPONDS TO O2, N2, CO, FUEL, CO2, NO, NOX, T AND
C     H2O FOR I=1 TO 9 RESPECTIVELY  (X(9,J) IS CALCULATED
C     IN THE PROGRAM)    J VALUES DENOTE THE RADIAL LOCATIONS
C     AT 0.5 CM INTERVALS WITH J=1 FOR R=0.0 AND J=11 FOR
C     R=5.0 CM    FOR I=1 TO 5 THE X VALUES ARE SPECIFIED AS
C     A FRACTION OF THE RESPECTIVE MAXIMUM VALUES XMAX,
C     WHICH ARE SPECIFIED IN PERCENTAGE BY VOLUME    NO AND
C     NOX ARE SPECIFIED IN PPM AND T IN K
C-----------------------------------------------------------------
      DIMENSION R(11),U(11),X(9,11),PROD(11),XMAX(5),RHOUR(11)
     1         ,SUM(9),AVG(9)
      INTEGER FUEL
      LOGICAL NAMER(13),NAMEU(13),NAMEX(13),NAMEXM(13),RUN(25)
C
C       ASSIGN LOGICAL UNIT NUMBERS TO FILE NAMES AND READ
C       FROM FILES
C
      WRITE(5,1)
1     FORMAT(' INPUT R VALUES, TYPE FILE NAME R.DAT')
      READ(5,100)NAMER
100   FORMAT(13A1)
      CALL ASSIGN(3,NAMER)
      READ(3,*)(R(I),I=1,11)
      WRITE(5,2)
2     FORMAT(' INPUT U VALUES,TYPE FILE NAME C***U.DAT')
      READ(5,100)NAMEU
      CALL ASSIGN(4,NAMEU)
      READ (4,*) (U(I),I=1,11)
      WRITE(5,4)
4     FORMAT(2X,'INPUT X(I,J) VALUES,  TYPE FILE NAME C***X.DAT')
      READ(5,100)NAMEX
      CALL ASSIGN(1,NAMEX)
      DO 3 I=1,8
      READ(1,*) (X(I,J),J=1,11)
3     CONTINUE
      WRITE(5,5)
5     FORMAT(' INPUT XMAX ARRAY,TYPE FILE NAME C***XM.DAT')
      READ(5,100)NAMEXM
      CALL ASSIGN(2,NAMEXM)
      READ(2,*)(XMAX(I),I=1,5)
C
C       READ DATA FROM TERMINAL
C
      WRITE (5,14)
14    FORMAT(' INPUT INLET FUEL(PPM) AND FUEL  , 1=C3H8, 2=CH4')
      READ (5,*) F,FUEL
      WRITE (5,15)
15    FORMAT(' INPUT RUN CONDITION')
      READ (5,151) RUN
```

```
151   FORMAT(25A1)
      WRITE (6,16) RUN
16    FORMAT(20X,25A1,/)
C
C     CALCULATION OF MOLE FRACTIONS ON A DRY BASIS
C
      DO 110 I=1,5
      DO 110 J=1,11
      X(I,J)=X(I,J)*XMAX(I)/100
110   CONTINUE
C
C     CALCULATION OF WATER,MOLE FRACTIONS ON A WET BASIS
C     AND CONVERSION OF ALL MOLE FRACTIONS TO PPM.
C
      DO 130 J=1,11
      IF (FUEL.EQ.2) GO TO 118
      X(9,J)= 4./3.*(X(3,J)+X(5,J))
      GO TO 119
118   X(9,J)= 2.*(X(3,J)+X(5,J))
119   DO 120 I=1,5
        X(I,J)= X(I,J)*1000000./(1+X(9,J))
120     CONTINUE
      X(9,J)= X(9,J)*1000000./(1+X(9,J))
130   CONTINUE
C
C     OUTPUT OF MOLE FRACTIONS (IN PPM),VELOCITY AND TEMPERATURE.
C
      WRITE(6,6)
6     FORMAT(1X,' R ',2X,'  U  ',3X,' O2  ',3X,' N2  ',2X,' CO  ',2X,
     1         'FUEL',2X,' CO2 ',2X,'  NO   ',1X,'  NOX  ',1X,'  T
     ',1X,
     2  '  H2O  ',/,1X,'CM ',2X,' M/S ',3X,' PPM ',3X,' PPM ',
     3  2X,' PPM ',2X,' PPM',2X,' PPM ',2X,'  PPM  ',1X,
     4  '  PPM  ',1X,'  K  ',1X,'  PPM  ',/)
      DO 7 J=1,11
      WRITE(6,8)R(J),U(J),(X(I,J),I=1,9)
8     FORMAT(1X,F3.1,2X,F5.2,1X,2(1X,F7.0),1X,F5.0,2(1X,F6.0),
     1  1X,F6.2,2X,F6.2,2X,F5.0,1X,F7.0)
7     CONTINUE
C
C     CALCULATION OF AVERAGE VALUES.
C
C
C     DENOMINATOR
C
      DO 9 I=1,11
      RHOUR(I) = R(I)*U(I)/X(8,I)
9     CONTINUE
C       INTEGRATION
C     SIMPSON'S RULE FOR INTEGRATION BETWEEN R=0.0 AND R=5.0
      CALL SIMPS(RHOUR,SUMO)
C     TRAPEZOIDAL RULE BETWEEN R= 5.0 AND 5.1 WITH VALUE AT 5.1 EQUAL
C     TO ZERO
      SUMO = SUMO +0.05*RHOUR(11)
```

```
C.
C       NUMERATOR
C
        DO 11 I=1,9
        DO 10 J=1,11
        PROD(J)=RHOUR(J)*X(I,J)
10      CONTINUE
C       INTEGRATION
        CALL SIMPS(PROD,SUM(I))
        SUM(I)=SUM(I)+0.05*PROD(11)
C
        AVG(I)=SUM(I)/SUMO
C
11      CONTINUE
C
C       OUTPUT OF AVERAGE VALUES.
C
        WRITE(6,12)(AVG(I),I=1,9)
12      FORMAT(/,6X,'AVG=',2X,2(1X,F7.0),1X,F5.0,2(1X,F6.0),1X,F6.2,
     1  2X,F6.2,2X,F5.0,1X,F7.0)
C
C       CALCULATION OF EFFICIENCIES.
C
        EFF1= (1.-AVG(4)/F)*100.
C
        IF (FUEL.EQ.2) GO TO 20
C
        EFF2= (1.-(AVG(4)+AVG(3)*67.63/484.22)/F)*100.
        GO TO 30
C
20      CONTINUE
        EFF2= (1.-(AVG(4)+AVG(3)*67.63/189.76)/F)*100.
C
30      CONTINUE
C
C       OUTPUT OF EFFICIENCY VALUES.
C
        WRITE (6,17) EFF1,EFF2
17      FORMAT(/,6X,'CHEMICAL EFFICIENCY (UNBURNT FUEL ONLY)  =',F7.3,
     1  '%',/,6X,'CHEMICAL EFFICIENCY (UNBURNT FUEL AND CO)=',F7.3,
     2  '%',//)
C
        STOP
        END
        SUBROUTINE SIMPS(Y,SUM)
        DIMENSION Y(11)
        SUM=0
        DO 10 I=1,4
10      SUM = SUM+4*Y(2*I)+2*Y(2*I+1)
        H=0.5
        SUM=H/3*(Y(1)+SUM+4*Y(10)+Y(11))
        RETURN
        END
```

```
C
C     PROGRAM EFF.FTN
C     ***************
C
C     THIS PROGRAM CALCULATES THE THERMAL EFFICIENCY FOR A
C     PROPANE FIRED RUN.  THE VARIABLE NAMES AND THE DATA
C     INPUT FORMAT ARE THE SAME AS FOR AVG.FTN.
C-----------------------------------------------------------
      DIMENSION R(11),U(11),X(9,11),XMAX(5),PROD(11),H(11)
      LOGICAL NAMER(13),NAMEU(13),NAMEX(13),NAMEXM(13),RUN(13)
C
C       ASSIGN LOGICAL UNIT NUMBERS TO FILE NAMES AND READ
C       FROM FILES.
C
      WRITE(5,1)
1     FORMAT(' INPUT FILE R.DAT')
      READ(5,100)NAMER
100   FORMAT(13A1)
      CALL ASSIGN(1,NAMER)
      READ(1,*)(R(I),I=1,11)
      WRITE(5,2)
2     FORMAT(' INPUT FILE C***U.DAT')
      READ(5,100)NAMEU
      CALL ASSIGN(2,NAMEU)
      READ(2,*)(U(I),I=1,11)
      WRITE(5,3)
3     FORMAT(' INPUT FILE C***X.DAT')
      READ(5,100)NAMEX
      CALL ASSIGN(3,NAMEX)
      DO 4 I=1,8
      READ(3,*)(X(I,J),J=1,11)
4     CONTINUE
      WRITE(5,5)
5     FORMAT(' INPUT FILE C***XM.DAT')
      READ(5,100)NAMEXM
      CALL ASSIGN(4,NAMEXM)
      READ(4,*)(XMAX(I),I=1,5)
C       READ DATA FROM TERMINAL.
      WRITE(5,6)
6     FORMAT(' INPUT RUN CONDITION')
      READ(5,100)RUN
      WRITE(5,8)
8     FORMAT(' INPUT (INLET TEMP)/1000,FUEL MASS RATE,P IN MM OF HG')
      READ(5,*)TI,FM,P
C
C     COEFFICIENTS FOR CP FOR O2,N2,CO,C3H8,CO2,H2O
C
      A1=7.361141
      B1=-5.369589
      C1=20.54179
      D1=-25.86526
      E1=15.94566
      F1=-4.85889
```

```
      G1=0.5861501
      A2=7.709928
      B2=-5.503897
      C2=13.12136
      D2=-11.67955
      E2=5.233997
      F2=-1.173185
      G2=0.103883
      A3=7.812249
      B3=-6.668293
      C3=17.28296
      D3=-17.28709
      E3=8.860125
      F3=2.314819
      G3=0.2447785
      A4=6.8008
      B4=28.71
      C4=62.349
      D4=-107.19
      E4=69.802
      F4=-21.101
      G4=2.4476
      A5=4.324933
      B5=20.80895
      C5=-22.9459
      D5=16.84483
      E5=-7.935665
      F5=2.121672
      G5=-0.2408713
      A9=7.98886
      B9=-1.506271
      C9=6.661376
      D9=-4.65597
      E9=1.696464
      F9=-0.3706212
      G9=0.03992444
C
C       CALCULATE MOLE FRACTIONS ON A DRY BASIS.
C
      DO 9 I=1,5
      DO 9 J=1,11
      X(I,J)=X(I,J)*XMAX(I)/100.0
9     CONTINUE
C
C       CALCULATE WATER AND MOLE FRACTIONS ON A DRY BASIS.
C
      DO 10 J=1,11
      X(9,J)=4.0*(X(3,J)+X(5,J))/3
       DO 20 I=1,5
        X(I,J)=X(I,J)/(1+X(9,J))
20     CONTINUE
      X(9,J)=X(9,J)/(1+X(9,J))
10    CONTINUE
```

```
      WRITE(6,200)RUN
200   FORMAT('-',10X,'THERMAL EFFICIENCY',10X,'RUN  ',13A1///10X,' R '
     1  ,5X,'   H    ',10X,'   C    ',3X,'  PROD '/)
C
C       EVALUATE INTEGRAND AT EACH RADIAL LOCATION.
C
      DO 12 J=1,11
      T=X(8,J)/1000.0
C
C       COEFFICIENTS FOR CP VALUE AT THE RADIAL LOCATION J.
      A=X(1,J)*A1+X(2,J)*A2+X(3,J)*A3+X(4,J)*A4+X(5,J)*A5+X(9,J)*A9
      B=(X(1,J)*B1+X(2,J)*B2+X(3,J)*B3+X(4,J)*B4+X(5,J)*B5+X(9,J)*B9)
     1  /2
      C=(X(1,J)*C1+X(2,J)*C2+X(3,J)*C3+X(4,J)*C4+X(5,J)*C5+X(9,J)*C9)
     1  /3
      D=(X(1,J)*D1+X(2,J)*D2+X(3,J)*D3+X(4,J)*D4+X(5,J)*D5+X(9,J)*D9)
     1  /4
      E=(X(1,J)*E1+X(2,J)*E2+X(3,J)*E3+X(4,J)*E4+X(5,J)*E5+X(9,J)*E9)
     1  /5
      F=(X(1,J)*F1+X(2,J)*F2+X(3,J)*F3+X(4,J)*F4+X(5,J)*F5+X(9,J)*F9)
     1  /6
      G=(X(1,J)*G1+X(2,J)*G2+X(3,J)*G3+X(4,J)*G4+X(5,J)*G5+X(9,J)*G9)
     1  /7
C
C       SENSIBLE ENTHALPIES AT THE LOCAL AND INLET TEMPERATURES.
      HT2=T*(A+T*(B+T*(C+T*(D+T*(E+T*(F+T*G))))))
      HT1=TI*(A+TI*(B+TI*(C+TI*(D+TI*(E+TI*(F+TI*G))))))
C
C       INCREASE IN SENSIBLE ENTHALPY AT RADIAL LOCATION J.
      H(J)=(HT2-HT1)
C
C       INTEGRAND (CONSTANT FACTORS ARE MULTIPLIED LATER)
      PROD(J)=R(J)*U(J)*H(J)/X(8,J)
      WRITE(6,11)R(J),H(J),C,PROD(J)
11    FORMAT(10X,F3.1,5X,F7.4,10X,F7.4,3X,F7.5)
12    CONTINUE
C
C       EVALUATE INTEGRAL OVER THE RADIUS.
C
      CALL SIMPS(PROD,SUM)
C       TRAPEZOIDAL RULE FROM R=5.0 TO R=5.1 CM
      SUM=SUM+0.05*PROD(11)
C
C       MULTIPLY CONSTANT FACTORS.
C       HE= INCREASE IN SENSIBLE ENTHALPY FLUX AT THE EXIT.
C     HE=SUM*100*(P/R)*2*PI=SUM*P*0.01007,  R=62400 MM.HG-CC/GM MOLE-K
C     P IN MM. OF HG.,  100 CONVERTS M/S TO CM/S.
C
      HE=0.01007*SUM*P
C
C       HEATING VALUE AT INLET TEMP TI
C       HV= VALUE AT STP,  Q= VALUE AT TI
C       (HV IN KCAL/GM MOLE,  Q IN KCAL/GM).
```

```
C
      HV=484.22
      A=5*A1+A4-3*A5-4*A9
      B=(5*B1+B4-3*B5-4*B9)/2.0
      C=(5*C1+C4-3*C5-4*C9)/3.0
      D=(5*D1+D4-3*D5-4*D9)/4.0
      E=(5*E1+E4-3*E5-4*E9)/5.0
      F=(5*F1+F4-3*F5-4*F9)/6.0
      G=(5*G1+G4-3*G5-4*G9)/7.0
      HT2=TI*(A+TI*(B+TI*(C+TI*(D+TI*(E+TI*(F+TI*G))))))
      T=0.293
      HT1=T*(A+TI*(B+TI*(C+TI*(D+TI*(E+TI*(F+TI*G))))))
      Q=(HV+HT2-HT1)/44.0
C
C       CALCULATE THERMAL EFFICIENCY (%).
C
      EFF=100*HE/(Q*FM)
      WRITE(6,13)SUM,HE,Q
13    FORMAT('0',10X,'SUM=',F6.4,5X,'HE=',F7.4,5X,'Q=',F6.3/)
      WRITE(6,14)EFF,TI,FM,P
14    FORMAT(10X,'EFF=',F7.3///10X,'TI=',F5.3,3X,'FM=',F6.4,'P=',F6.2)
      STOP
      END
C
C
      SUBROUTINE SIMPS(Y,SUM)
C     SIMPSONS RULE FOR 11 POINTS; STEP SIZE=0.5
      DIMENSION Y(11)
      SUM=0.0
      DO 10 I=1,4
10    SUM=SUM+4*Y(2*I)+2*Y(2*I+1)
      H=0.5
      SUM=H/3*(Y(1)+SUM+4*Y(10)+Y(11))
      RETURN
      END
```

```
C
C     PROGRAM EFFM.FTN
C     ****************
C
C     THIS  PROGRAM CALCULATES THE THERMAL EFFICIENCY FOR A
C     METHANE FIRED RUN   COMMENT CARDS FOR EFF FTN APPLY
C     FOR THIS PROGRAM ALSO.
C-----------------------------------------------------------------
      DIMENSION R(11),U(11),X(9,11),XMAX(5),PROD(11),H(11)
      LOGICAL NAMER(13),NAMEU(13),NAMEX(13),NAMEXM(13),RUN(13)
      WRITE(5,1)
1     FORMAT(' INPUT FILE R.DAT')
      READ(5,100)NAMER
100   FORMAT(13A1)
      CALL ASSIGN(1,NAMER)
      READ(1,*)(R(I),I=1,11)
      WRITE(5,2)
2     FORMAT(' INPUT FILE C***U.DAT')
      READ(5,100)NAMEU
      CALL ASSIGN(2,NAMEU)
      READ(2,*)(U(I),I=1,11)
      WRITE(5,3)
3     FORMAT(' INPUT FILE C***X.DAT')
      READ(5,100)NAMEX
      CALL ASSIGN(3,NAMEX)
      DO 4 I=1,8
      READ(3,*)(X(I,J),J=1,11)
4     CONTINUE
      WRITE(5,5)
5     FORMAT(' INPUT FILE C***XM.DAT')
      READ(5,100)NAMEXM
      CALL ASSIGN(4,NAMEXM)
      READ(4,*)(XMAX(I),I=1,5)
      WRITE(5,6)
6     FORMAT(' INPUT RUN CONDITION')
      READ(5,100)RUN
      WRITE(5,8)
8     FORMAT(' INPUT (INLET TEMP)/1000,FUEL MASS RATE,P IN MM OF HG')
      READ(5,*)TI,FM,P
C
C     COEFFICIENTS FOR CP FOR O2,N2,CO,CH4,CO2,H2O
      A1=7.361141
        B1=5.369589
      C1=20.54179
      D1=-25.86526
      E1=15.94566
      F1=-4.85889
      G1=0.5861501
      A2=7.709928
      B2=-5.503897
      C2=13.12136
      D2=-11.67955
      E2=5.233997
```

```
      F2=-1.173185
      G2=0.103883
      A3=7.812249
      B3=-6.668293
      C3=17.28296
      D3=-17.28709
      E3=8.860125
      F3=2.314819
      G3=0.2447785
        A4=7.918404
        B4=-11.41722
        C4=63.73457
        D4=-75.25691
        E4=43.29269
        F4=-12.56702
        G4=1.49695
      A5=4.324933
      B5=20.80895
      C5=-22.9459
      D5=16.84483
      E5=-7.935665
      F5=2.121672
      G5=-0.2408713
      A9=7.98886
      B9=-1.506271
      C9=6.661376
      D9=-4.65597
      E9=1.696464
      F9=-0.3706212
      G9=0.03992444
      DO 9 I=1,5
      DO 9 J=1,11
      X(I,J)=X(I,J)*XMAX(I)/100.0
9     CONTINUE
      DO 10 J=1,11
      X(9,J)=2*(X(3,J)+X(5,J))
10    CONTINUE
      WRITE(6,200)RUN
200   FORMAT(///,10X,'THERMAL EFFICIENCY',10X,'RUN:  ',13A1///10X,' R '
     1  ,5X,'   H    ',10X,'   C    ',3X,'  PROD '/)
      DO 12 J=1,11
      T=X(8,J)/1000.0
      A=X(1,J)*A1+X(2,J)*A2+X(3,J)*A3+X(4,J)*A4+X(5,J)*A5+X(9,J)*A9
      B=(X(1,J)*B1+X(2,J)*B2+X(3,J)*B3+X(4,J)*B4+X(5,J)*B5+X(9,J)*B9)
     1  /2
      C=(X(1,J)*C1+X(2,J)*C2+X(3,J)*C3+X(4,J)*C4+X(5,J)*C5+X(9,J)*C9)
     1  /3
      D=(X(1,J)*D1+X(2,J)*D2+X(3,J)*D3+X(4,J)*D4+X(5,J)*D5+X(9,J)*D9)
     1  /4
      E=(X(1,J)*E1+X(2,J)*E2+X(3,J)*E3+X(4,J)*E4+X(5,J)*E5+X(9,J)*E9)
     1  /5
      F=(X(1,J)*F1+X(2,J)*F2+X(3,J)*F3+X(4,J)*F4+X(5,J)*F5+X(9,J)*F9)
     1  /6
```

```
      G=(X(1,J)*G1+X(2,J)*G2+X(3,J)*G3+X(4,J)*G4+X(5,J)*G5+X(9,J)*G9)
     1  /7
      HT2=T*(A+T*(B+T*(C+T*(D+T*(E+T*(F+T*G))))))
      HT1=TI*(A+TI*(B+TI*(C+TI*(D+TI*(E+TI*(F+TI*G))))))
      H(J)=(HT2-HT1)
      PROD(J)=R(J)*U(J)*H(J)/X(8,J)
      WRITE(6,11)R(J),H(J),C,PROD(J)
11    FORMAT(10X,F3.1,5X,F7.4,10X,F7.4,3X,F7.5)
12    CONTINUE
      CALL SIMPS(PROD,SUM)
      SUM=SUM+0.05*PROD(11)
C     HE=SUM*100*P/R*2*PI=SUM*P*0.01007;  R=62400 MM.HG-CC/GM MOLE-K
C     P IN MM. OF HG.
      HE=0.01007*SUM*P
C     HEATING VALUE AT TEMP TI
        HV=189.76
      A=2*A1+A4-A5-2*A9
      B=(2*B1+B4-B5-2*B9)/2.0
      C=(2*C1+C4-C5-2*C9)/3.0
      D=(2*D1+D4-D5-2*D9)/4.0
      E=(2*E1+E4-E5-2*E9)/5.0
      F=(2*F1+F4-F5-2*F9)/6.0
      G=(2*G1+G4-G5-2*G9)/7.0
      HT2=TI*(A+TI*(B+TI*(C+TI*(D+TI*(E+TI*(F+TI*G))))))
      T=0.293
      HT1=T*(A+TI*(B+TI*(C+TI*(D+TI*(E+TI*(F+TI*G))))))
      Q=(HV+HT2-HT1)/16.0
      EFF=100*HE/(Q*FM)
      WRITE(6,13)SUM,HE,Q
13    FORMAT('0',10X,'SUM=',F6.4,5X,'HE=',F7.4,5X,'Q=',F6.3/)
      WRITE(6,14)EFF,TI,FM,P
14    FORMAT(10X,'EFF=',F7.3///10X,'TI=',F5.3,3X,'FM=',F6.4,'P=',F6.2)
      STOP
      END
C
C
      SUBROUTINE SIMPS(Y,SUM)
C     SIMPSONS RULE FOR 11 POINTS, STEP SIZE=0.5
      DIMENSION Y(11)
      SUM=0.0
      DO 10 I=1,4
10    SUM=SUM+4*Y(2*I)+2*Y(2*I+1)
      H=0.5
      SUM=H/3*(Y(1)+SUM+4*Y(10)+Y(11))
      RETURN
      END
```